MULTISTRANGE BARYON PRODUCTION IN HIGH ENERGY ELECTRON-PROTON COLLISION

NOORATIKAH BINTI MOHAMMAD NASIR

FACULTY OF SCIENCE
UNIVERSITY OF MALAYA
KUALA LUMPUR

2018

MULTISTRANGE BARYON PRODUCTION IN HIGH ENERGY ELECTRON-PROTON COLLISION

NOORATIKAH BINTI MOHAMMAD NASIR

DISSERTATION SUBMITTED IN FULFILMENT OF THE REQUIREMENTS FOR THE DEGREE OF MASTER OF SCIENCE

DEPARTMENT OF PHYSICS
FACULTY OF SCIENCE
UNIVERSITY OF MALAYA
KUALA LUMPUR

2018

UNIVERSITY OF MALAYA

ORIGINAL LITERARY WORK DECLARATION

Name of Candidate: **NOORATIKAH MOHAMMAD NASIR**

[redacted]

Matric No: **SGR130090**

Name of Degree: **MASTER OF SCIENCE**

Title of Dissertation: **MULTISTRANGE BARYON PRODUCTION IN HIGH ENERGY ELECTRON-PROTON COLLISION**

Field of Study: **EXPERIMENTAL PHYSICS**

I do solemnly and sincerely declare that:

(1) I am the sole author/writer of this Work;
(2) This Work is original;
(3) Any use of any work in which copyright exists was done by way of fair dealing and for permitted purposes and any excerpt or extract from, or reference to or reproduction of any copyright work has been disclosed expressly and sufficiently and the title of the Work and its authorship have been acknowledged in this Work;
(4) I do not have any actual knowledge nor do I ought reasonably to know that the making of this work constitutes an infringement of any copyright work;
(5) I hereby assign all and every rights in the copyright to this Work to the University of Malaya ("UM"), who henceforth shall be owner of the copyright in this Work and that any reproduction or use in any form or by any means whatsoever is prohibited without the written consent of UM having been first had and obtained;
(6) I am fully aware that if in the course of making this Work I have infringed any copyright whether intentionally or otherwise, I may be subject to legal action or any other action as may be determined by UM.

Candidate's Signature [redacted] Date: 18/7/18

Subscribed and solemnly declared before,

Witness's Signature [redacted] Date: 18/7/18

Name: PROF DR WAN AHMAD TAJUDDIN WAN AHMAD

Designation: PROFESSOR

MULTISTRANGE BARYON PRODUCTION IN HIGH ENERGY ELECTRON-PROTON COLLISION

ABSTRACT

A search for Ξ^-'s decaying to $\Lambda\pi^-$ combinations is carried out to calculate the total cross sections in electron-proton collisions at HERA. The analysed data were collected using the ZEUS detector during the running period of 2002-2007 with an integrated luminosity of 323 pb^{-1}. The data analysis was done using online and offline analysis at center-of-mass energy of $\sqrt{s}$ = 318 GeV. Strange and multistrange baryon production phenomenology such as String Model is reviewed, as it is not fully understood yet. The cross section carried out has been compared with ARIADNE Monte Carlo (MC) simulation predictions.

Keywords: baryon production, electron-proton, strange quark

PENGELUARAN BARYON MULTIANEH DALAM PERLANGGARAN ELEKTRON-PROTON TENAGA TINGGI

ABSTRAK

Satu carian untuk Ξ^- yang mereput kepada $\Lambda\pi^-$ dijalankan untuk mengira jumlah keratan rentas dalam pelanggaran elektron-proton di HERA. Data yang dikumpulkan dianalisis menggunakan alat pengesanan ZEUS pada tahun 2002-2007 dengan nilai kilauan bersepadu 323 pb-1. Analisis data dilakukan dengan menggunakan kuasa pada tenaga pusat $\sqrt{s} = 318$ GeV. Fenomenologi seperti Model String dalam penghasilan barion kuark aneh dan multianeh disemak kerana ia masih belum difahami sepenuhnya. Keratan rentas kajian yang dilakukan terhadap data telah dibandingkan dengan ramalan simulasi Monte Carlo (MC) Ariadne.

Kata kunci: pengeluaran baryon, elektron-proton, kuark aneh

ACKNOWLEDGEMENTS

Praised be to Almighty, Who guided me to complete this thesis, and I would not have found the way had it not been that He had guided me.

I would like to take this opportunity to acknowledge my incalculable personal debt to my supervisor Prof Dr Wan Ahmad Tajuddin bin Wan Abdullah for all the advice, information and encouragement he freely provided over the year. His invaluable spirit and support had encouraged me to finish this writing successfully. Not to forget, many thanks to Prof Dr Zainol Abidin bin Ibrahim, for his morale support and sharing his life experience stories.

It is an honour for me to be part of ZEUS collaboration and many thanks to ZEUS members for their guidance during my first stay at DESY and even help answering my questions remotely through emails, especially Shasha. Apart from that, I would like to thank NCPP members, especially Kak Mira, Kak Khasmi, and Ami for always being there to keep me moving forward. Not to forget, my ZEUS partner, Nuha.

Last but not least, million thanks to my parents; Ummi and Abah for their blessings, my siblings, friends, and my loved ones.

TABLE OF CONTENTS

LIST OF FIGURES

LIST OF TABLES

LIST OF SYMBOLS AND ABBREVIATIONS

α	:	Alpha
ep	:	electron-proton
ξ	:	Parton
K	:	Kaon Meson
q	:	Quark
$\bar{q}$	:	Anti-Quark
γ	:	Photon
λ^0	:	Lambda Baryon
Ξ^-	:	Xi Baryon
Σ^+	:	Sigma Baryon
N_{dof}	:	Number degrees of freedom
Q^2	:	Photon Virtuality
$W^\pm$	:	$W^\pm$ Gauge Boson
Z^0	:	Z^0 Gauge Boson
χ^2	:	Chi-square
ARIADNE	:	A Program for Simulation of QCD Cascades Implementing the Colour Dipole
BCAL	:	Barrel Calorimeter
BGF	:	Boson-gluon Fusion
BMVD	:	Barrel Micro Vertex Detector
BW	:	Breit Wigner
CAL	:	Uranium Scintillator Calorimeter
CC	:	Charged Current
CDM	:	Colour Dipole Model
CERN	:	European Organization for Nuclear Research

CTD	:	Central Tracking Detector
DESY	:	Deutsches Elektronen-Synchrotron
DIS	:	Deep Inelastic Scattering
DJANGOH	:	Interface between HERACLES (QED corrections to order α_{QED}) and LEPTO/ARIADNE (QCD matrix elements and parton showers/colour dipole radiation) to give complete *ep* events
EM	:	Electromagnetic
EMC	:	Electro-Magnetic Calorimeter
FCAL	:	Forward Calorimeter
FLT	:	First-Level Trigger
FMVD	:	Forward Micro Vertex Detector
FORTRAN	:	FORmula TRANslation
GFLT	:	Global First Level Trigger
H1	:	H1 Detector
HERA	:	Hadron Electron Ring Accelerator
HERA-B	:	HERA-B Detector
HERACLES	:	NC and CC *ep* interactions (using parameterizations of structure functions or parton densities) with radiative corrections: single photon emission from the lepton line, self-energy corrections and the complete set of one-loop weak corrections can be included
HERMES	:	HERMES Detector
ID	:	Identification
JETSET	:	The Lund string model for hadronization of parton systems
LEP	:	Large Electron-Positron
LEPTO	:	Deep inelastic lepton-nucleon scattering based on LO electroweak cross sections (incl. lepton polarization), first order QCD matrix elements, parton showers and Lund hadronisation giving complete events. Soft colour interaction model gives rapidity gap events
LER	:	Low Energy Run
MC	:	Monte Carlo

MER	:	Middle Energy Run
MVD	:	Micro Vertex Detector
NC	:	Neutral Current
ORANGE	:	Overlying Routine for Ntuple Generation
PDF	:	Probability Distribution Function
PETRA	:	PETRA Experiment
PHP	:	Photoproduction
PHYTIA	:	General purpose generator for ee, pp and ep interactions, based on LO matrix elements, parton showers and Lund hadronisation
QCD	:	Quantum Chromodynamics
QED	:	Quark Electrodynamics
QPM	:	Quark Parton Model
RAPGAP	:	A full Monte Carlo suited to describe deep inelastic scattering, including diffractive DIS and LO direct and resolved processes
RCAL	:	Rear Calorimeter
SINISTRA	:	Electron Finder
SLAC	:	Stanford Linear Accelerator Center
SLT	:	Second Level Trigger
SRTD	:	Small Rear Tracking Detector
STT	:	Straw Tube Tracker
SU(3)	:	Special Unitary Group
TLT	:	Third Level Trigger
VCTRACK	:	V(XD)C(TD)TRA(C)K
WA	:	Wan Abdullah
XX	:	20^{th} century
ZEPHYR	:	ZEUS PHYsics Reconstruction Program
ZEUS	:	ZEUS Detector

ZSMSM	:	ZEUS Standard Software System
ZTT	:	Track Finding Software Packages
ZUFOS	:	ZEUS Unidentified Flying ObjectS

CHAPTER 1: INTRODUCTION

1.1 The Standard Model

The never-ending question about what matter consists of is very fundamental. It has mesmerised many generations of physicists in the past and will still be topical in the future. Everything in the universe, from our solar system to the most distant galaxy, all of it can be traced back to the Big Bang (Linde et al., 1994). The Big Bang theory is the current cosmological model that describes the origin, early history, and evolution of the universe. About 13.8 billion years ago, the universe was no larger than an atom. It remains a mystery where this "primordial atom" came from until now. After matter began to form, there was a kind of "war" between antimatter and matter. In the early universe, there would have been an equal amount of matter and antimatter created. Because they both have opposite charges, they cancel each other out. If there was an equal amount of both, why does the universe have so much matter? For some unknown reason, there was a slight imbalance in the ratio of matter and antimatter. The matter that was slightly more than antimatter survived is the one that makes up the world around us.

Ernest Rutherford (Rutherford, 1911) revealed at the early XX century, an intrinsic structure of the atom by scattering α particles on a thin gold foil. His idea leads to the beliefs that an atom is built of a combination neutron and proton inside the nucleus and electron orbiting the nucleus. This increases the curiosity in understanding in depth of the building blocks of matter and their interactions, where many experiments in high energy physics have been conducted such as at DESY, CERN and SLAC.

After inflation, the first forms of matter began to form. Quarks were formed and soon combined to form protons and neutrons, which would combine to form atomic nuclei. Due to the extreme temperatures of the early universe, however, the protons and

neutrons could not capture electrons to form atoms. It would be another 380,000 years until the first atoms formed. During this period, the temperature was cold enough to allow the nuclei to capture electrons, creating the first atoms. The illustration of atoms, nucleus, and quarks are shown in Figure 1.1.

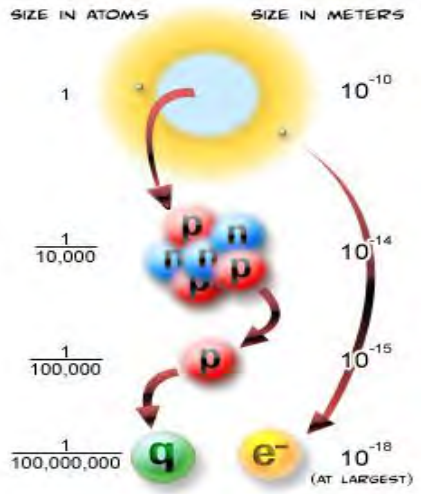

Figure 1.1: The size of the atom (Berkeley Lab, 2014).

A theory called The Standard Model (Herrero, 1999) that has been developed by the physicist to explain what the world is made up and what holds it together. The discoveries believe that leptons and quarks made up particles. Each group consists of six flavours, which comes in three generations. The first generation which is the lightest, (up and down quark) makes the most stable particles, followed by less stable second generations, (charm and strange quark) and third generations, (top and bottom quark).

Same goes to the leptons group, they are similarly arranged in three generations with paired – the lightest, (electron and electron neutrino), the heavier, (muon and muon neutrino), and the most massive, (tau and tau neutrino).

Not only that, Standard Model also tells us about the four fundamental forces in the universe. Nature is controlled by just four significant forces; namely gravity, the strong nuclear force, electromagnetism, and the weak nuclear force. During the first moments

of the universes life, all the forces in the universe were all united as a single "super force." Immediately after the Big Bang, these four forces were united as a single super-force, yet due to the rapid expansion and cooling down of the universe the super force began to break and broke the symmetry.

The first force to break off from the super-force was gravity. Gravity is by far the weakest of the forces. It certainly does not appear that way. Every particle of matter exerts some gravitational pull on every other particle, which is why gravity dominates large scale structures in the universe. Unlike the other forces, gravity works on much bigger scales, so its effects are more noticeable, yet carries the most weakling forces. The strong nuclear force was the next force to break from the original super-force. The strong force, as the name suggests, is the strongest of the four forces and are used to bind the elementary particles of matter to form larger particles, such as binding quarks together to form protons and neutrons (Honc, 2011). The third force to break from the super-force was the electromagnetic force. The electromagnetic force is the attraction between unlike poles. It is responsible for holding atoms together. The positive charge is likely to be attracted by the negative charge. And to hold protons together, neutrons are also drawn to the positive charge of protons. The very last force to arise in the universe was the weak nuclear force. This force is weaker than both the strong force and electromagnetic force, yet it is still stronger than gravity. It is responsible for the process of radioactive decay within atoms.

Each of these forces also has a particular kind of particle which carries the force. For electromagnetism, photons (particles of light) carry the electromagnetic force. Gluons, which are particles that act as a type of glue that holds particles such as quarks together, carries the strong force. W and Z bosons carry weak force (Loveland, 2017). It remains unknown; however, what particle carries the gravitational force. Scientists have proposed the existence of the graviton, yet its existence remains unknown. To date,

scientists have no complete theory of quantum gravity, and without any one of these, scientists will never fully understand our universe. Figure 1.2 shows the Standard Model.

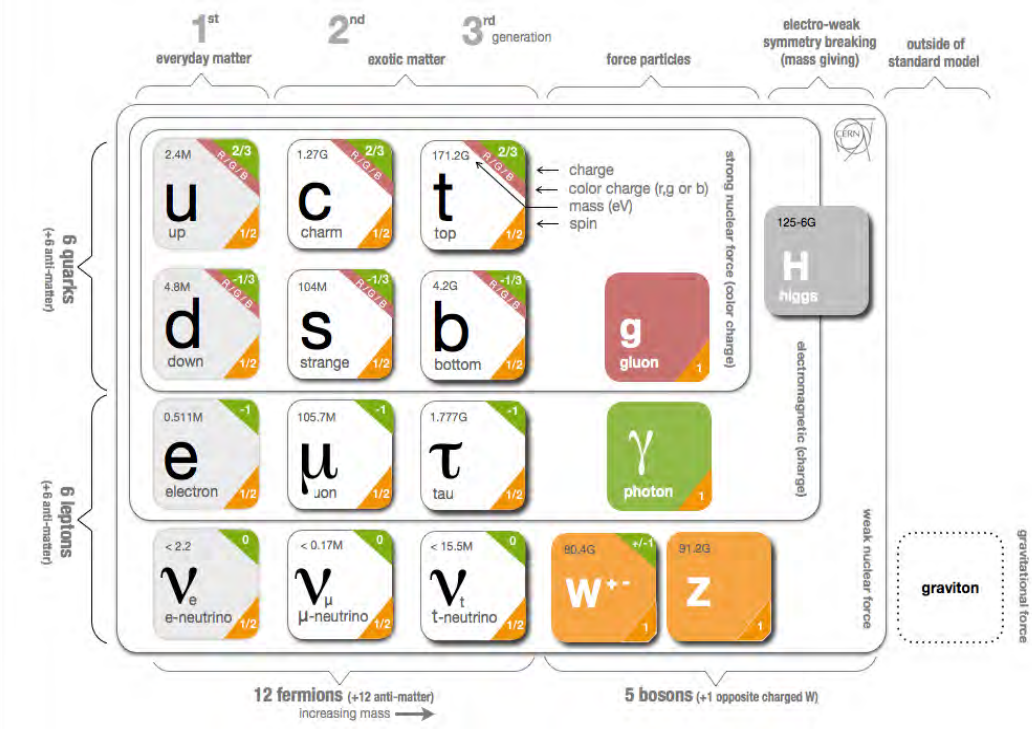

Figure 1.2: The Standard Model (CERN Collaboration et al., 2014).

1.2 Objectives

This thesis is devoted to strange analysis production. Therefore, the objectives of this research are:

1. To study the efficiency of doubly-strange baryon Ξ^- production in Monte Carlo and Data respectively as the indications on mechanism of baryon production in hadronization.
2. To implement optimization cuts in Monte Carlo and Data analysis so that the signal can be enhanced.

1.3 Thesis Layout

This thesis is systematized in the following way: Chapter 1 gives a brief introduction to the standard model in particle physics, objectives associated in this research, and thesis layout is also in this chapter. In the following Chapter 2 physics concept that describes the processes involved in the electron-proton collision is presented. The HERA physics, doubly-strange production mechanism, deep inelastic scattering, and quark parton model is also discussed here. A description of the experimental conditions and procedures used to operate the analysis, the HERA collider and the ZEUS detector where some essential components of the detector part were explained can be found in Chapter 3. Chapter 4 tells about Monte Carlo simulations in general, event selection, and the particle tracks reconstruction. In Chapter 5, the offline selection of events is included here, the brief description for triggers and cuts selected, and identification of candidates to reconstruct Ξ^- baryon, matching analysis and some optimization cuts are included here. Chapter 6 discussed about the related results and discussion on the analysis efficiency and cross sections in Monte Carlo and HERA II data. The conclusion of this research is in Chapter 7.

CHAPTER 2: PHYSICS OVERVIEW

In this chapter, various studies which have been done related to physics that involved in the electron-proton collision are reviewed. An introduction to strange baryon production is also presented here, as well as kinematics and phase space at HERA.

2.1 Electron-proton collision at HERA

In 1992, the very first electron-proton (ep) collider in the world (Hilton, 1999), the Hadron Electron Ring Accelerator, HERA (Szuba et al., 2012) started running at *Deutsches Elektronen-Synchrotron*, DESY to study the internal proton structure. It has about 30 GeV of electrons and 920 GeV of protons (820 GeV until the end of 1997), giving a fixed centre-of-mass energy of 318 GeV (Brock et al., 2009). With the aim of increasing luminosity, a long shut down in 2000 and 2001 was intended to upgrade the machine and detectors. After the collision happened, many particles were produced, and one of the particles is Ξ^-. This study focuses on the search of strange baryon production through the measurement of inclusive baryon production in ep neutral current deep inelastic scattering using ZEUS detector (Szuba et al., 2012).

Having two strange quarks (down, strange, strange), $\Xi^-$are much more sensitive to strange production where this weak decaying particle has the spin of ½. The selected decay mode for the searched particle is $\Xi^- \rightarrow \Lambda^0 + \pi^-$ (Patrignani, 2016). The production of strange particle in high energy electron-proton collision is one of the many studies by various researchers in strange production. The discovery of strange quarks in cosmic rays before the quarks model was proposed makes the searches become more interesting, as it has long lifetimes (Mohammad Nasir & Wan Abdullah, 2015). Apart from that, the motivation for this analysis is that the strange hadron production is not well understood in hadronic collisions, as its measurements at HERA

lag behind those experiment at LEP. For the record, there is a disagreement between HERA and LEP regarding the fragmentation of strange hadrons measurements, i.e., $\Lambda_s \approx 0.2$ and $\Lambda_s \approx 0.3$ respectively.

2.2 Doubly-strange production mechanism

Researchers agreed that deep study in Neutral Current in Deep Inelastic Scattering (D' Agostini & Nigro, 1997) about production of the strange particle could give information of s-quarks in the nucleon. The first so-called "strange" particles — K mesons with a mass of about 500 MeV — were observed in cosmic rays in the same period. They were followed by the first strange baryons given the name hyperons, such as λ^0, Σ^+ and Ξ^- (Okun, 2012). They were known as strange because these particles were created repeatedly and rapidly (through the strong interaction) but then decayed moderately to strongly interacting particles by the weak interaction. The doublets K^+ and K^0 were discovered with positive strangeness and the corresponding doublets antiparticles K^- and K^0 with negative strangeness. Anti$K$ were always created together alongside K mesons in any collisions of non-strange particles, be it mesons or with hyperons. This is to ensure that total strangeness was conserved (Borisovich, 2012).

The possible mechanism processes involved in multi-strange baryon production are highlighted in the next section.

2.2.1 Boson Gluon fusion

The production of strange quark can also be seen in boson-gluon fusion (BGF) in Figure 2.1. It is a process where gluon from proton couples with photon emitted via a virtual strange anti-strange quark (Ziegler, 2002). The production of light quarks in deep inelastic scattering is taken into account as it contributes to high cross sections. Apart from that, light quarks can be produced from the decaying of heavier quarks which are

in the higher generations, but due to small cross-section of strange quark being produced, usually, this decaying method is neglected.

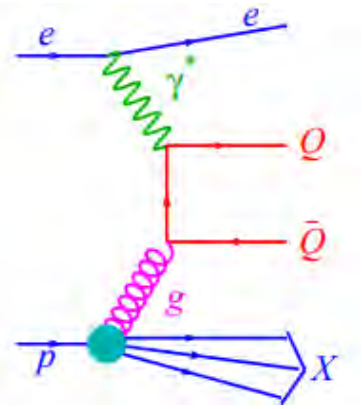

Figure 2.1: Boson gluon fusion (Zur Nedden, 2009).

2.2.2 Fragmentation

Other than that, this light quark could also come from fragmentation process. See Figure 2.2. During this process, the strange quarks happens to appear, which means the quarks are not straightforwardly involved in hard scattering, but it come out from gluon splitting in parton shower. The colourless hadrons due to changes in quarks and gluons at perturbative region of QCD must be simulated by fragmentation models, as it is not calculable. Lund string model is a successful model that describes this process. One of the simulation programs that help described such process is JETSET Monte Carlo. The program is based on Lund string model where the production of meson can be designed to begin from the initial quark, q_0. A new duo of $q_1\bar{q}_1$ may be formed, creating a new meson $q_0\bar{q}_1$ and leaves the other q_1 behind. This quantum mechanical tunnelling approach from Lund model was generated so that the duo $q_i\bar{q}_i$ led to the string separation. The concept is that both generated quarks are being produced at the equal point though it tunnels into the allowed region within a certain range. The iteration keeps on following for the next fragmentations.

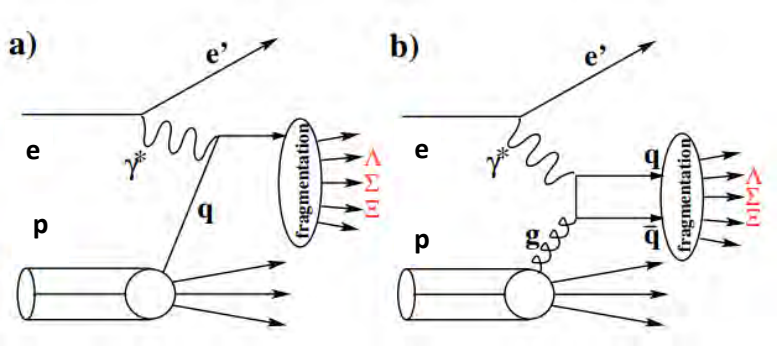

Figure 2.2: The origin of strange quarks in DIS (a) a quark, q, that receives a large momentum transfer in the proton (b) a quark-antiquark pair, $q\bar{q}$ appear from BGF process (Ziegler, 2002).

2.2.3 Excitation of flavour

The production of strange quark can be described by giving such example that quarks inside hadrons are held strongly by the carrier, gluons. Flavour excitation as in Figure 2.3 is a process where gluon inside the proton could transform into quark-antiquark pairs, and therefore a "sea" of quarks is present inside the hadron. Having a short period, depending on $\Delta\tau \sim \frac{\hbar}{m_q}$ usually most of light quark-antiquark will be emitted in the sea as pairs. As a result of fluctuations, the strange quarks might be struck, and a large momentum transfer received so that the pair cannot recombine to its original state. The phenomenon is known as flavour excitation.

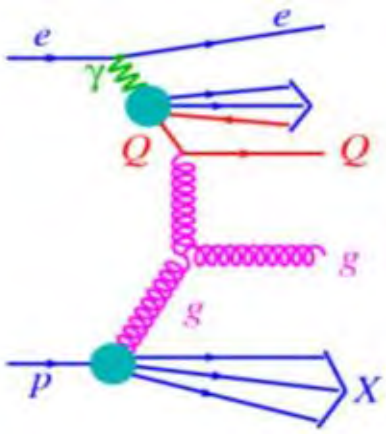

Figure 2.3: Flavour excitation where gluon transform into quark-antiquark pairs (Zur Nedden, 2009).

2.3 Deep Inelastic Scattering (DIS)

The aim of accelerating electrons to very large energies and allows it to combine near side of static proton as the existence of quarks is known as deep inelastic scattering. DIS studies are interesting because it can be used to extract the momentum distributions of the partons inside the proton, and elucidate the theory of strong interaction. Figure 2.4 shows Feynman diagram of DIS process. Different types of exchanged bosons in electron-proton collisions can be classified into two classes, namely Neutral Current (NC) and Charged Current (CC).

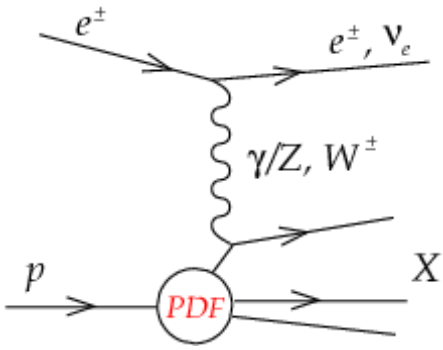

Figure 2.4: Deep Inelastic Scattering (Placakyte, 2011).

2.3.1 Neutral Current

Neutral Current DIS is a process which occur when the exchanged of mediator Z^0 or γ occur when an electron interacts with the proton. The large scattering angle allows the scattered electron to be detected. See Figure 2.5.

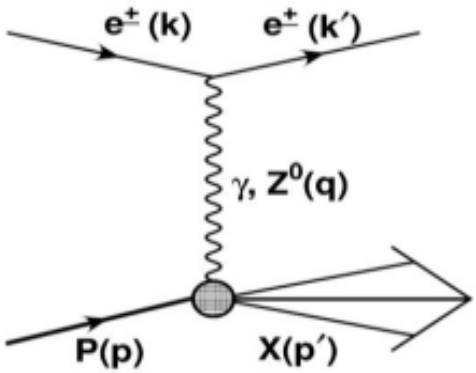

Figure 2.5: Neutral Current in DIS (Zolkapli, 2013).

2.3.2 Charged Current

Charge Current DIS occur when the exchanged of charged $W^{\pm}$ boson as mediator, where the electron transforms into a neutrino and escapes the detector, as in Figure 2.6.

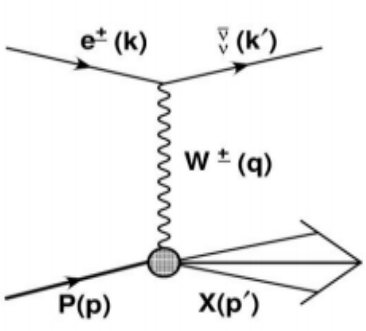

Figure 2.6: Charged Current in DIS (Zolkapli, 2013).

The equation for both NC and CC interactions can be written respectively as,

$$e + p \rightarrow e' + X \tag{2.1}$$

$$e^{+}\,(e^{-}) + p \rightarrow\ \bar{v}(v) + X \tag{2.2}$$

The ep scattering is classified by the photon virtuality, Q^2. There are two regimes, namely Deep Inelastic Scattering (DIS) and Photoproduction (PHP). Both events can be differentiated by $Q^2$where this variable is used to separate electron-proton into different regions of phase space. DIS belongs to a region with $Q^2 > 1$ GeV^2 while PHP is in the $Q^2 \ll 1$GeV^2 region.

2.4 HERA kinematics and phase space

Figure 2.7 discusses the interactions that took place at HERA and their kinematics. Most of HERA kinematic phase space occurs by the exchange of γ mediator. The four-momentum of incoming and scattered lepton are represented by $e(k)$ and $e'(k')$

respectively, while $p(P)$ and $p'(P')$ are the four-momentum of incoming and scattered proton. Q^2 is known as the squared of large 4-momentum-transfer at lepton vertex, which means exchanged boson virtuality. The center-of-mass energy squared, s is fixed for fixed beam energies and as for HERA, it has $\sqrt{318}$ GeV. In proton (p) system, W^2 is virtual photon (γ^*)'s center-of-mass, and H defines a set of all final state particles except for scattered electron and proton. ε is the Bjorken scaling variable of four-momentum of incoming proton.

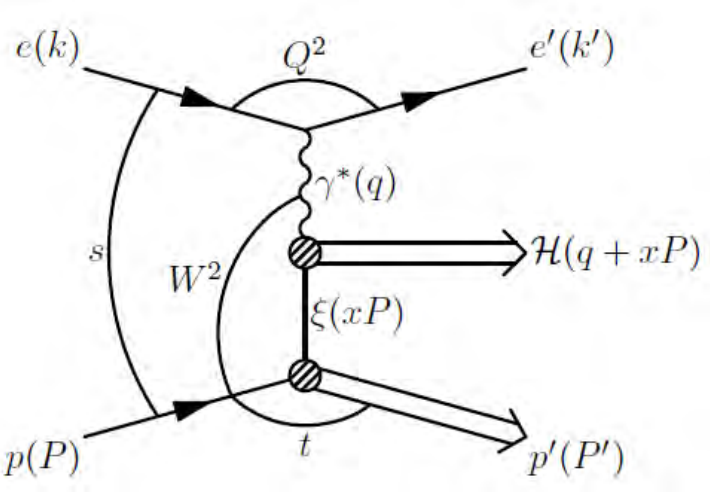

Figure 2.7: HERA kinematics (Guzik, 2011).

The scattering can be described using the Lorentz variables where these four variables are correlated to each other, and only 3 of them are independent. The variable x is known as Bjorken scaling variable, the partial longitudinally momentum of hit quark inside proton. While on the other hand, inelasticity y is the respective electron energy transfer to the proton, in rest frame of proton. The equation is as shown.

$$Q^2 = -q^2 = -(k - k')^2 \tag{2.3}$$

$$x = \frac{Q^2}{2p.q} \tag{2.4}$$

$$y = \frac{q.p}{k.p} \tag{2.5}$$

$$s = (k + p)^2 \tag{2.6}$$

As x and y are two independent variables, usually it is described as (x, Q^2) or (y, Q^2) for DIS inclusive kinematics.

2.5 Proton Structure

Figure 2.8 shows cross sections for both HERA I and HERA II in Neutral Current and Charged Current for H1 and ZEUS experiments. Neutral Current contains three structure functions, F_2, F_L and xF_3 which can be written in general form as,

$$\frac{d^2\sigma^{NC}(ep)}{dxdQ^2} = \frac{2\pi\alpha^2}{Q^4 x}[Y_+ F_2^{NC}(x, Q^2) - y^2 F_L^{NC}(x, Q^2) \mp Y_- xF_3^{NC}(x, Q^2)] \tag{2.7}$$

where $Y_\pm = 1 \pm (1 - y)^2$ and α, is the coupling constant of electromagnetic. At high Q^2, it is often to neglect the mass terms. For low Q^2, the structure functions F_2, F_L are given by γ^* exchange, while the parity-violating xF_3 arising from γZ^0 interference is being ignored (Cooper-Sarkar et al., 1998).

The Charge Current differential cross section carried by $W^\pm$ is

$$\frac{d^2\sigma^{CC}(ep)}{dxdQ^2} = \frac{G_F^2}{4\pi x} \frac{M_W^4}{(Q^2 + M_W^2)^2}[Y_+ F_2^{CC}(x, Q^2) - y^2 F_L^{CC}(x, Q^2) \mp Y_- xF_3^{CC}(x, Q^2)] \tag{2.8}$$

where $G_F = \frac{\pi\alpha}{\sqrt{2}\sin 2\theta_w M_W^2}$ is the Fermi coupling constant, M_W, is mass $W^\pm$, and θ_w, is Weinberg angle. At $Q^2 \ll M_W^2$ the CC cross section is mostly cover up to NC as $\frac{\sigma^{CC}}{\sigma^{NC}} \sim \frac{Q^4}{M_W^4}$.

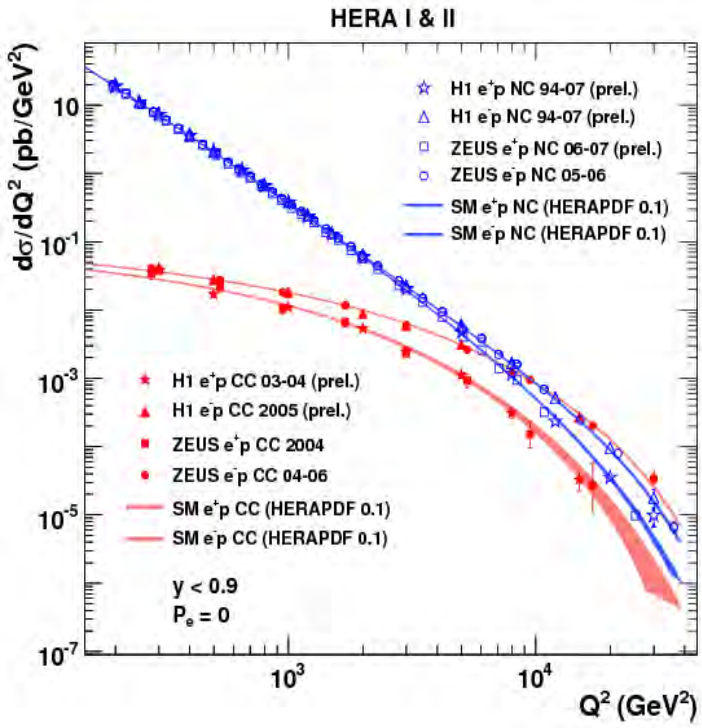

Figure 2.8: Charge Current (CC) and Neutral Current (NC) cross sections at DIS (Q^2dependence) as measured by ZEUS and H1 experiments (Zenaiev, 2017).

2.6 Quark Parton Model

Proposed by Feynman (Feynman, 1969), Quark Parton Model, QPM can be used to define the fraction of the proton's momentum carried by a parton (Chekanov et al., 2007). Parton is a set point-like object, which does not interact with each other. QPM can be understood well in *ep* scattering model as electron bounced back when hits on one of the partons. Thus, with a resolution that improves energy, DIS event gives a very clean way of probing the internal hadronic structure. In this case, it is deep as photon penetrates deeply into the proton, and due to the proton breaks up, it is known as inelastic. Figure 2.9 illustrates QPM.

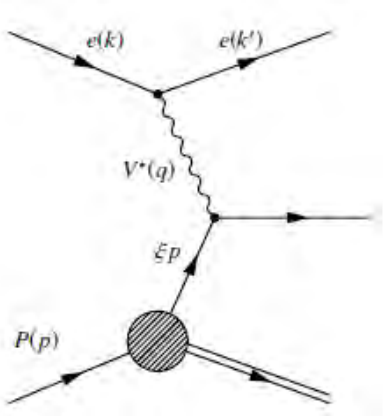

Figure 2.9: *ep* scattering in QPM (Zenaiev, 2017).

Neglecting the proton and parton masses, M and m respectively, a simple relation can be derived for the fractional of proton momentum transported by a parton,ξ using momentum conservation (Chekanov et al., 2007). It corresponds approximately to the Bjorken scaling variable, x (Bjorken, 1969).

$$0 \approx m^2 = (\xi p + q)^2 = \xi^2 M^2 + 2\xi p.q^2 = \frac{\xi Q^2}{x} - Q^2; \Rightarrow \xi = x \qquad (2.9)$$

The Bjorken variable x corresponds to the proton momentum carried by proton in hard scattering. In Quark Parton Model, both structure functions F_1 and F_2 are free from Q^2 but rely on x. The structure functions F_1 and F_2 is as follows:

$$F_1(x) = \frac{1}{2} \sum_i e_i^2 f_i(x) \qquad (2.10)$$

$$F_2(x) = \sum_i e_i^2 x f_i(x) \qquad (2.11)$$

where e_i is the charge of the i-th parton in units of the elementary charge and f_i is the parton distribution functions (Perez & Rizvi, 2013) that define all the possibility to

search a parton of the i-th with the momentum fraction in a proton. This has been proven at SLAC which conducts the experiments on DIS (Miller, 1972).

Anyhow, if there would be three valence quarks in the proton, then the sum of their fractional momenta would be equal to 1, as in the equation written,

$$\sum_i \int f_i(x) x dx = 1 \tag{2.12}$$

However, this quantity is near to 0.5, which is about 50% of the proton momentum carried by neutral particles, as proven experimentally (Eichten et al., 1973). It was found to be the gluons of QCD in the e^+e^-collisions at PETRA in the events with three hadronic jets (Brandelik et al., 1979). The gluon discovery established QCD in the way that it is the theory of strong interactions. Protons are filled with low x gluons, which can split into quark-antiquarks pairs, producing the sea quark.

2.7 Quantum Chromodynamics

Theoretically, inclusive deep inelastic lepton hadron scattering is an important process in perturbative quantum chromodynamics, QCD (Gell-Mann, 2015). In 1970s, a quantum theory of strong interactions was developed, where it includes a new gauge boson known as gluon. The "charge" of the strong force is called "colour", and each quark comes in three colours, namely red, green or blue. See Figure 2.10. Particularly, the colour changes are conserved in all physical process, where gluon transmitted this colour force.

Symmetrically, anti-coloured particles are being produced in conjunction of their corresponding coloured particles. It turns into effectively favourable to create new quark-antiquark duo in case they are far away against one another. These quark-

antiquark duos will after that, combine to produce the colourless particles such as mesons or hadrons.

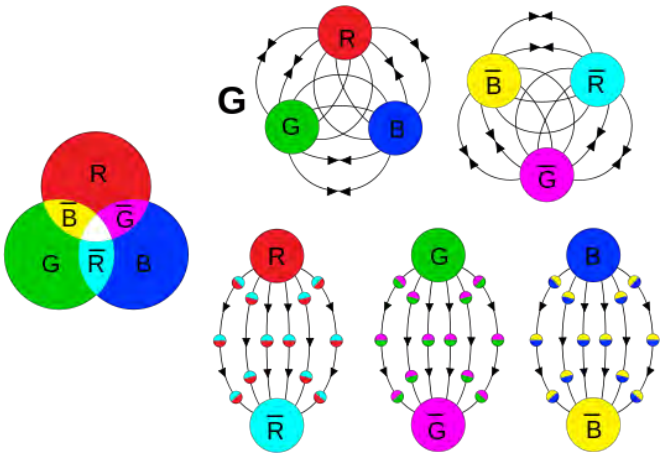

Figure 2.10: Colour fields for a quark, antiquark, and meson (Parker, 1994), (Mansfield, 2011).

QCD described that quarks are confining, by means quarks and gluons does not remain as confined matters. No strong force could fragment baryon into its constituents, as well as the quarks, even if it is the strongest. In lieu of breaking into any small pieces, the baryon produces extra particles through the self-interacting and quantum-mechanical dynamics of the gluons field that hook up the quarks inside the baryon, via hadronization process (Webber, 2000).

There are a few differences between quantum chromodynamics (QCD) and quantum electrodynamics, QED (Cohen-Tannoudji et al., 1989). Unlike photons, the gluons respond directly to one another in the presence and motion of colour charge as they can unbalance colour charge. Other than that, the gluons' reaction towards the colour charge are more effective compared with photons in QED when being deliberate by the coupling constant.

QCD can be categorised as non-abelian gauge theory (Altarelli & Wells, 2017) with quark-gluon interaction being simulated by the SU(3) group structure of the colour charges. The fermion wave-functions can be written as

$$\psi(x) \to \psi'(x) = e^{ig(t-\theta(x))}\psi(x), \tag{2.13}$$

where g is a constant defining the coupling strength while $t-\theta$ is the product of colour group generators alongside vector space-time phase functions in colour space. The group generators t^a satisfies

$$[t^a, t^b] = if^{abc}t^c, \tag{2.14}$$

where f^{abc} is the structure constant. The gluon field-strength tensor can be defined as

$$F_a^{\mu v} = \delta^\mu A_a^v - \delta^v A_a^\mu + g f_{abc} A_b^\mu A_c^v, \tag{2.15}$$

where $A_a (a = 1-8)$ are the gluon fields while the final term symbolizes synergy of gluons amidst themselves in a way that they too, lift colour charges. The quark spinor fields ψ_i revolutionize when triplets under SU(3) with $i = 1-3$ brimming the three colour indices. The Lagrangian density are as equation shown,

$$\mathcal{L}_{QCD} = \sum_f \psi_f^i (i\gamma_\mu D^\mu - m_f)_{ij} \psi_f^j - \frac{1}{4} F_a^{\mu v} F_{\mu v}^a \tag{2.16}$$

where m_f are mass parameters, the covariant derivative D_{ij}^μ is

$$D_{ij}^\mu = \delta_{ij}\delta^\mu + ig(t^a)_{ij} A_a^\mu \tag{2.17}$$

and $(t^a)_{ij}$ are 3 x 3 Hermitian matrices, that the significant triplets portrayal of SU(3) are $(\lambda^a)_{ij}/2,$ where Gell-Mann matrices is denoted by λ_a.

The same coupling constant g couples the gluon fields to themselves in $F_a^{\mu v}$, with gluon to the quark fields covariant derivative (D_{ij}^{μ}). QCD is the strong force quanta – the spin 1 massless gluons – carries charge colour and hence couple with another gluon, but in QED the photon does not couple with another photon.

CHAPTER 3: EXPERIMENTAL CONDITIONS

In this chapter, a brief explanation about the HERA collider built at DESY and some other experiments were introduced. The ZEUS detector and some other important components were in this chapter. The trigger system used was also included.

3.1 The HERA collider

The Hadron-Elektron-Ring-Anlage, HERA ring accelerator at the DESY laboratory in Hamburg is to date the world's only lepton-hadron collider with the tunnel circumference of 6.4 km and built about 25 m below the ground level. The construction finished in 1987, when later on the accelerator, was installed in 1990. October 1991 had been observed to be the first collisions recorded. A center-of-mass energy of $\sqrt{s} = 318$ GeV (300 GeV until 1998) provided by HERA, which is higher than in the previous fixed-target DIS experiments. The two different rings were used to accelerates electrons and protons to the final energies of 27.5 GeV and 920 GeV (820 GeV in HERA I) (Antonelli, 2009). Figure 3.1 shows the HERA ring.

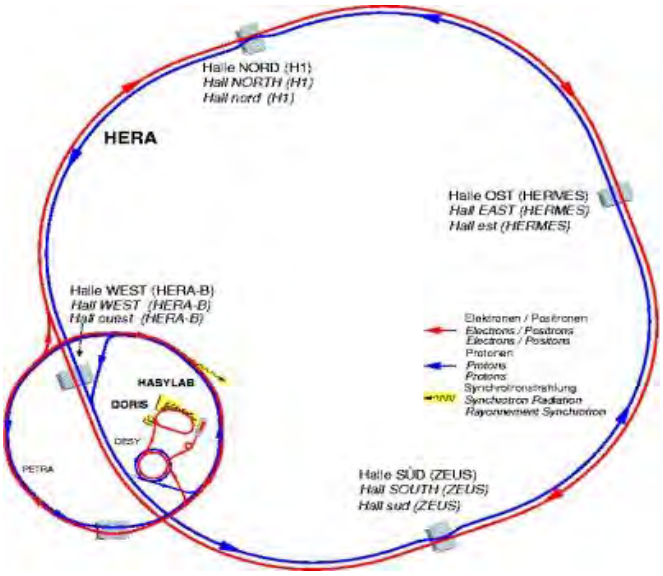

Figure 3.1: The HERA accelerator together with injection system PETRA (Verena Schonberg, 2006).

Both beams of electron and proton were kept in 180 bunches, where each bunch crossing rate was approximately about 10 MHz. The two general purpose colliders, ZEUS and H1 detectors were placed at North and South halls respectively, wherein these both regions the collisions happened. These two operated over 16 years of HERA operation.

Other than that, HERMES and HERA-B were another two additional experiments found in HERA, constructed in purpose to operate the fixed target condition. In 1994 up until 2007, HERMES experiment studies the spin effects in lepton-nucleon interactions by using a polarised nuclear target (Baumgarten et al., 2003). Meanwhile, HERA-B operated between 1998 until 2003 (Zur Nedden & HERA B Collaboration, 2004) was invented to understand *B*-meson physics as well as the nuclear effects inside proton-beam halo near a nuclear wire target interaction. The main components of the ZEUS detector are briefly described below. A description of the H1 detector and its main sub-detectors can be found elsewhere (Abt, et al., 1997; Andrieu et al., 1993; Appuhn et al., 1997; Pitzl et al., 2000).

3.2 The ZEUS detector

A detailed description of the ZEUS detector can be found elsewhere (ZEUS collaboration & Holm U, 1993; Derrick et al., 1992). Zeus is a multipurpose detector weighted 3600 tons with 12 m x 10 m x 19 m dimensions (Hilton, 1999). Figure 3.2 shows the detector. The discovery in high energy physics world is affected for the adventure in more and higher energies, that let us dig into ever more deeply inside the admirable structure of the particles. Of course, by having higher energies increased the multiplicity of particles. The purpose of this detector is to discover the energies upon extreme precision, directions and nature of single particles and jets produced in the collisions.

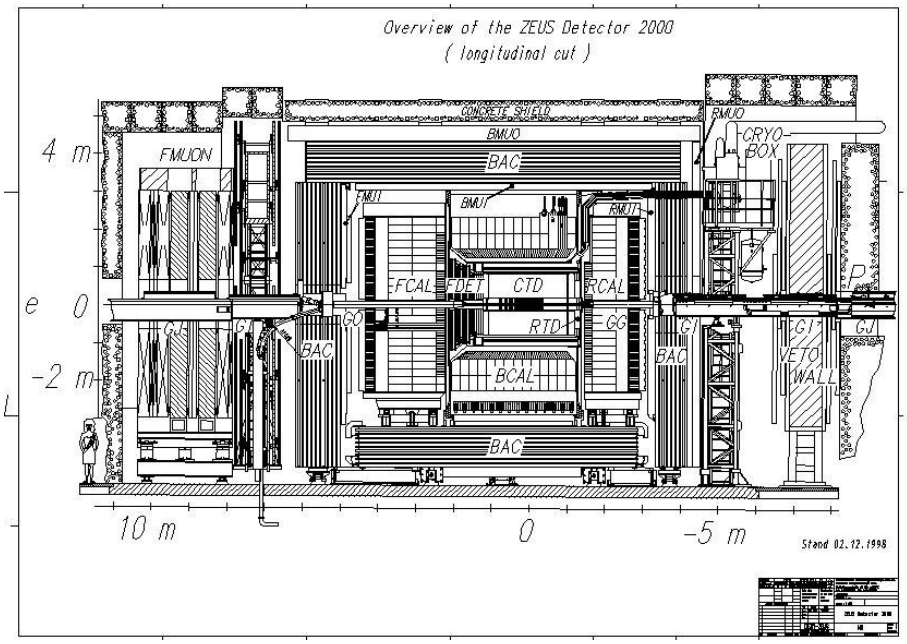

Figure 3.2: The ZEUS detector (Polini, 2007).

3.2.1 Central Tracking Detector

The CTD was built in a shape of cylindrical wire drift chamber that contained 72 cylindrical drift chamber layers, with 9 super layers (SL). The SL is divided into five axial and four stereo cells with ($\pm 5°$), each has eight layers of sense wires. See Figure 3.3. This component ascertains the trajectory extent of charged particles.

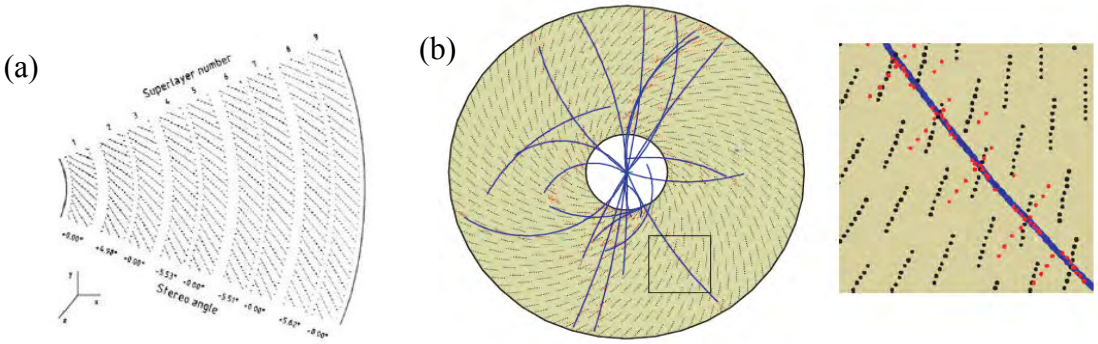

Figure 3.3: The Central Tracking Detector. (a) The wire arrangement in one octant in xy view. (b) The event displays from ZEUS CTD, displaying sense wires with tracks being reconstructed. (Ziegler, 2002).

CTD has a magnetic field of 1.43 T; perpendicularly to the electric field afford with a light superconducting solenoid around the tracking detector. The drift cells are tilted by 45° to the radial direction, allowing aligned tracks coming from the interaction point to lie across slightly at one cell in SL. Inside the CTD, there are several mixtures of gaseous, such as argon (Ar), carbon dioxide (CO_2), and ethane (C_2H_6) which functions as ionisation gas for the charged particles that pass through it. The charged particles can be reconstructed within an angular range of $15° < \theta < 164°$. The ionised electrons accelerate along the way in a uniform electric field of a cell to the sense wires. A "hit in SL" is defined when the electric pulse is induced in the sense wire by ionisation, and the spatial coordinates of the hit of the cell are calculated by time and pulse height. The transverse momentum of the full-length track's resolution is $\sigma(P_T)/\ P_T = \sqrt{\left(0.0058_{P_T}\right)^2} + \sqrt{(0.0016)^2}$ (P_T is in GeV). Good acceptance is in the region of $-1.75 < \eta < 1.75$.

The description about tracks reconstruction and secondary vertices can be found elsewhere (Hall-Wilton et al., 1999). The tracks reconstruction by CTD hits only is crucial because the mixed use of CTD and other tracking detectors needs a pleasant ability and understanding of the corresponding alignments, and multiple scattering at the components border that is not specified.

3.2.2 Calorimeter

Uranium scintillator calorimeter, CAL is the heart in ZEUS detector. It is used to reconstructs the energy, direction of particle showers, and the particle's position, to identify the reconstructed objects, to determine the energy deposited in calorimeter cells, and to search the jets by clustering the cells. See Figure 3.4.

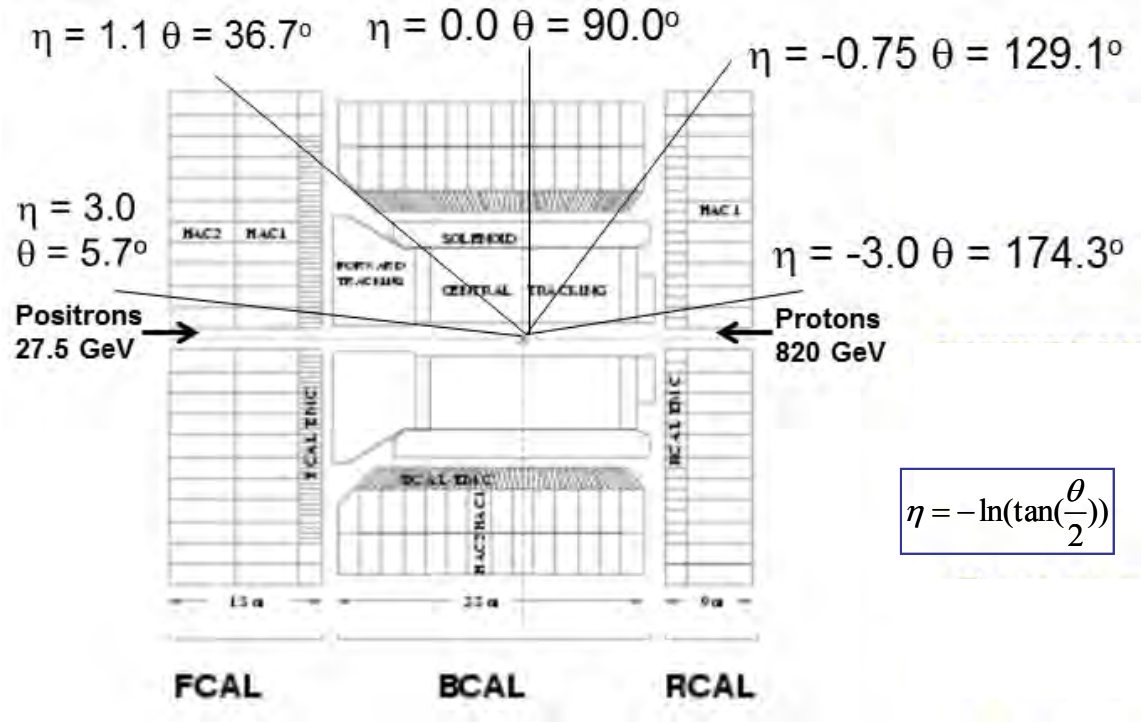

Figure 3.4: ZEUS calorimeter structure (ZEUS Collaboration, 2008).

CAL contained plates of depleted uranium interleaved with plastic scintillator in order to attain compensation and the excellent achievable energy resolution in hadrons. Once the particle enters the calorimeter, it loses most of its energy via collisions in the high-density material which then produces a shower of particles in the sandwich structure. The scintillator tiles form towers which are read out via wave length shifter bars, light guides, and photomultipliers (ZEUS collaboration & Holm, 1993). A tiny light signal is produced when the electrically charged particles traversed the scintillator plates. It is directly equivalent at the energy of particle and therefore, as the particle's energy boost, the light signal increases.

Interaction point in ZEUS experiment is situated in the calorimeter. By stacking the modules next to each other, the construction is possible. The blue scintillator light is absorbed in wavelength shifting material and re-emitted as green light with the help of photomultiplier.

The calorimeter is segmented longitudinally into electromagnetic and one or two hadronic sections. Typical tower sizes are 5 cm x 20 cm in the electromagnetic section and 20 cm x 20 cm in the hadronic section. The calorimeter is divided into a forward (FCAL), a barrel (BCAL), and a rear part (RCAL) with 7, 5 and 4 absorption lengths, respectively (ZEUS collaboration & Holm, 1993). Three parts of CAL covering polar angles are as follows,

- the FCAL, from $2.2° < \theta < 39.9°$ consisting 23 modules,
- the BCAL, from $36.7° < \theta < 129.1°$ consisting 32 modules, and
- the RCAL, from $128.1° < \theta < 176.5°$ consisting 23 modules

An active area in the forward direction which is the photon beam direction, begins at 60 $mrad$. The solid angle coverage corresponds to 99.8% in the forward hemisphere and 99.5% in the backward hemisphere (ZEUS collaboration & Holm, 1993).

The high-resolution calorimeter is encircled with a backing calorimeter that calculates the energy of delayed showering particles. The backing calorimeter acts as absorber the iron plates that create the magnet yoke (ZEUS collaboration & Holm, 1993) . Aluminium tubes conducted in proportional mode are used for readout (Elliot & Teresa, 1998). The ratio of electromagnetic particles energy response to the hadronic particles energy response is near to one in the calorimeter. Resolution is defined as $\frac{\sigma E}{E} = \frac{0.18}{\sqrt{E}}$ for electrons and $\frac{\sigma E}{E} = \frac{0.35}{\sqrt{E}}$ for hadrons, where ZEUS detector has the best resolution of $\frac{e}{h} = 1.00 \pm 0.05$.

Identification of particles is from the deposited signal in calorimeter. For example, leptons and photons lose their energy as soon as they enter a calorimeter via electromagnetic interactions, while muon only lost some small fraction. Hadrons such as protons and pions lose their energy through the strong and electromagnetic interactions, which needs more material to be absorbed.

3.2.3 Micro vertex detector

During the break in year 2000-2001, a silicon-strip vertex device is installed. This important sub detector was installed with the purpose of improving the space resolution of tracks in the vicinity of the interaction point. Divided into two independent components, it is known as barrel micro vertex detector (BMVD) and forward micro vertex detector (FMVD).

About 600 silicon-strips modules were used to build BMVD, which were grouped in three cylindrical layers around the beampipe as seen in Figure 3.5. The double-sided modules with strips on the opposite side sensors were perpendicular, so that $r\phi$ and rz position hit can be measured. The polar angle that can be covered by BMVD is around $30° < \theta < 150°$. A single hit has a space resolution about $24\ \mu$m and the two-track separation resolution was $120\ \mu$m. Organised in four forward wheels, FMVD consists of 112 silicon-strip wedge shaped sensors. Its polar angle covers in the range of $\theta > 7°$.

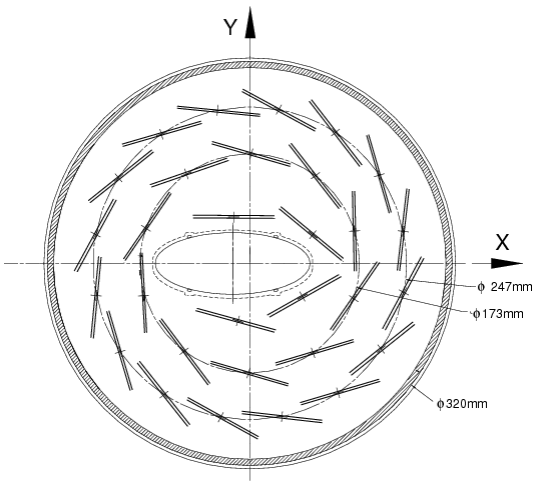

Figure 3.5: Cross section of BMVD in XY plane (Korcsak-Gorzo, 2007).

3.2.4 Luminosity

The luminosity, $\mathcal{L}$ measurements has been described in detailed that are available elsewhere (Adamczyk et al., 2014). It is the amount of process over the cross section of some specific process, given by $\mathcal{L} = \frac{R}{\sigma}$ measured in pb^{-1} / year, where $1\,\mathrm{pb} = 10^{-40}\mathrm{m}^{-2}$. The amount of high energy photons from the bremsstrahlung process, $ep \rightarrow ep\gamma$ is used to measure the luminosity. This involved QED process, where it has high rate and cross section can be easily calculated. The first phase of HERA has recorded that a photon calorimeter used to measure the rate of bremsstrahlung photons. It is positioned in the tunnel for about $100\,\mathrm{m}$ downstream where the electron and proton beams were separated. Bremsstrahlung photons moved through a straight vacuum chamber and an aluminium exit window before entering the photon calorimeter.

In 1992 to 2000, the ep HERA collider acquired its first phase of progression, known as "HERA I". Both colliders, H1 and ZEUS recorded integrated luminosities of approximately $120\,pb^{-1}$of $e^{+}p$ and $15\,pb^{-1}$ of $e^{-}p$ collisions (Andruszków et al., 2001).

The long shutdown has been used to upgrade the collider and detector machine, to gain the luminosity four times, and also to afford longitudinally polarised lepton beams to experiments. By increasing luminosity, the beam is stronger on focusing and slightly larger beam currents. With HERA-II as the new phase, ZEUS and H1 experiments reported roughly about $200\,pb^{-1}$ of $e^{+}p$ and $200\,pb^{-1}$ of $e^{-}p$. Figure 3.6 shows the integrated luminosity successfully recorded by ZEUS detector.

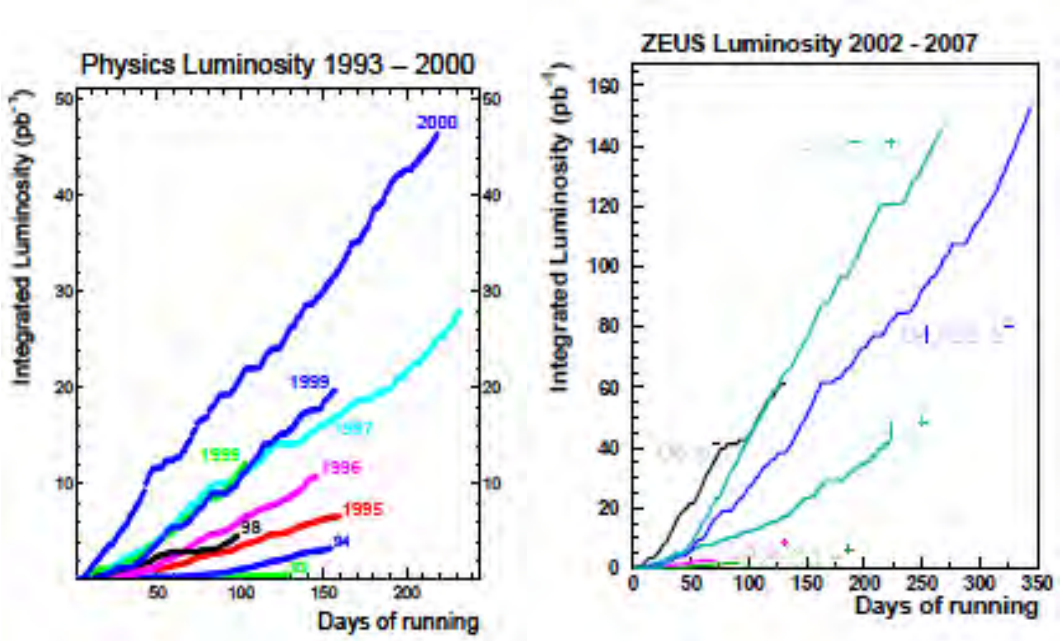

Figure 3.6: The ZEUS luminosity. ZEUS detector recorded the luminosity in different periods of time when a long shutdown in year 2000-2001 (Klein, 2008).

The final three months of HERA operation has shown that data for low energy run (LER) of 460 GeV and middle energy run (MER) of 575 GeV were taken, with approximately 13 pb^{-1} and 7 pb^{-1} recorded data, respectively. The main reason LER and MER data took place was because of the calculation of the longitudinal proton structure function, F_L.

After a great success data taking period, the lepton-hadron colliders end the operations in the middle of year 2007. Up until today, with almost 450 physicists through the international collaborators, the data taking continues to probe the proton structure and study the HERA physic unique.

3.2.5 Small rear tracking detector

Small rear tracking detector, SRTD installed in the detector contained sensitively segmented scintillator strips. With the aim of improving the electron and other charged particle measurement in the small-angle area about the beam pipe direction (Bamberger et al., 1997). This allows an accurate reconstruction of kinematic variables in the low x and Q^2 region with the resolution of $\sigma_{x,y} = 2.7$ mm. Figure 3.7 shows SRTD in rear direction. In HERA kinematic region, the angle of scattered energy θ does not cover more than $165°$. Hence, the precision of electron position is not well calculated. It is important to have precise electron impact position in consequence of kinematic variables reconstruction. Not only that, SRTD affords fast timing at the first-level trigger (FLT) to reject backgrounds outside the point of interaction.

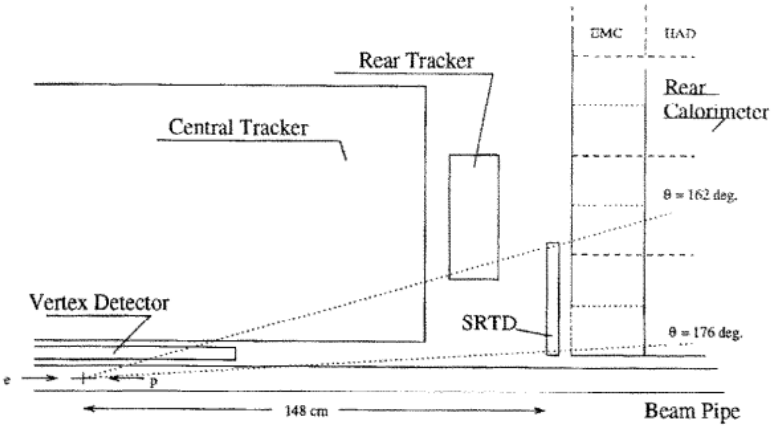

Figure 3.7: ZEUS detector in rear direction view (Bamberger, et al., 1997).

3.3 The trigger system

The purpose of online trigger system is to detect intriguing physics events such as DIS and PHP. These events provide an understanding of interesting HERA physics together with suppress background-induced events thoroughly. ZEUS experiment had three-level triggering system, namely First Level Trigger, FLT, Second Level Trigger, SLT, and Third Level Trigger, TLT.

FLT (Smith et al., 1995; Heath et al., 1992) is a hardware trigger system in individual sub-detector which functioned to send information signal to Global First Level Trigger (GFLT) for trigger decision. GFLT also used to synchronise sub-detectors with HERA bunch-crossing clock to produce fast decision to eliminate beam gas events.

SLT received the decision events from FLT, and then based on software trigger it processed this information which were used on charged particle tracks, the interaction vertex, calorimeter timing cuts, and global energy sums (Quadt et al., 1999).

TLT (Bhadra et al., 1989) processed events that were passed by SLT that accept the choice according on global information from an event. Events which pass this stage are recorded to tape and available for offline reconstruction. It is a commodity processor farm where it refined electron and jet finding and advanced physics filters are available here. Figure 3.8 shows a dataflow through the trigger system. Figure 3.8 is the ZEUS trigger system.

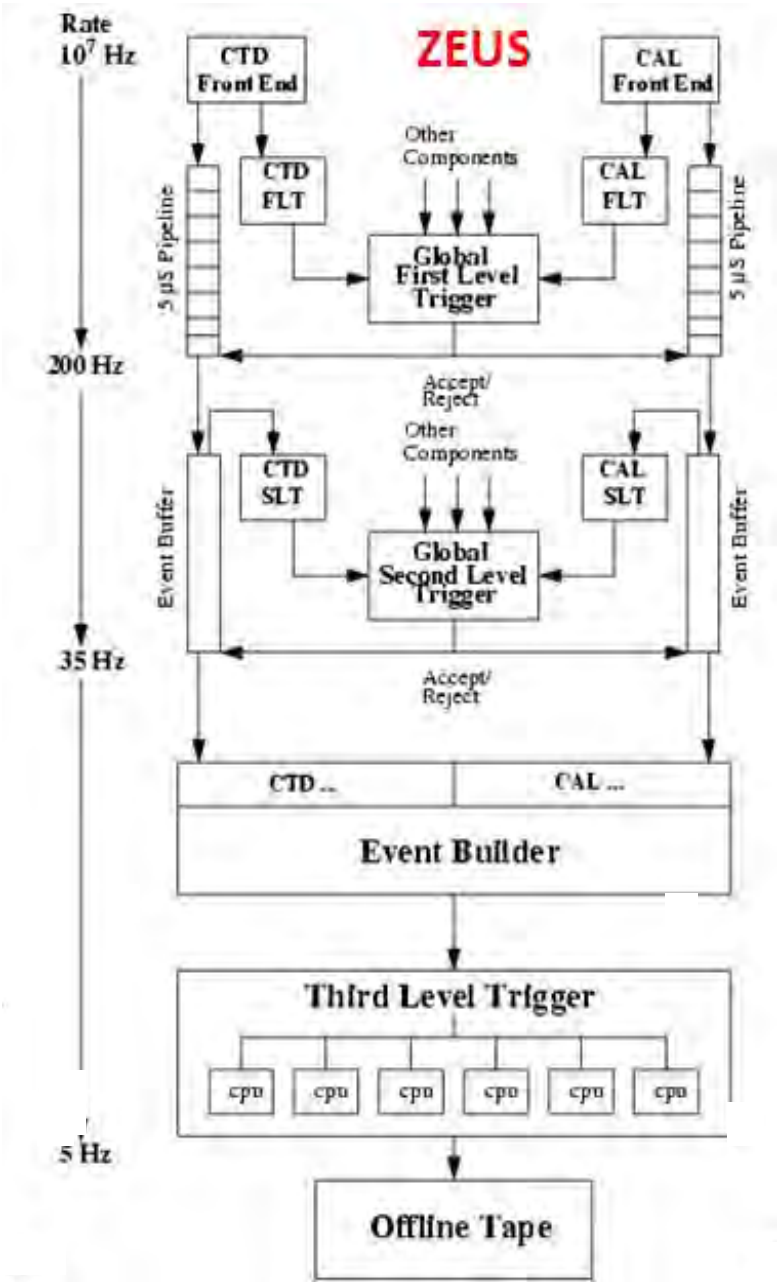

Figure 3.8: ZEUS trigger chain with rates at each trigger level (Lajoie, 2009).

CHAPTER 4: OFFLINE ANALYSIS

In this chapter, it is all about events. Event simulation, event selection, and event reconstruction were described. Apart from that, the reconstruction of tracks, vertexes, and electron and hadronic were also included.

4.1 Event Simulation

In high energy physics, Monte Carlo simulations is a very important tool that are used to calculate the efficiency of interested events, estimating the rate of background, evaluating the kinematic reconstruction correctness, as well as studying the calculated cross section in the entire kinematic range.

By having MC event samples, it can be used to determine the detector response, adjusting the correct data to the hadron level, along with computing predictions to be distinguished with the real data analysis (ZEUS Collaboration, 2003).

Every detector has their respective response to the underlying physics processes. The cross sections cannot be perfectly measured if the acceptance level is limited. Therefore, to model the detector response, the commonly used MC simulations (Metropolis & Ulam, 1949) have two different stages, namely underlying physics simulations and detector response simulations. Brief descriptions about these two stages were described in the next section.

4.1.1 Underlying physics simulation

It is carried out by certain MC generators, that generates a set of entire particles at the stable final states. The underlying physics processes includes simulation of hard scattering, hadronisation, parton showers, and particle decays. ARIADNE (Lönnblad, 1992), RAPGAP (Jung, 1995), and PHYTIA (Sjöstrand et al., 2006) are some of event generators that are widely used in ZEUS experiment.

4.1.2 Detector response simulation

In this phase, the generated final-state particles move onward over a detector simulation. MOZART (Haas, 1992) is a program, originally based on GEANT 3.21 (Allison et al., 1987) was used to perform the ZEUS detector simulation. Then, simulated events were passed over the trigger system as well as ZEUS Physics Reconstruction program, ZEPHYR. Lastly, MC events were recorded as a regular data in the tape, then processed by exactly the identical reconstruction and selection algorithms. The algorithm may also contain extra information on generated or true information. Figure 4.1 shows the ZEUS event analysis.

Overlying Routine for Ntuple Generation, or better known as ORANGE is a software library that executes a user-selected subset of analysis routines (Bindi, 2008). ZSMSM software package can be turned on by using suitable control card. It was made up of various blocks of variables, the Ntuple are described in the documentation which appears with each released (Zolkapli, 2013). Some blocks used in this analysis were FMCKIN2, V0lite, Tracking, etc.

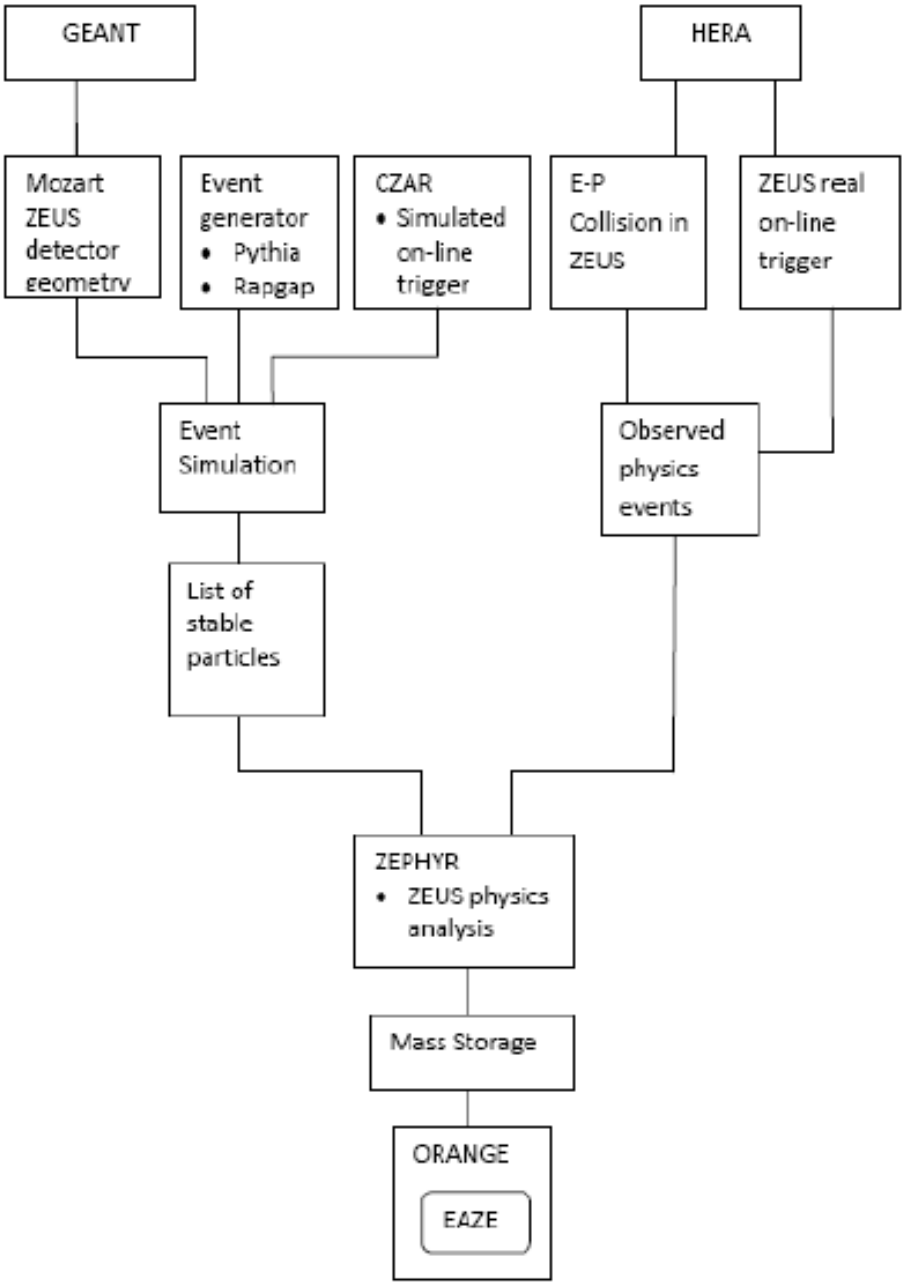

Figure 4.1: The ZEUS event analysis.

4.2 Event Selection

Two steps were involved during the events selection, namely online selection and offline selection. Online selection is the actual time for the events where the resolution reached cannot be undo, thus data will be vanished forever. Meanwhile, offline selection took place when decision can still be considered and can be processed.

4.2.1 Online Selection

At online event selection, the detector performed to pick the physics events interests, where the only information available is tracking and coarse calorimeter. Events chosen depends on energy deposits inside CAL to be constant among an isolated positron. On top of that, events consist of high transverse energy, E_T in conjunction with CTD track were also selected (ZEUS Collaboration, 2003).

During online selection too, there are some needs upon Conservation of Energy-Momentum, δ in order to choose the interested events. The timing fact from the calorimeter functioned to remove events that disagree in correspondence to the bunch-crossing time.

4.2.2 Offline Selection

It is a process where the interest events in the calorimeter were characterized by scattered electron or positron so that their kinematic variables can be determined. SINISTRA (Abramowicz et al., 1995) is an electron finder which functions to determine the best candidates of electron and the scattered electron.

4.3 Event Reconstruction

The same simulation program that was pre-owned by the ZEUS Monte Carlo was chosen to operate the reconstructed events. The kinematic variables Q^2, x and y can be reconstruct using these three methods below.

4.3.1 Electron method

Uses energy and scattering angle that coming from electron only, this method that can be calculated as follows:

$$Q^2_{\mathrm{el}} = 2E_e E_{e'}(1 + \cos\theta_e), \tag{4.1}$$

$$x_{\mathrm{el}} = \frac{Q^2_{\mathrm{el}}}{sy_{\mathrm{el}}}, \tag{4.2}$$

$$y_{\mathrm{el}} = 1 - \frac{E'_e}{2E_e}(1 - cos\theta_e), \tag{4.3}$$

where E_e is the incoming electron energy, $E_{e'}$ and θ_e are the energy and angle of the scattered electron respectively. Electron method is greatly affected by electron energy and position. It becomes optimal at low Q^2, due to ZEUS detector is more precise in the rare zone.

4.3.2 Jacquet-Blondel method

Depending on parameters of the hadronic final state, this approach has an advantage of using this method is it can be used if the scattered electron cannot be detected such as CC in DIS. Below is the kinematics described:

$$Q^2_{\mathrm{JB}} = \frac{P^2_{T\,\mathrm{had}}}{1-y_{\mathrm{JB}}}, \tag{4.4}$$

$$x_{\mathrm{JB}} = \frac{Q^2_{\mathrm{JB}}}{s y_{\mathrm{JB}}}, \tag{4.5}$$

$$y_{\mathrm{JB}} = \frac{\delta_{\mathrm{had}}}{2E_e}, \tag{4.6}$$

where $P_{T\ \mathrm{had}}$ and δ_{had} are given by

$$P_{T\ \mathrm{had}} = \sqrt{\sum_i (P^i_{x\,\mathrm{had}})^2 + (P^i_{y\,\mathrm{had}})^2}, \tag{4.7}$$

$$\delta_{\mathrm{had}} = \sum_i (E^i_{\mathrm{had}} - P^i_{z\mathrm{had}}), \tag{4.8}$$

where $\left(P^i_{x\,\mathrm{had}},\ P^i_{y\,\mathrm{had}},\ P^i_{z\,\mathrm{had}},\ E^i_{\mathrm{had}}\right)$ is the 4-momenta of every hadronic final state while the total goes to overall hadronic energy, not including the scattered electron. The scattered electron does not need to be detected in this procedure, therefore it can be practised at CC and PHP events, though it consists low Q^2 resolution in DIS events.

4.3.3 Double-Angle method

It is a combination from Electron method and Jacquet-Blondel method described above (Bentvelsen et al., 1992), (Hoeger, 1991). The kinematic variables are as in the relations.

$$Q^2_{\mathrm{DA}} = 4E_e^2 \frac{\cot(\frac{\theta_e}{2})}{\tan(\frac{\theta_e}{2}) + \tan(\frac{\theta_{\mathrm{had}}}{2})}, \tag{4.9}$$

$$x_{\mathrm{DA}} = \frac{Q^2_{\mathrm{DA}}}{s y_{\mathrm{DA}}}, \tag{4.10}$$

$$y_{\mathrm{DA}} = \frac{\tan(\frac{\theta_{\mathrm{had}}}{2})}{\tan(\frac{\theta_e}{2}) + \tan(\frac{\theta_{\mathrm{had}}}{2})}, \tag{4.11}$$

where hadronic angle θ_{had} is

$$\tan\left(\frac{\theta_{\mathrm{had}}}{2}\right) = \frac{\delta_{\mathrm{had}}}{P_{T_{\mathrm{had}}}} \tag{4.12}$$

The angular resolution in hadronic system is always preferred compared to electron method, but Q^2_{JB} and x_{JB} are worse than the scattered electron, Q^2_{el} and x_{el}.

4.4 Reconstruction of Tracks

Particle trajectories were reconstructed by the hits in the tracking detectors such as CTD, MVD, and STT. It is important to look into account all the error on the hit measurement, the multiple scattering occurred, and also the present of any dead material distribution inside the detector. The detector components such as CTD, CAL and SRTD are important in selecting the NC DIS events. CTD for example, measures point of the first vertex as well as track positron. CAL determines the energy of the scattered electron and hadronic final state. SRTD functions to locate the impact point of scattered positron. Ever since the detector upgrade, new improvement of track reconstruction was built. In ZEUS, Kalman filter algorithm (Kalman, 1960) and ZTT tracks (Lisovyi, 2011) were used.

4.4.1 Kalman Filter Algorithm

This filter is an iteratively procedure for reconstruction of tracks from the measured hits, works by building tracks from the furthermost layer or point of the tracking system directed toward the center. This algorithm makes the track to “trail the measurement” over the detector (Avery, 1992), which is different from another global approach where it fit all calculations to a single set of track parameters.

By all means, this algorithm used all the information and will not give any bad track parameters by increasing another calculation. For instance, adding hits will not cause in increasing ambiguity of the track parameters. It is difference from any track fitting methods as the program filters the track backwardly, such that the parameters on the further part of the track unsatisfactorily driven compared to the nearer part. Kalman filter allows tracks to be fitted in a separate portion, for example tracks can be used and fitted inside drift chambers before projecting into silicon detector alongside entire covariance matrix. This approach ensures the silicon hits can be added so that it does not need to do the entire fit again and thus make the fitting process much faster.

4.4.2 ZTT tracks

ZTT is the ZEUS software of track finding packages. It combines the information from CTD and MVD detectors, where there were two stages of track reconstructed, namely pattern recognition and refinement trajectory.

The first stage was done by VCTRACK package (Hartner, 1998). VCTRACK is a software FORTRAN package that was used in ZEUS experiment for vertex and track finding. This program helps to find the first vertex and following vertices of the interested events, apart from searching for the right tracks. For every track reconstructed, it needs to have CTD hits, even though other tracking detectors might exploit. In 9^{th} SL of CTD, the track density was low than the nearby interaction point. About three combination hits in CTD from the outer layer would result in the forming of tracking seeds. This seed was extrapolated inwardly, and any additional hits were gathered with increased in precision. To guide the trajectory, a large “virtual” hit was joined at the beam line. Subsequently a “road” of hits from the CTD through the MVD to the intersection point successfully formed, the least-squares of a track was fit by the chosen hits on the road in favour of finding out parameters of helix at the helix origin

(Zenaiev, 2017). Generally, tracking reconstruction at ZEUS experiment has hits in only sub-detector, namely CTD-only and MVD-only tracks.

The second stage, refinement trajectory was done by Kalman algorithm to enhance correctness of helix parameters in the area of the intersection point. The information for this second stage was taken from the fit output of pattern recognition. There were several steps involved in track fit; prediction, filtering and smoothing.

Global trajectory parameterization (Spiridonov, 2008) of tracks used in this experiment includes helix parameters (Hartner, 1998), which are defined at tracks closest approached to the z-axis. There are five helix parameters, as shown.

$$\tilde{x}^T = (\phi_H, \frac{Q}{R_H}, QD_H, z_H, \cot\theta), \tag{4.13}$$

where

ϕ_H =angle of xy-projection of track direction with the x-axis,

$\frac{Q}{R_H}$ = helix curvature signed by a particle charge, Q,

QD_H = signed minimal distance to Z-axis,

z_H = z-coordinate at point of closest approach,

$\cot\theta$ = cotangent of track w.r.t z-axis.

The ZEUS detector (ZEUS collaboration, 1993) coordinate system shown in Figure 4.2 is an orthogonal right-handed. The x-plane is pointing perpendicular to the beams in the direction of the centre of HERA collider, while y-plane directing perpendicularly upward to collider plane, while z-plane is in the proton direction, parallel into beam pipe. The beam point, where interaction occurs is the origin of this Cartesian coordinate system. The azimuthal angle, ϕ is determined with respect to x-axis in r-ϕ plane and the

polar angle, θ is often used to calculate the pseudorapidity, η which was defined as $\eta = -\ln(\tan\theta/2)$.

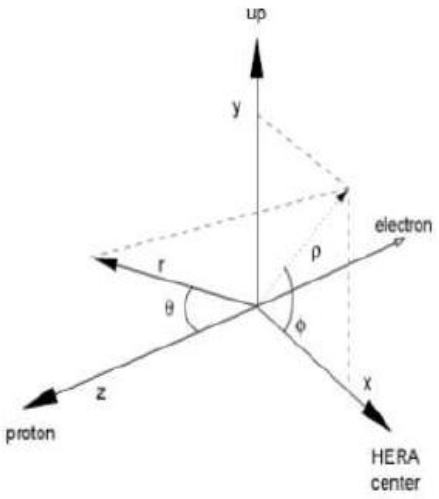

Figure 4.2: ZEUS coordinate system.

4.5 Vertex Reconstruction

Vertex means the spot where decays or interaction occurred. There were two main reasons of doing vertex in ZEUS experiment. The main reason was to determine the significance position of the beam point collision and also determine the right momenta track upon the particular point. Apart from that, reconstruction of vertices plays a role in estimating the probability of the tracks coming from the certain vertex. For instance, in event selection, the probability might be taken from vertex fit quality such as $\chi^2$of vertex fit. It is very important to make sure both beam point of collision and vertex of Ξ^- decay was identified correctly in the event. VCTRACK package did the vertex and track finding, where full description can be found elsewhere (Close, 2004).

The first vertex fit was determined to be as near as the averaged of beam point. The point where collisions happened is known as beam point (Mankel, 2006). The secondary vertex for neutral strange particle Λ^0 can be traced as it has distinctive signature.

Therefore, the ability to provide better tracking is crucial for their inspection. In ep collision, they were created abundantly (Boogert, 2003).

4.6 Electron and Hadronic Reconstruction

Scattered electron is crucial as it helps in differentiating the NC DIS events from the CC DIS events, because it leaves clear signature spot of undetected neutrino escapes. SINISTRA (Abramowicz et al., 1995) together with probabilistic EM (Kappes, 2001) were the main electron finders in this experiment.

ZEUS Unidentified Flying Objects, or better known as ZUFOS (Tuning, 2001) stored some info from the calorimeter and the tracking in order to gain accurate measurement of hadronic energy. The purpose of ZUFO was to stand for one final state particle. It is where the track momenta resolution given by $\frac{\sigma(p_T)}{p_T} = ap_T \oplus b \oplus cp_T$, gave more excellent energy for lower particle momenta and the resolution of the calorimeter was developed for higher particle energy $\frac{\sigma(E)}{E} \sim 1/E$. Calorimeter gives information for the neutral particles and the charged particles were given with information from the tracking, where the energy used were usually below 10 GeV.

CHAPTER 5: RECONSTRUCTION OF Ξ^-BARYON

In this chapter, the samples and luminosity used for both MC and HERA II data, the selections of cuts implemented on trigger, DIS, box and geometry are described. The Ξ^- and Λ identification are also being described here, including the matching analysis, optimization cuts, and some results and discussion on the analysis in MC and HERA II data.

5.1 MC and Data Samples

Different physical processes used different generators, depending on which they are likely most suited. The MC generator used in this analysis was Inclusive ARIADNE NC DIS at Low Q2 (Lönnblad, 1992), a simulation program of QCD cascades implementing the colour dipole model (CDM). ARIADNE simulates the production of inclusive light favours in DIS events.

ARIADNE gives perfect definition of the observed hadronic final state in inclusive DIS (Aaron et al., 2010) where simulated events were take place for the entire event generator. Note that ARIADNE was used only in studies which involved the light flavour background, such as detector resolutions and efficiencies.

An analysis (Libov, 2013) was done to evaluate tracking inefficiency for charged pions as a result of interactions in hadronic inside detector substantial and how good the MC simulation reproduced such interactions. Table 5.1 shows the full MC samples achieved by the ZEUS detector. The total number of events collected for HERA II was 268 million events. A summary of luminosity of the generated samples for each period for Monte Carlo is given in Table 5.2.

Table 5.1: Number of events for HERA II MC samples.

Run period	Beam	N_{ev}, 10^6
2003/2004	e^+p	31
2005	e^-p	87
2006	e^-p	34.7
2006/2007	e^+p	116

Table 5.2: Integrated luminosity MC samples for each year.

Run period	Beam	Integrated Luminosity, $\mathcal{L}(pb^{-1})$
2003/2004	e^+p	41
2005	e^-p	133
2006	e^-p	55
2006/2007	e^+p	142

Meanwhile, Table 5.3 is the data sample used in this work that was collected during 2003-2007 years in HERA II running periods. The total number of events was about 355 million events. The total luminosity collected by ZEUS detector with center of mass of 318 GeV was about 360 pb^{-1}as shown in Table 5.4.

Table 5.3: Number of events for HERA II real data samples.

Run period	**Beam**	$\mathbf{N_{ev}, 10^6}$
2003	e^+p	3.7
2004	e^+p	47.5
2005	e^-p	132.2
2006	e^-p	44.2
2006	e^+p	86.6
2007	e^+p	41.2

Table 5.4: Integrated luminosity data samples for each year.

Run period	**Beam**	**Integrated Luminosity, $\mathcal{L}(pb^{-1})$**
2003/2004	e^+p	36
2005	e^-p	134
2006	e^-p	53
2006/2007	e^+p	137

5.2 Trigger Selection

FLT helps in triggering with an output rate below 1 kHz. In FLT, a very short time is needed for the decision to be made, which is to select events originating from ep collision. This also includes general background rejection and reconstructed of the scattered electron. FLT requires at least a single of the following being satisfied (Ziegler, 2002):

- total energy in the electromagnetic sections of the CAL needs to be greater than 15 GeV.
- an isolated electron was found in FCAL or BCAL; in addition, a track had been found in the CTD
- an isolated electron was identified in RCAL; in addition, more than 2GeV had to be found in the EMC section of RCAL
- total transverse energy was greater than 18 GeV
- total transverse energy was greater than 12 GeV and at least one track must have been found in the CTD
- a signal in SRTD and a track was found

A programmable transputer network builds the SLT. The events that passed FLT were sent to the SLT. More practical programs can be created such as algorithms involving cuts and applying some selections to remove noise events. It is important to keep the rate under 100 Hz. At SLT, at least two requirements had to be fulfilled (Ziegler, 2002):

- more than 2.5 GeV in the EMC of RCAL or BCAL or more than 10 GeV in hadronic section
- $E - P_Z + 2 * E_{lumi,\gamma} > 29$ GeV, where $E - P_Z = \Sigma E_i(1 - cos\theta_i)$, E_i is the energy of the ith calorimeter cell, θ_i is the polar angle and the sum runs over all

cells and $E_{lumi,\gamma}$ is the energy deposited in the photon calorimeter of the luminosity monitor system.

All final events were then passed through TLT, which discussed in the next section. Events passed the TLT were recorded to tape, alongside ready for use for offline reconstruction in the study.

5.3 DIS Selection

The DIS selection with both beams $e^- p$ and $e^+ p$ were taken into account. The DIS kinematic region was restricted for photon virtuality in the range of $20 < {Q^2}_{el} < 200$ GeV, Bjorken scaling variable $3.10^{-4} < x_{el} < 2.10^{-2}$ and elasticity $y_{el} < 0.7$. The selected events for DIS third level trigger required DIS03, which means (Ziegler, 2002):

- one of the available electron finders found a positron with an energy above 4 GeV
- $E - P_Z > 30$ GeV

The following selections are required to ensure good DIS events as written in the published paper attached (Abramowicz et al., 2016):

- $E_{e\prime} > 10$ GeV, where the purpose was to ensure high efficiency of SINISTRA and to reject all the PHP background having fake scattered positron.
- $20 < {Q^2}_{\text{el}} < 200$ GeV, where it is DIS phase space.
- $3.10^{-4} < x_{\text{el}} < 2.10^{-2}$, where it has best resolution at low Q^2
- $y_{el} < 0.7$, where it removes events with low energy forward going photons which are misidentified as leptons.
- $y_{\text{JB}} > 0.04$, reject events with poorly reconstructed hadronic system and ensures sufficient accuracy for double-angle method.

- $41 < E - P_Z < 60$ GeV, the lower cut reduces undetected scattered electron while the latter cut rejected cosmic ray events particles.
- $|\mathrm{Z_{vertex}}| < 50$ cm, where it is the Z coordinate of a primary vertex position.

5.4 Box Cut and Geometry Cut

In general, box cut means to get certain geometric position of the scattered electron, and to ensure it reaches proper part of the calorimeter. It is important for comparing data to MC for extraction of cross section purpose.

Box cut applied to the scattered electron position on the RCAL surface outside of a rectangle around the beampipe. It is to reject events where the electron went through edges of the CAL, with $|x| > 13$ cm and $|y| > 13$ cm. The offline box cut of SINISTRA are stricter compared to the online, due to a difference between online and offline version of SINISTRA.

Geometry cut is to remove regions of the calorimeter, where the scattered electron reconstructed is low as well as difficult to simulate because of their geometrical complexity, such as (Zenaiev, 2017):

- electrons in the regions of cracks between the RCAL, BCAL and FCAL, super cracks in HERA II, were rejected, $164 < z < 174$ cm, $-104 < z < -98.5$ cm,
- electrons in the overlap region between the RCAL and BCAL $\left(\sqrt{x^2 + y^2}\right) > 175$ cm on the RCAL surface,
- the "chimney" cut, to remove a region in the RCAL where cooling tubes and supply cables for the solenoid were mounted as $|x| < 12$ cm if $y > 80$ cm.
- the region of gaps between halves of the RCAL were removed, $6.5 < x < 12$ cm if $y > 0$ and $-14 < x < -8.5$ cm if $y < 0$.

5.5 Ξ^- Selection

Having two strange quarks and a down quark, Ξ^- and their charge conjugated Ξ^+ is a weakly decaying particle with $\tau = 1.64 \pm 0.02$ s. The selected main decay for this analysis is $\Xi^- \rightarrow \Lambda + \pi^-$ with $B_r = 99.89 \pm 0.04$ % (Patrignani, 2016). The reconstruction of Ξ^- were based on charged detection of the tracks found in CTD when reconstructing displaced tertiary vertices. Since Ξ^- has two daughters Λ and π^-, the reconstruction also needs to consider the decay channel of Λ which decays into a proton and a pion. Table 5.5 below summarise decay chains for this analysis.

Table 5.5: Decay channel of Ξ^- and Λ^0.

	Contents	**Mass/GeV**	B_r	$\tau/10^{-10}$s	$c\tau$/cm
$\Xi^- \rightarrow \Lambda + \pi^-$ $\bar{\Xi}^+ \rightarrow \bar{\Lambda} + \pi^+$	dss	1.321±0.07	99.89±0.04	1.64 ± 0.02	4.91
$\Lambda \rightarrow p^+ + \pi^-$ $\bar{\Lambda} \rightarrow \bar{p} + \pi^+$	uds $\bar{u}d\bar{s}$	1.115±0.006	63.9±0.5	2.63±0.02	7.89

5.5.1 Λ Candidate Identification

A Λ candidate is a neutral baryon which can never be seen directly using CTD, but since the decay products are charged proton and pion, it can be identified as both leave a track that can be easily reconstructed back. Having a lifetime of 10^{-10} s, Λ is known as a weakly decaying particle that it will move few centimetres before decaying, thus an obvious secondary vertex is detected separated from the primary vertex. In the time of the reconstruction, all secondary vertex tracks were taken into consideration.

Λ events were required to have a strange hadron candidate, decaying into two oppositely charged tracks. These two charged particles were then fitted into a displaced secondary vertex, as in Figure 5.1. To build Λ event all reconstructed secondary vertices of an event were considered. The invariant mass of each reconstructed candidate, $m(p\pi)$ was solved by designating the proton mass ($m_p = 938.2720$ MeV) to the particle with the higher momentum than the other daughter, ($m_\pi = 139.5702$ MeV). To ensure precise invariant mass reconstruction, vectors of the momentum has to be at the decay vertex, with all tracks used must be vertex tracks. The reconstruction for Λ were by V0lite block as it contains information for the charged daughters.

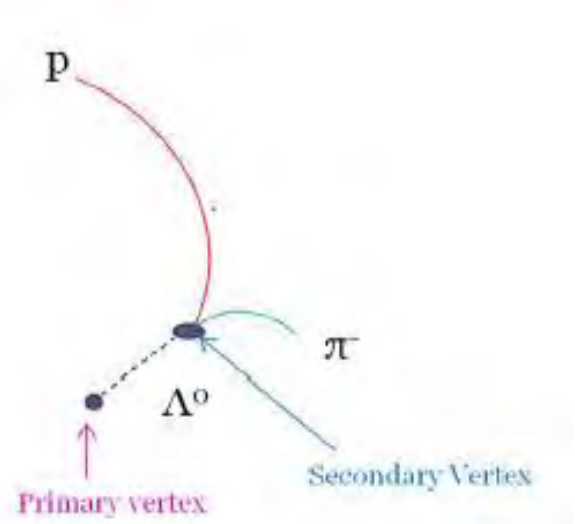

Figure 5.1: The decay of Λ^0candidate that decays into p and π^- (Zolkapli, 2013).

5.5.2 Ξ^- Identification with Reconstructed Displaced Tertiary Vertex (dtv)

As a weakly decaying particle, Ξ^- decay near the first vertex, although it is quite distant from the decay vertex. Hence, the reconstruction of decay vertex for Ξ^-can be differentiated from first vertex just like the reconstruction of the secondary vertices of Λ decays, known as displaced tertiary vertex.

The reconstruction of displaced tertiary vertex of $\Xi^-$is by combining the neutral daughter candidates with entirely charged CTD tracks in an event. The necessity for CTD track are (Ziegler, 2002):

- at least three hits in superlayers;
- track transverse momenta, $P_T > 0.15$ GeV and
- track pseudorapidity, $|\eta| < 1.75$

See Figure 5.2. Displaced tertiary vertex was found by searching the nearest distance of closest approach, dca among a Λ candidate and a charged CTD track. After that, the central of a line associating the points of dca on Λ and CTD track describes the displaced tertiary vertex. The daughter particles, Λ and π^-must come from the same Ξ^- decay vertex. Therefore, dca cannot be too large. As a heavier daughter candidate, Λ takes higher fraction of Ξ^-momentum and thus flies nearly the same direction with Ξ^-. This helps to reject background combinations which do not comes from Ξ^- decay.

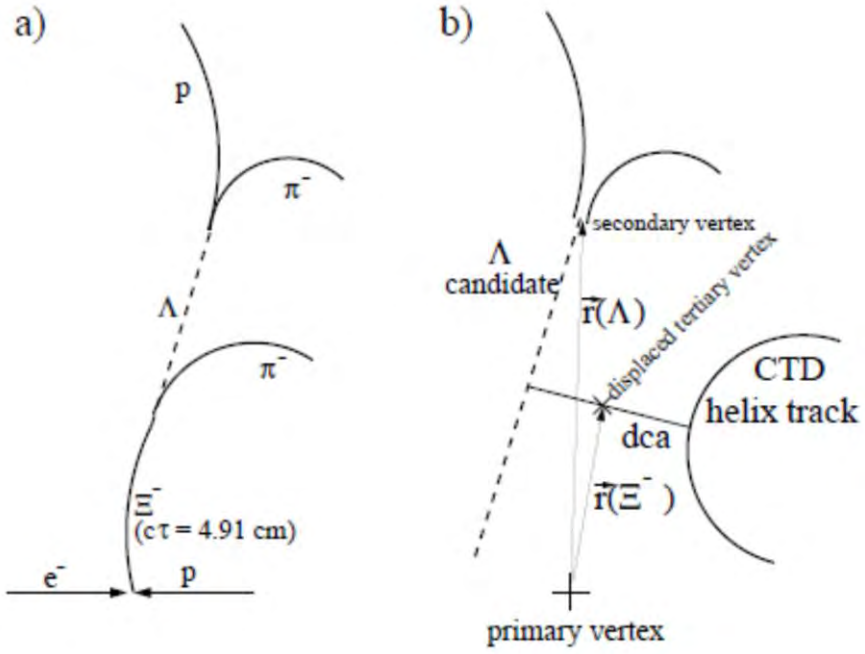

Figure 5.2: The (a) decay chain upon ep collision while (b) is where dtv and dca is located (Ziegler, 2002).

5.6 Matching Analysis

In this study, steps of matching between the truth and reconstructed Ξ^- candidate were invented. This is because the complications may occur from the MC reweighting and control plots.

An approach of MC reweighting should be applied at the generator level only, where by in inclusive event quantities, the kinematics weights such as Q^2 are considered. Meanwhile, in control plots it is only applied for the interested candidates only. For instance, if the weights were to be applied for both events and candidates, the uniqueness is lost. Weights are unique when it is applied for event at generator and reconstruction level.

The idea of matching is quite simple, it is to look at the particle ID, the momenta, as well as the directions, which can be done with any suitable MC sample in the Common Ntuples format. Some values of p_T and η were adjusted to get good enough matching efficiency, but in principle different analysis might give different efficiency outcome.

The matching was done by taking into account whether the truth-level particles comes from Ξ^- baryon candidate in the studied decay channel, with all the daughter tracks (Λ and π^-) were well matched to truth-level. It is therefore, the reconstructed Ξ^- candidate was then said to be successfully matched to the truth-level. The correct charge combination of decay chain Ξ^-, which is Λ decay and π^- is known as the sample of signal, while the wrong combination or the one that is not coming from the decay channel is known as background sample. Figure 5.3 and Figure 5.4 are plots of particles that undergone matching procedure.

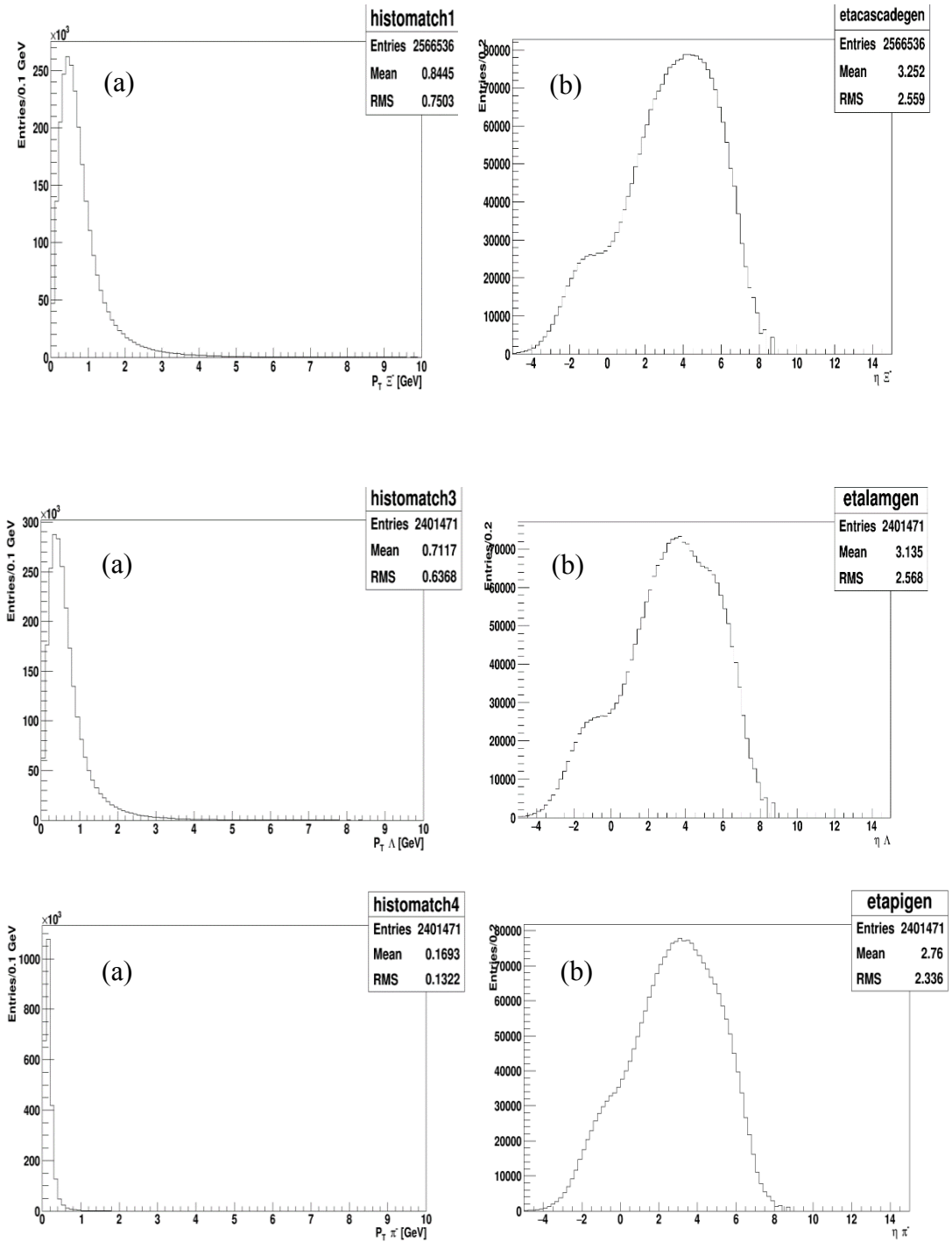

Figure 5.3: The (a) transverse momentum, p_T^{gen} and (b) pseudorapidity, η^{gen} of matched Ξ^- and the daughters, Λ and π^- respectively.

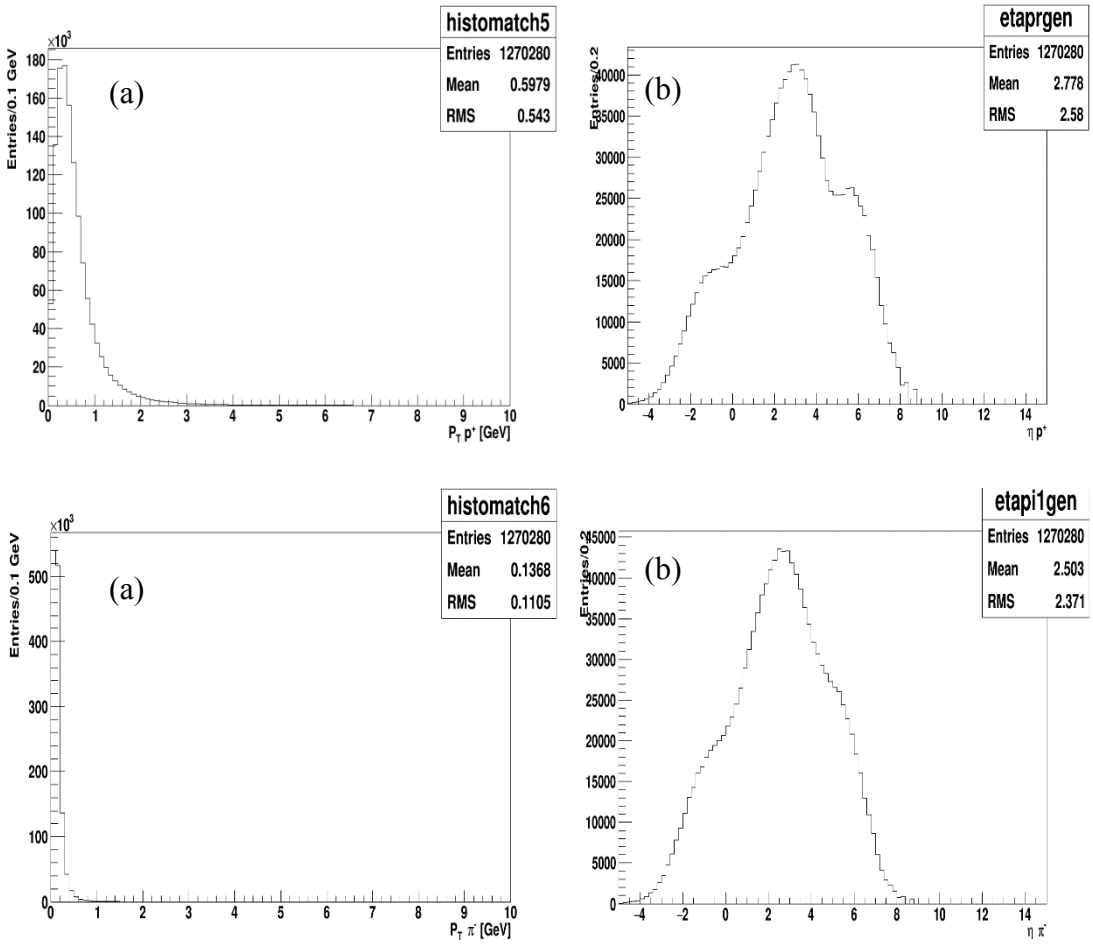

Figure 5.4: The (a) transverse momentum, p_T^{gen} and (b) pseudorapidity, η^{gen} of matched Λ daughters, p and π^- respectively.

In contemplation of limiting the combinatorial background and exclude the unsatisfactorily calculated secondary vertices, Λ event candidate is said to be found if the following requirements are fulfilled (Zolkapli, 2013):

- events have at least one secondary vertex;
- the secondary vertex is required to have two different charged tracks, with the p or $\bar{p}$ mass was assigned to the track with larger momentum and the π or $\bar{\pi}$ to the other track for V0lite candidate.
- hits in superlayers 1 to 3, to have advantage for the algorithms to reconstruct secondary vertices of the considerable resolution enhancement, and to restrict the CTD region where track acceptance is mostly high

- $p_T > 0.15$ GeV, transverse momentum has to be larger than 0.15 GeV, as lower p_T gives the chances of not well measured p_T because of the spiral by magnetic field is very close to the beam axis
- $|\eta| < 1.75$, to stay away from edge of acceptance that exists due to cut on $p_T$and $|\eta|$set by requirements of three superlayers.

Figure 5.5 shows the matched and unmatched distributions of Λ. The mass peak is around 1.116 GeV. The unmatched Λ dominates the distribution due to large η at generator level (Refer Figure 5.3 (b) and Figure 5.4 (b)).

The azimuthal angle, ϕ and the polar angle, θ was measured according to the x −plane and z −plane, there was symmetry imbalance between forward and rear side of the detector. The ZEUS detector was designed with longer side on forward calorimeter than the rear calorimeter, due to large difference in proton and electron momentum. As a result, this gives huge number of particles being boosting towards the forward direction.

Figure 5.6 shows the correlation distributions of transverse momentum, p_T^{gen} and pseudorapidity, η^{gen} of matched Λ at generator level, while Figure 5.7 shows the reconstructed Ξ^- successfully matched to the generator-level.

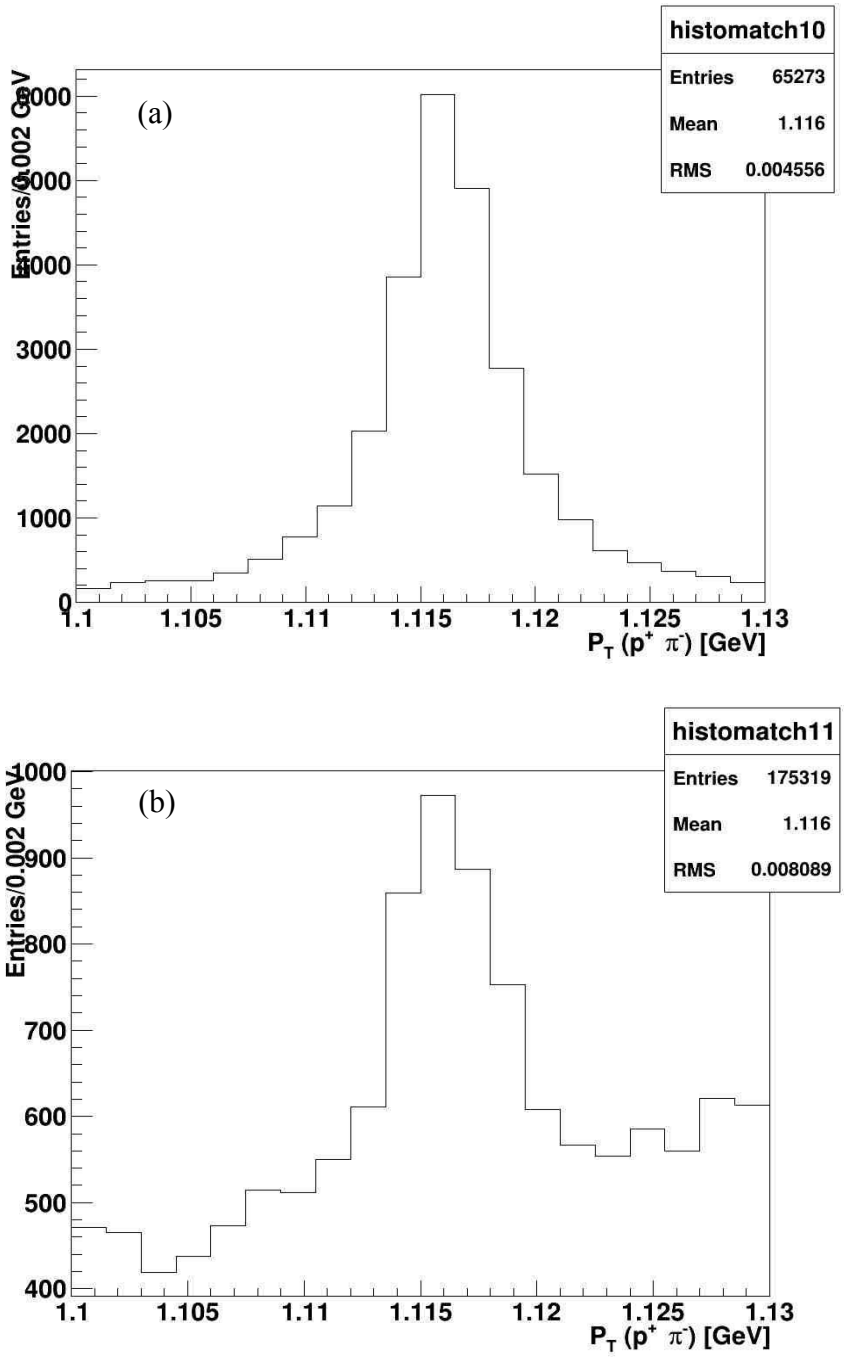

Figure 5.5: The simulated (a) matched Λ and (b) unmatched Λ.

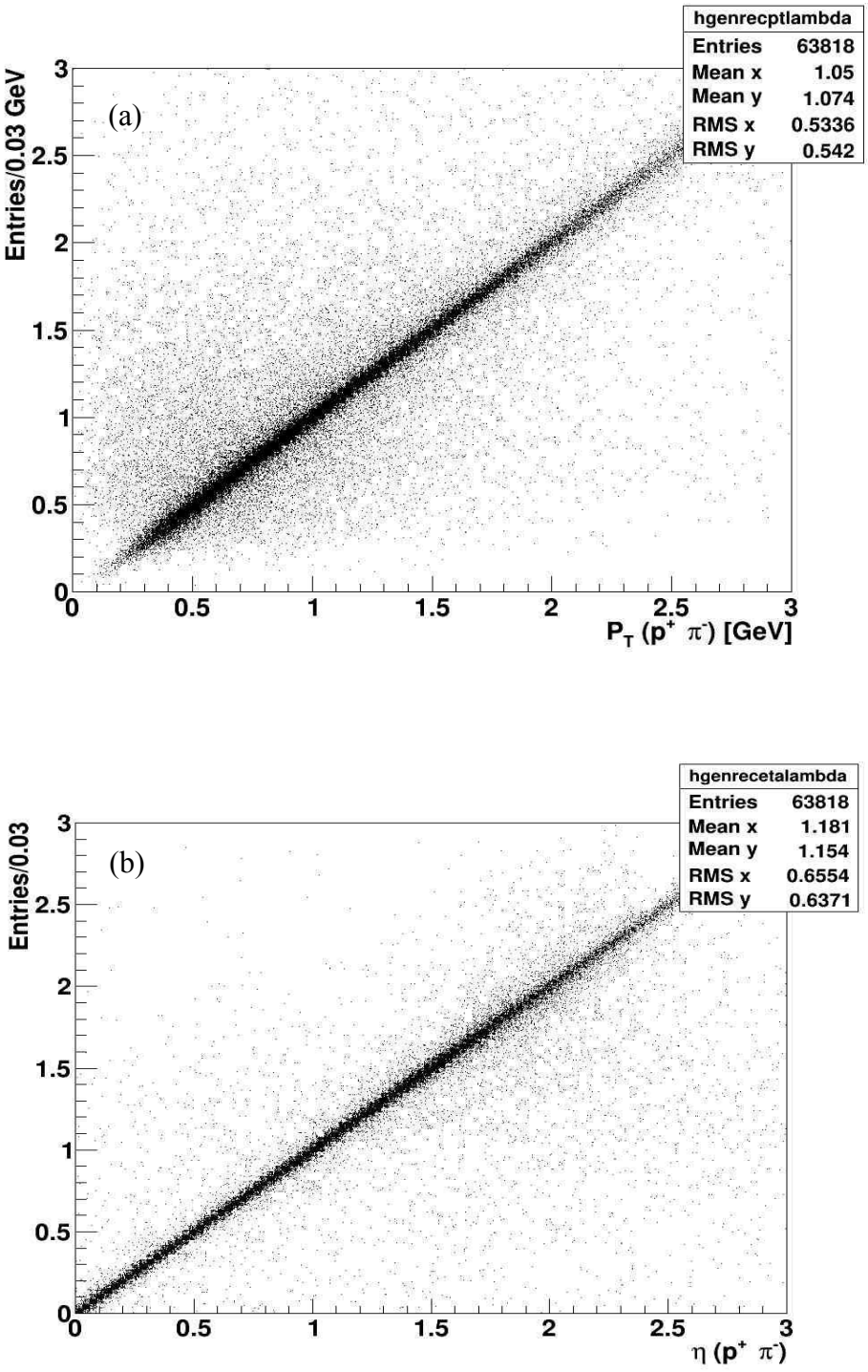

Figure 5.6: The correlation in (a) p_T^{gen} and (b) η^{gen} between generator level and reconstructed level of Λ.

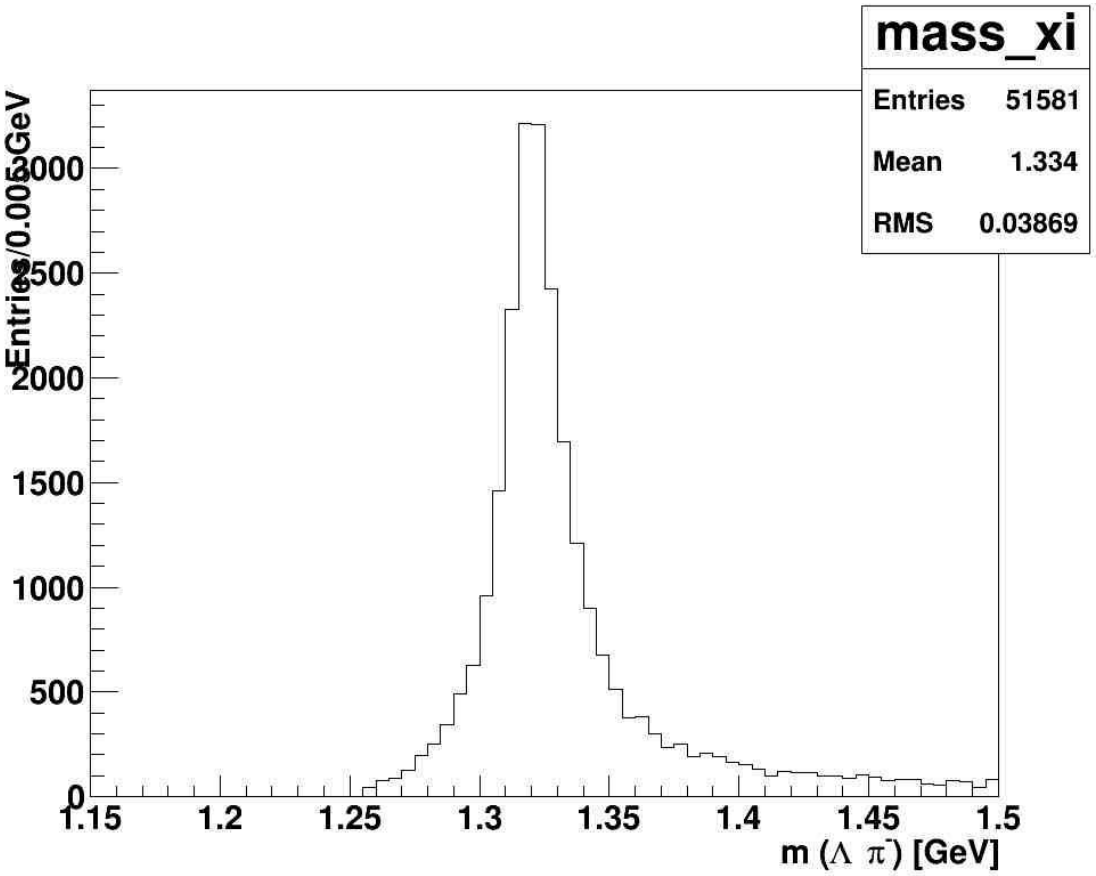

Figure 5.7: The matched reconstructed Ξ^-.

5.7 Optimization Cuts

Separation between the one that carries the interest information, signal and the other one that consists of noise, background is one of the common problems faced by physicists in High Energy Physics (Narsky, 2006). It is perhaps difficult to decide in determining which one is suitable cuts for both signal and background due to the characteristics of signal and background itself. For instance, usually in HEP world, one typically wants to optimize a figure-of-merit (FOM) in the signal area that can be expressed as signal and background, S and B. This FOM can be written as $\frac{S}{\sqrt{S+B}}$, where it is the ratio of signal to the background. It is common for the analysts to express the cleanliness or peak of the signal with the presence of fluctuations of observed signal and background. To get good analysis and reliable result, the higher the ratio the better it is.

There are a lot of methods that have been developed to solve this problem. For example, feed forward back propagation neural network (Cowan, 1990) and Fisher discriminant (Fisher, 1936) are the most chosen by HEP community since then till nowadays. There were many other approaches as well, but it is always important to note that the choice of method chosen for the problem must be driven by the specifics of the analysis itself. Below are the lists of cuts that have been selected for this analysis.

- the Λ candidates are defined as all Λ event candidates with invariant mass of $1.112 < m(p\pi) < 1.121$. (Figure 5.8)
- $(0.2 < p_T\Lambda =< 1.0)$ && $(1.2 < p_T\Lambda =< 1.5)$. (Figure 5.9)
- $(-2.25 < \eta_\Lambda < -0.25)$ && $(0. < \eta_\Lambda < 2.)$. (Figure 5.10)
- $\phi_\Lambda > 0.1$ (Figure 5.11)
- collinearity of the secondary vertex > 0.009 (Figure 5.12)
- $\chi^2$of the secondary vertex < 3.8. (Figure 5.13)
- $dca_\Lambda$of the secondary vertex < 0.6. (Figure 5.14)
- $d_0\pi < 5.5$. (Figure 5.15)
- $0.1 < d_0\Xi^- < 2.2$. (Figure 5.16)
- $dca_z > 0.2$. where dca_zstands for distance of closest approach in Z axis where it belongs to Λ candidate, Z_Λ, and π^-candidate, Z_{π^-}, ie: $dca_z = Z_\Lambda - Z_{\pi^-}$. (Figure 5.17)
- collinearity of the primary vertex > 0.09. (Figure 5.18)

(a)

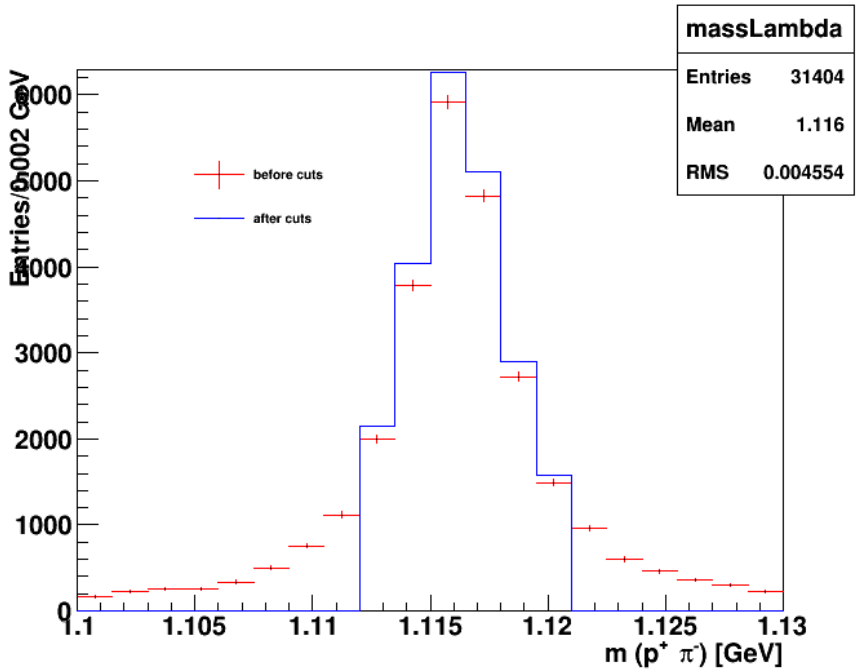

(b)

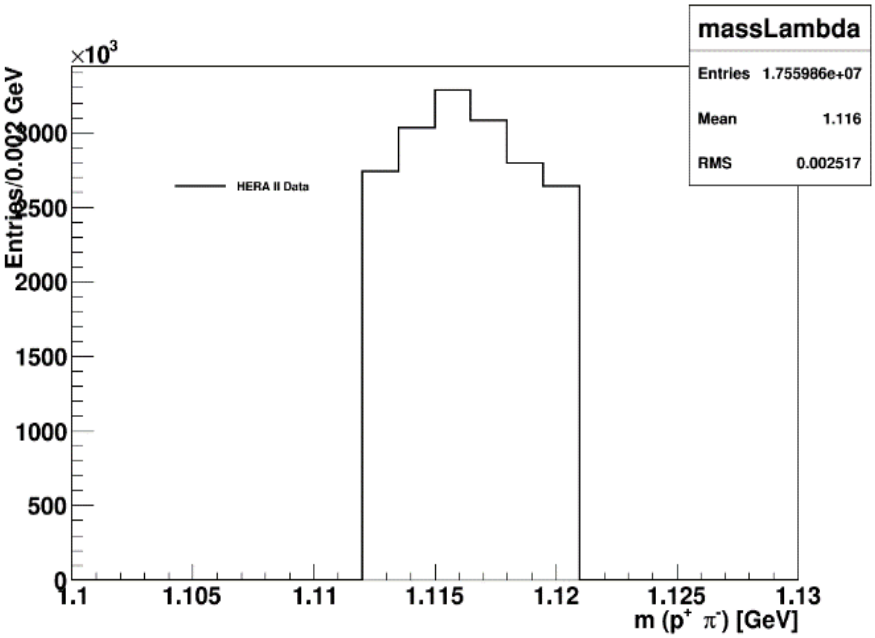

Figure 5.8: The distribution of mass Λ for (a) ARIADNE MC and (b) HERA II data.

(a)

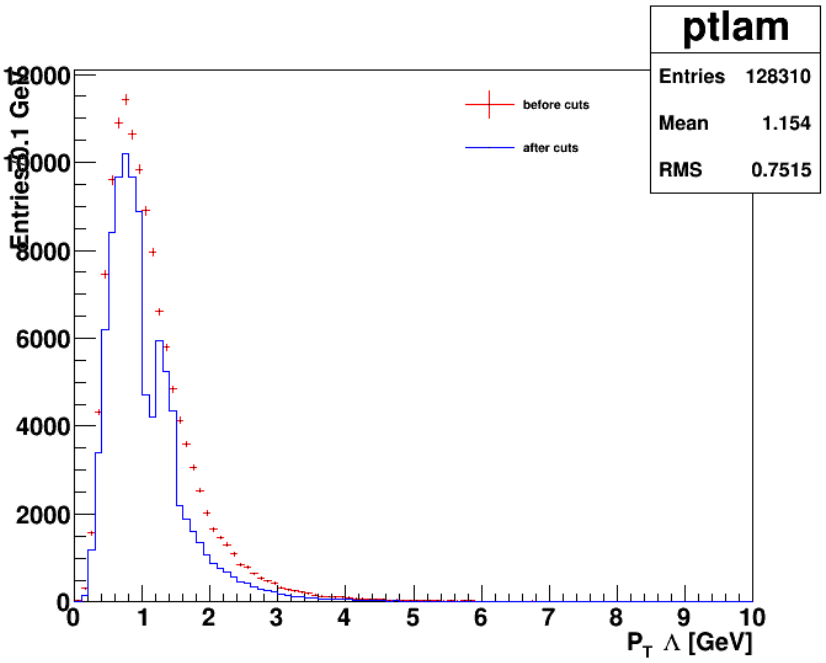

(b)

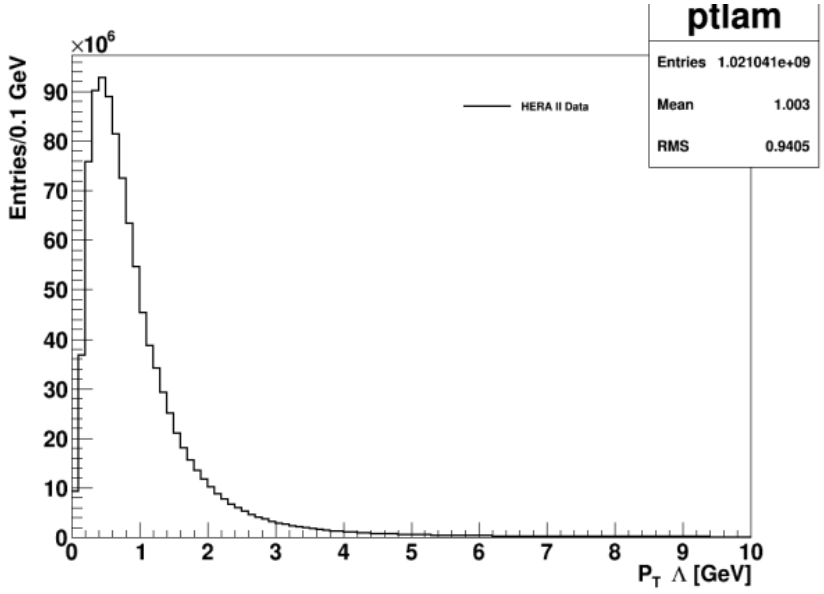

Figure 5.9: The distribution of P_T of Λ for (a) ARIADNE MC and (b) HERA II data.

(a)

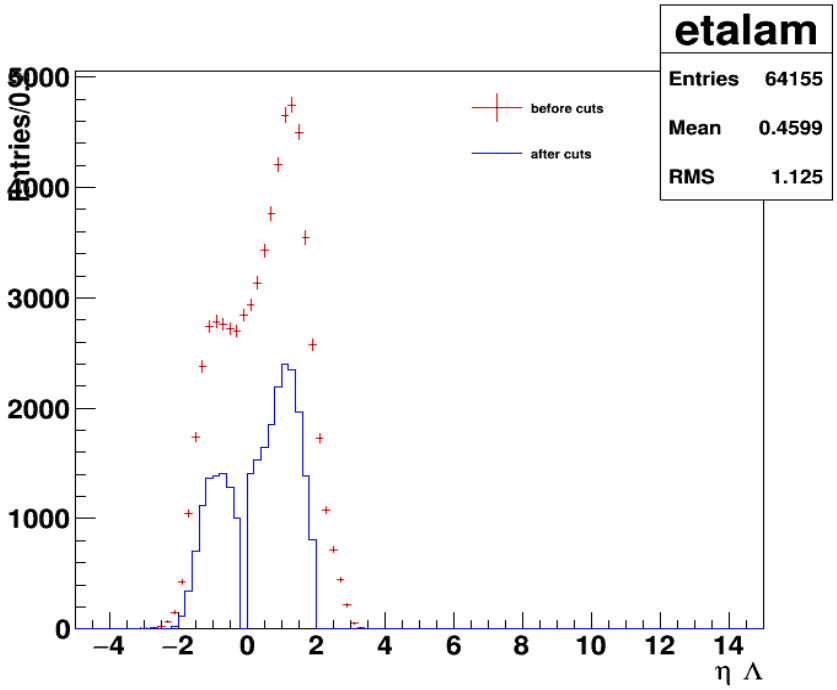

(b)

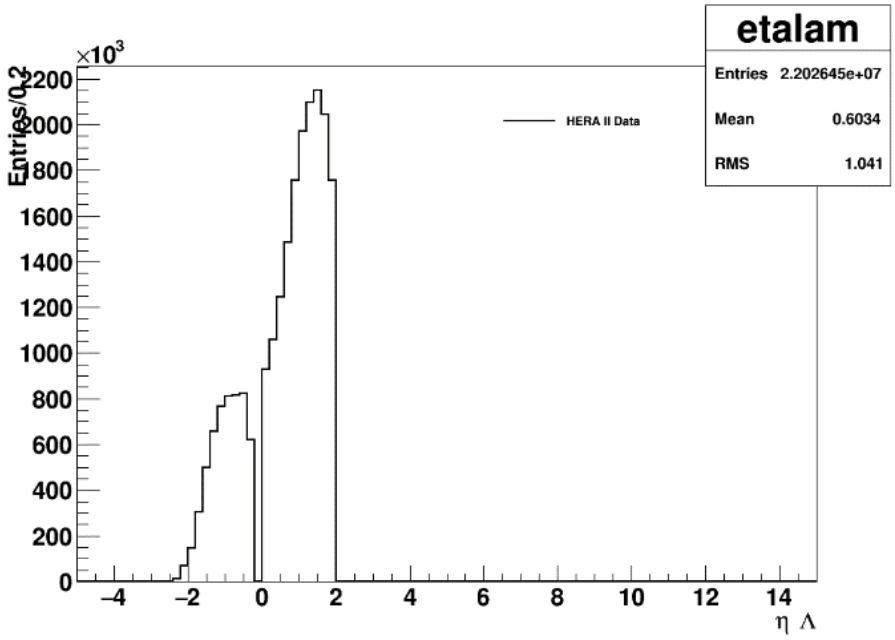

Figure 5.10: The distribution of η Λ for (a) ARIADNE MC and (b) HERA II data.

(a)

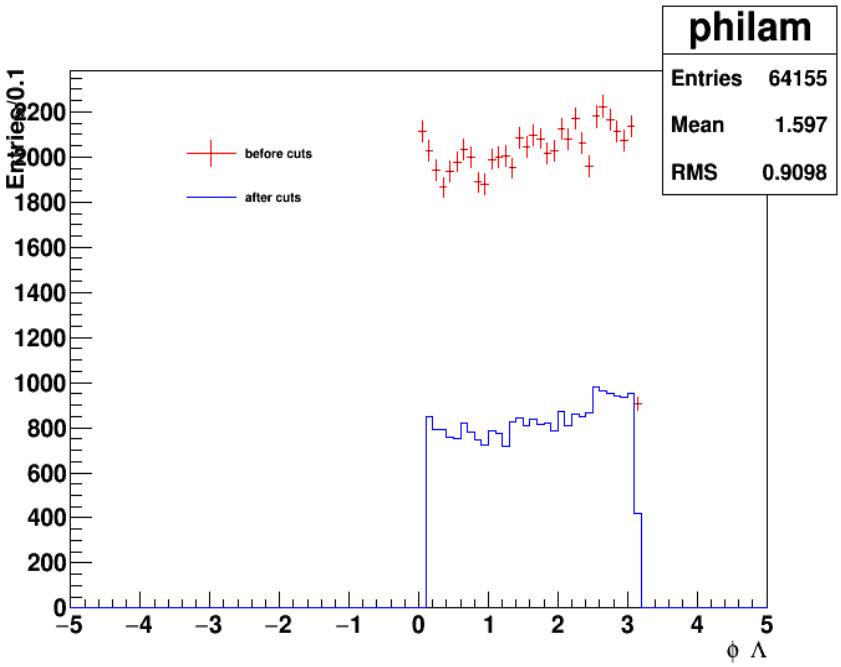

(b)

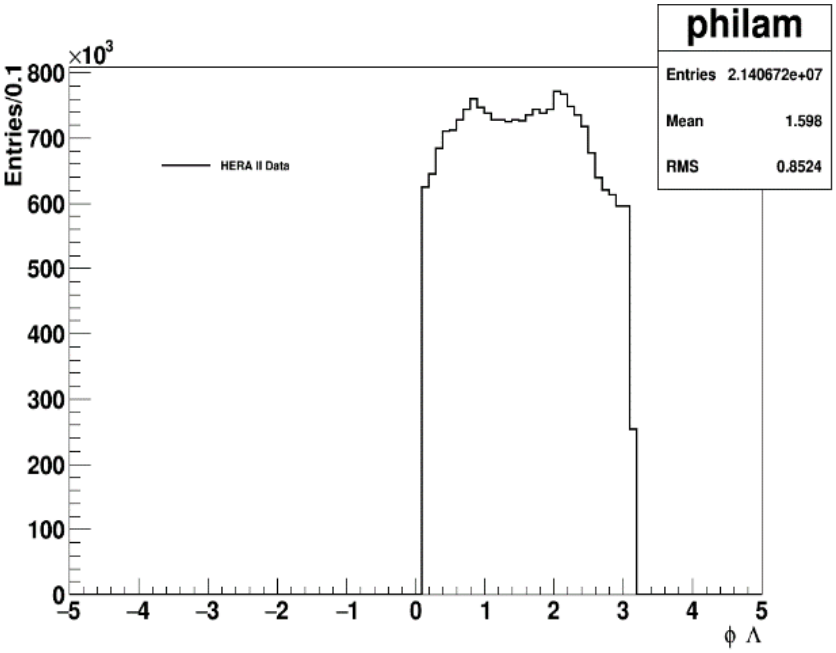

Figure 5.11: The distribution of ϕ_Λ for (a) ARIADNE MC and (b) HERA II data.

(a)

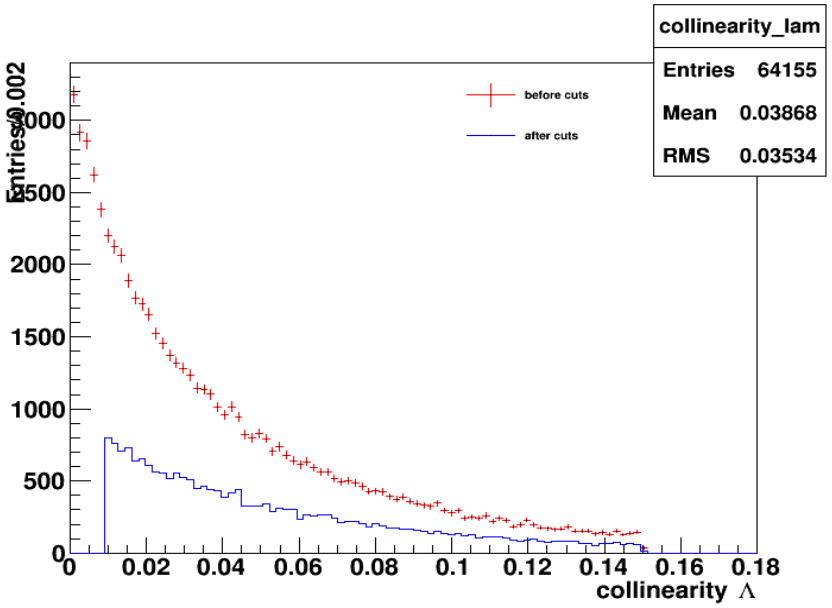

(b)

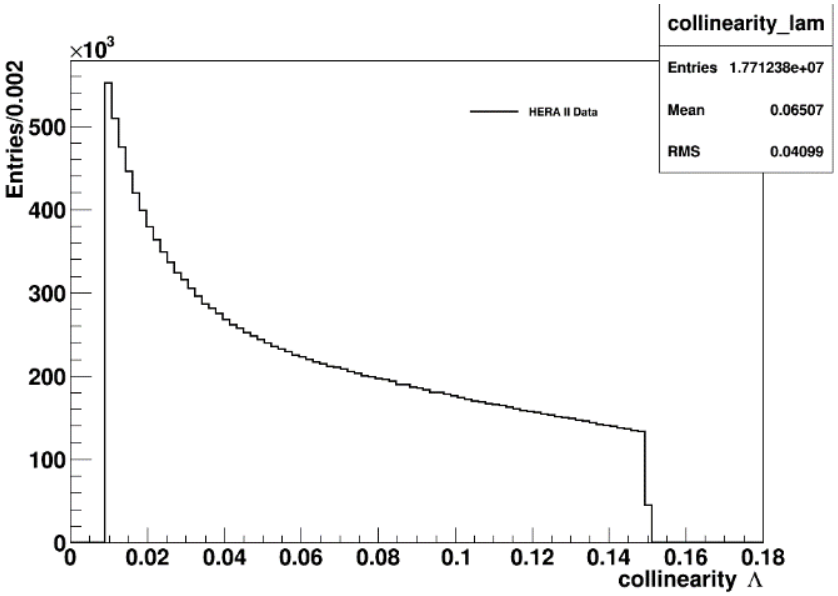

Figure 5.12: The distribution of collinearity Λ for (a) ARIADNE MC and (b) HERA II data.

(a)

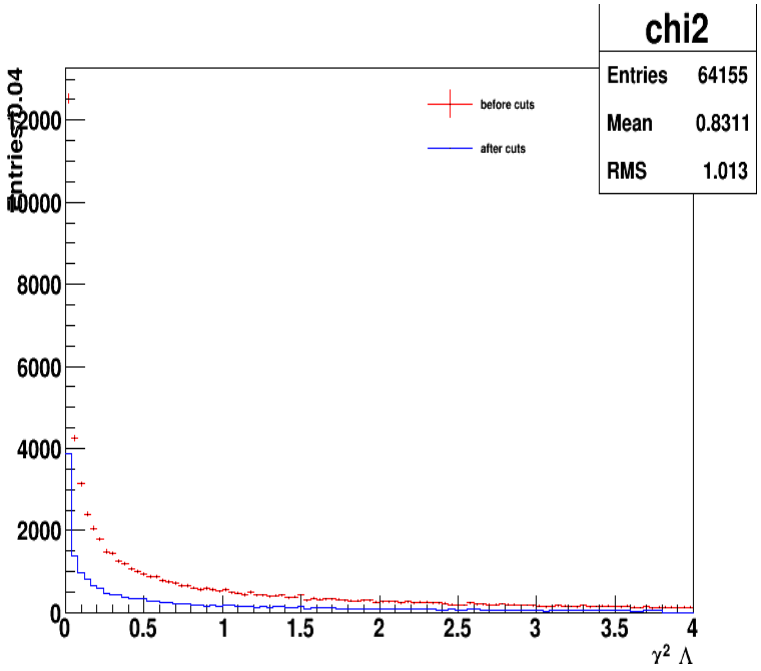

(b)

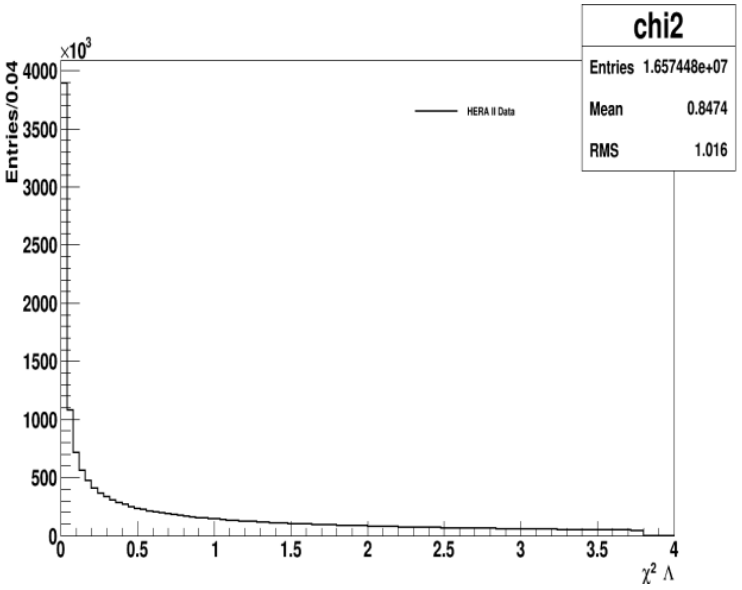

Figure 5.13: The distribution of χ^2 Λ for (a) ARIADNE MC and (b) HERA II data.

(a)

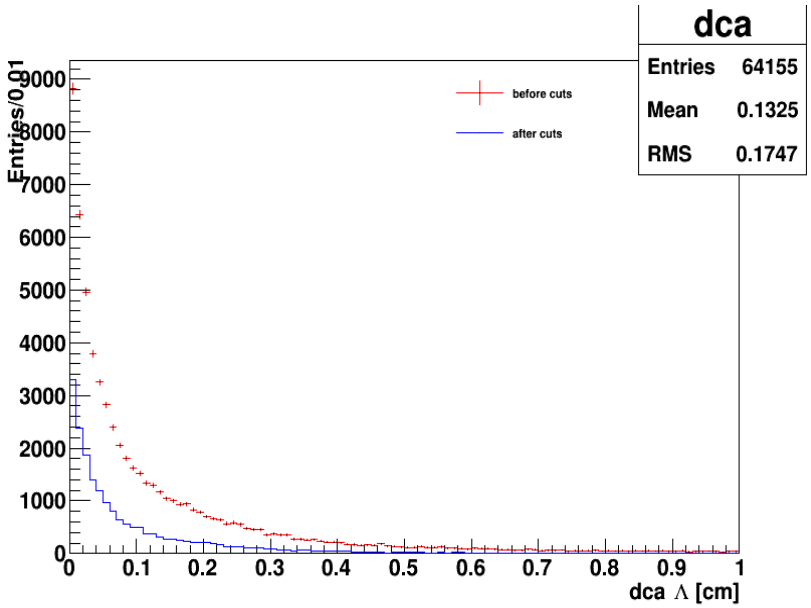

(b)

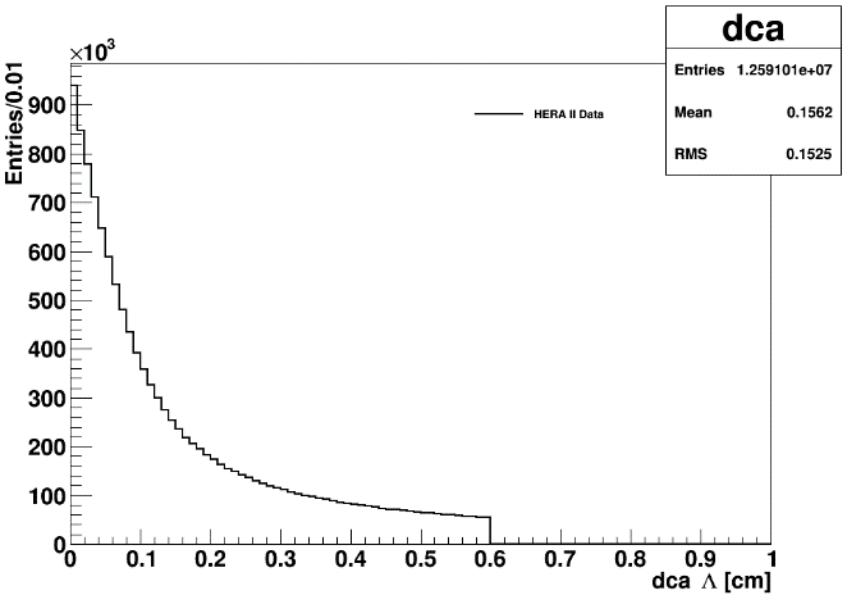

Figure 5.14: The distribution of dca of Λ for (a) ARIADNE MC and (b) HERA II data.

(a)

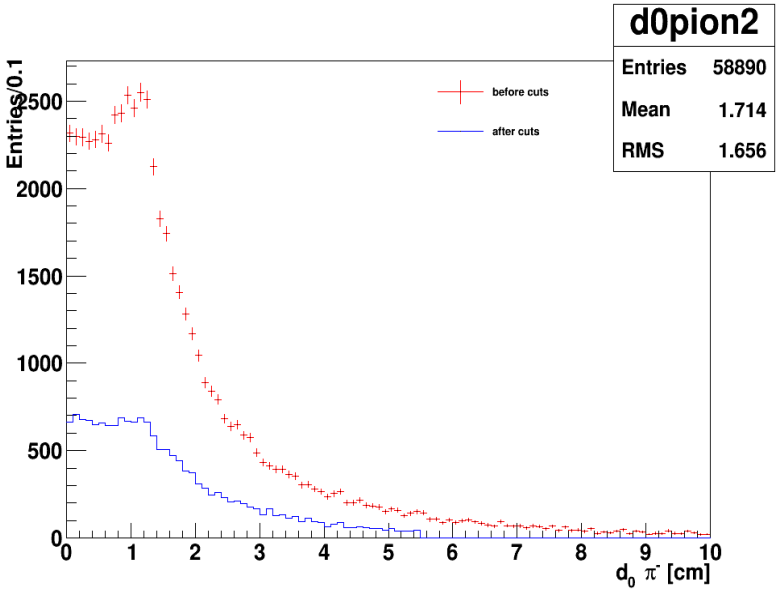

(b)

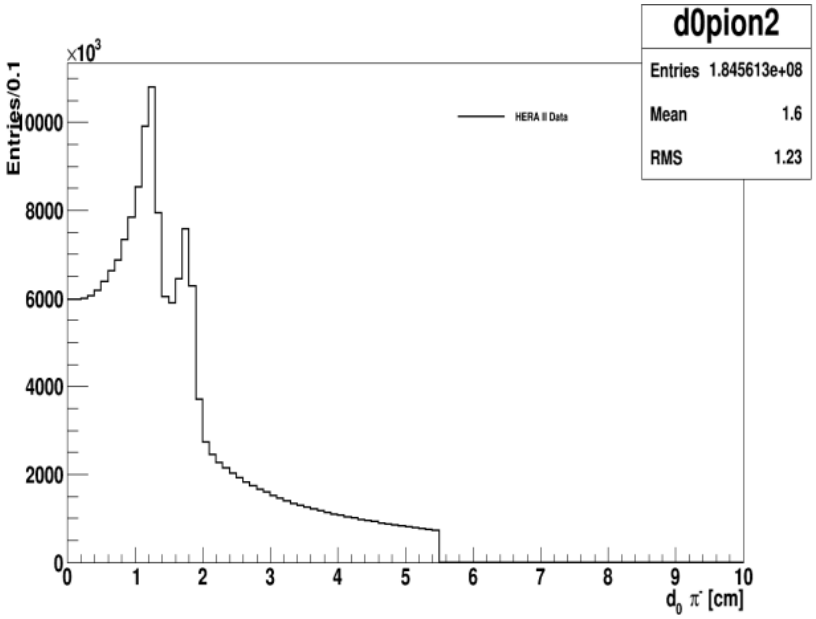

Figure 5.15: The distribution of $d_0\pi$ for (a) ARIADNE MC and (b) HERA II data.

(a)

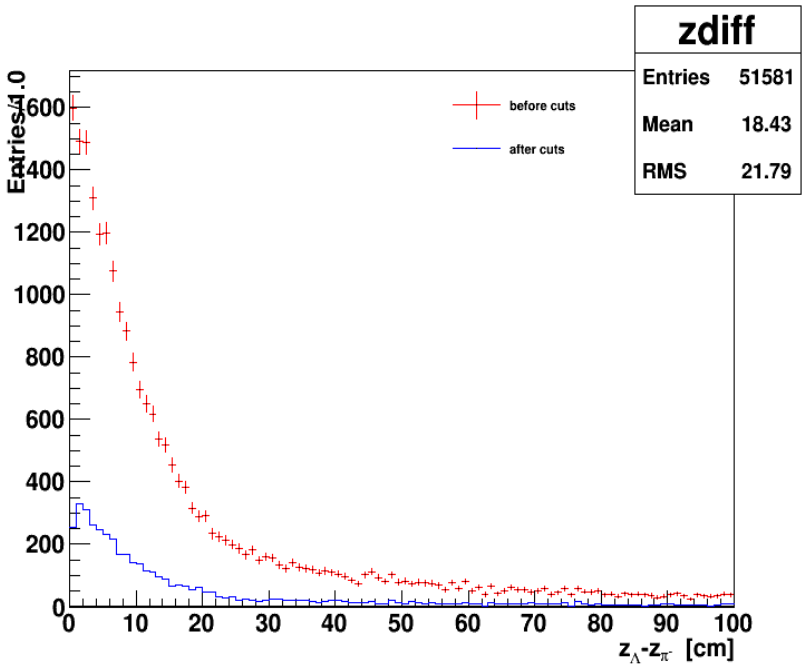

(b)

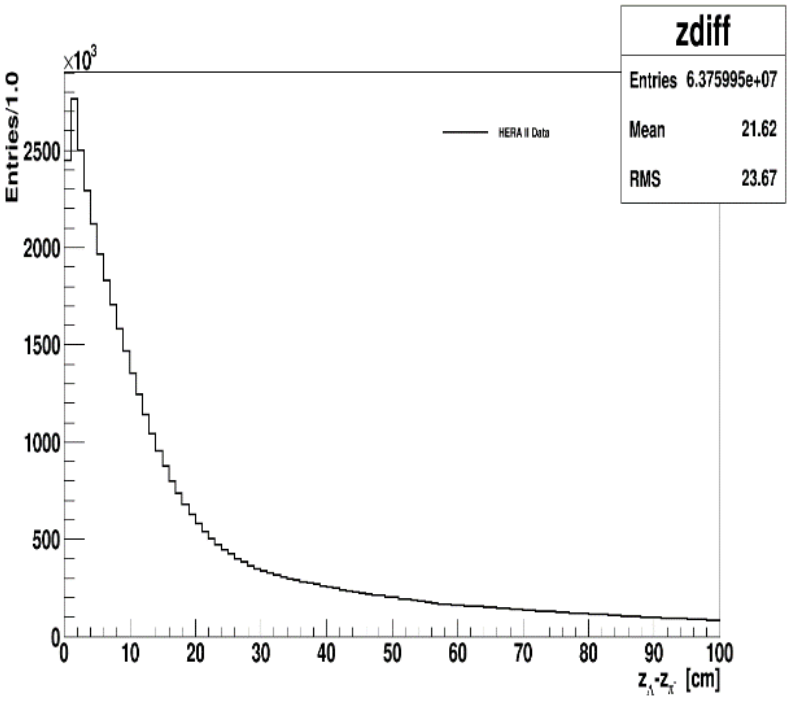

Figure 5.16: The distribution of dca_z for (a) ARIADNE MC and (b) HERA II data.

(a)

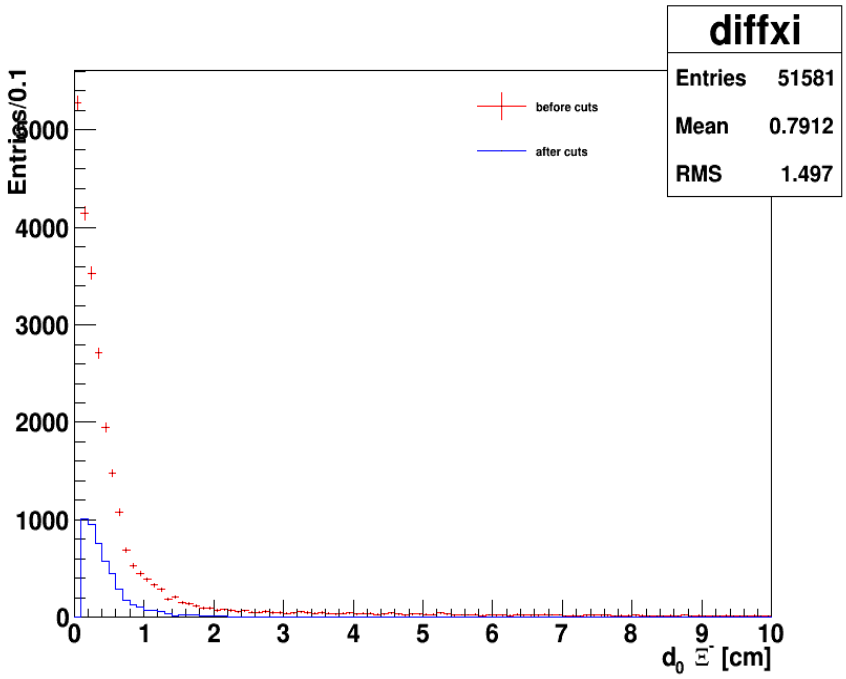

(b)

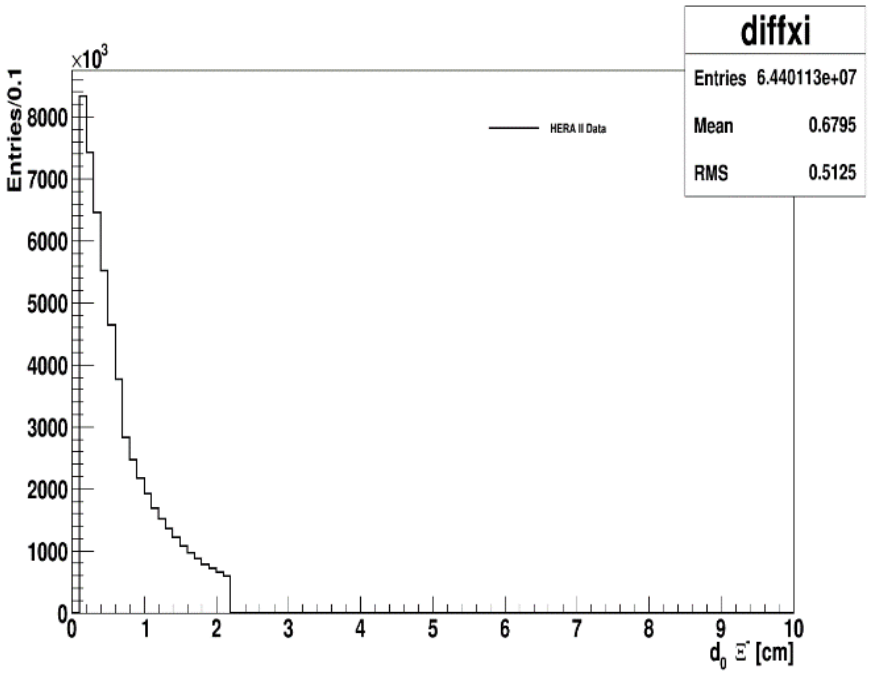

Figure 5.17: The distribution of $d_0\Xi^-$ for (a) ARIADNE MC and (b) HERA II data.

(a)

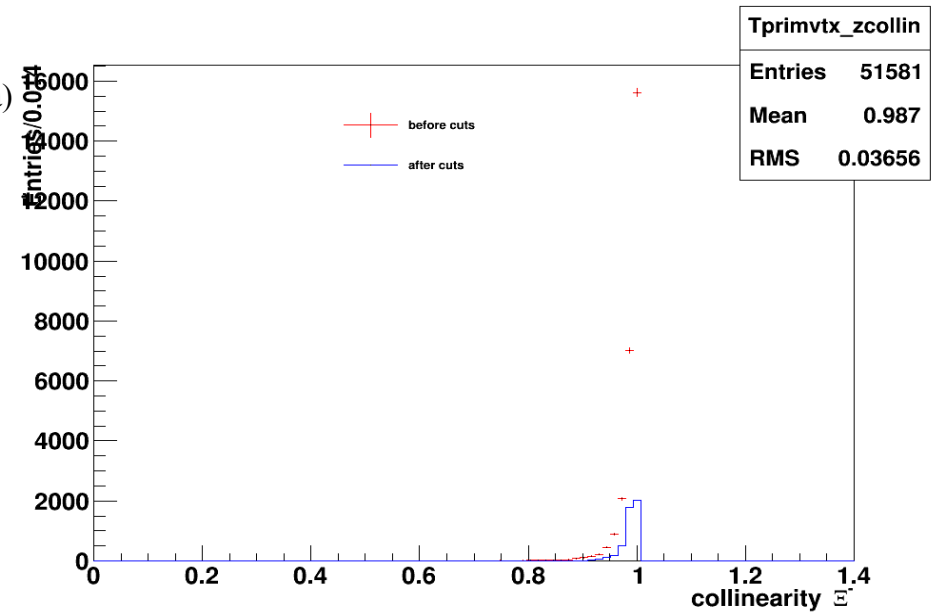

(b)

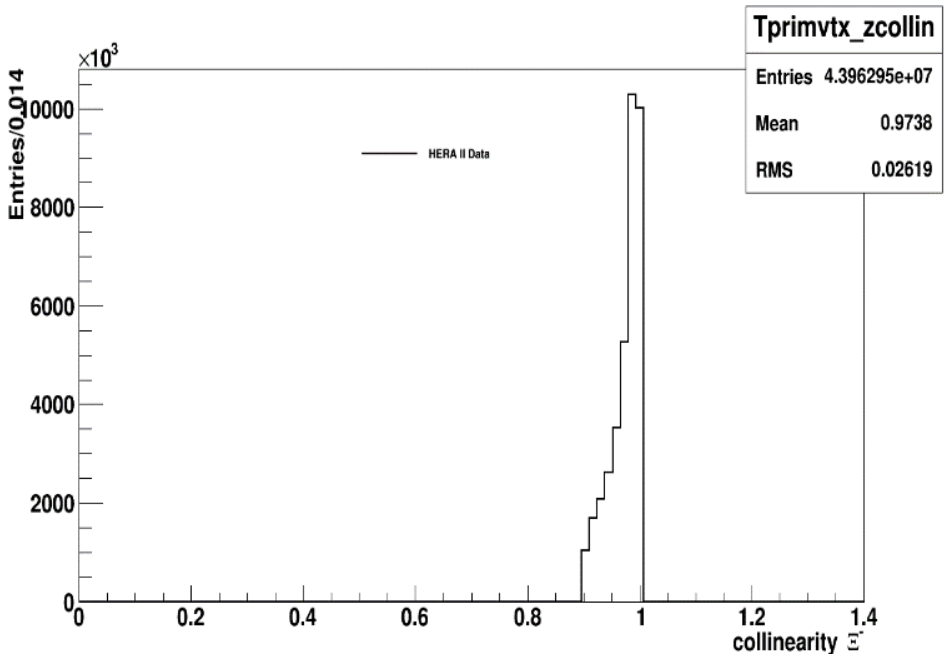

Figure 5.18: The distribution of collinearity of the primary vertex for (a) ARIADNE MC and (b) HERA II data.

CHAPTER 6: RESULTS AND DISCUSSION

6.1 Acceptance, Efficiency, and Purity

The reconstructed particles at hadron level undergone correction through the detector acceptance, $\boldsymbol{A}$. By definition, acceptance means how far detector understands the process behind it whereby it is the ratio of the reconstructed all the possible candidates at the detector level, $\boldsymbol{\varepsilon}$ to the total of simulated candidates at the hadron level, $\boldsymbol{P}$. Equation 6.1 shows how acceptance works.

$$A = \frac{\boldsymbol{\varepsilon}}{P} \tag{6.1}$$

where ε stands for efficiency and P is the purity.

While acceptance is depending on efficiency and purity it is important to take note on both definitions of ε and P. Efficiency is the ratio of the simulated particles at the hadron level in the reconstructed signal at the detector level. It is defined as in Equation 6.2.

$$\varepsilon = \frac{N_{MC}^{rec}}{N_{MC}^{gen}} \tag{6.2}$$

where N_{MC}^{rec} is the total number of reconstructed particles at generator level and N_{MC}^{gen} stands for the total number of generated particles at generator level.

Purity on the other side means the ratio of the real particles to the total of candidates, where Equation 6.3 defines.

$$P = \frac{N_{MC}^{rec}}{N_{data}^{rec}} \tag{6.3}$$

Table 6.1 shows the efficiency of truth particle produced at generator level. It can be seen that about 0.0156 or 1.56 % $\Xi^-{}_{truth}$'s produced per event. This is then followed by 93.57 % for both Ξ^-'s daughter particle, Λ_{truth} and $\pi^-{}_{truth}$. As for both Λ's daughter, $p^+{}_{truth}$ and $\pi^-{}_{truth}$, the efficiency is about 52.90 %. The analysis then searched for the track matching efficiency which was done by finding the track match of three particles. This track efficiency only gives 8 %. According to branching ratio of the selected decay channel Ξ^-, it is supposed to be about 99.89 %, while for decay channel Λ, 67.8%. The reason behind efficiency fall might be probably because of large η produced at generator level.

The efficiency of reconstructed particle produced at generator level is in Table 6.2. After going through several cuts, Ξ^{-rec}_{MC} gives about 0.00404 or 0.4 ± 0.0039 %. Plot for Ξ^{-rec}_{MC} is as shown in Figure 6.1.

Table 6.1: Efficiency at generator level.

N_{ev}, 10^6	164.5	
$\Xi^-{}_{truth}$	2 566 536	0.0156
Λ_{truth}	2 401 471	0.9357
$\pi^-{}_{truth}$	2 401 471	0.9357
$p^+{}_{truth}$	1 270 280	0.5290
$\pi^-{}_{truth}$	1 270 280	0.5290
$p^+{}_{truth}, \pi^-{}_{truth}, \pi^-{}_{truth}$	194 693	0.08

Table 6.2: Efficiency of Λ and Ξ^-.

	Before Optimization Cuts	After Optimization Cuts	Candidate survived (%)
Λ_{MC}^{rec}	65273	31404	48.11
Ξ^{-rec}_{MC}	51581	10370	20.10

(a)

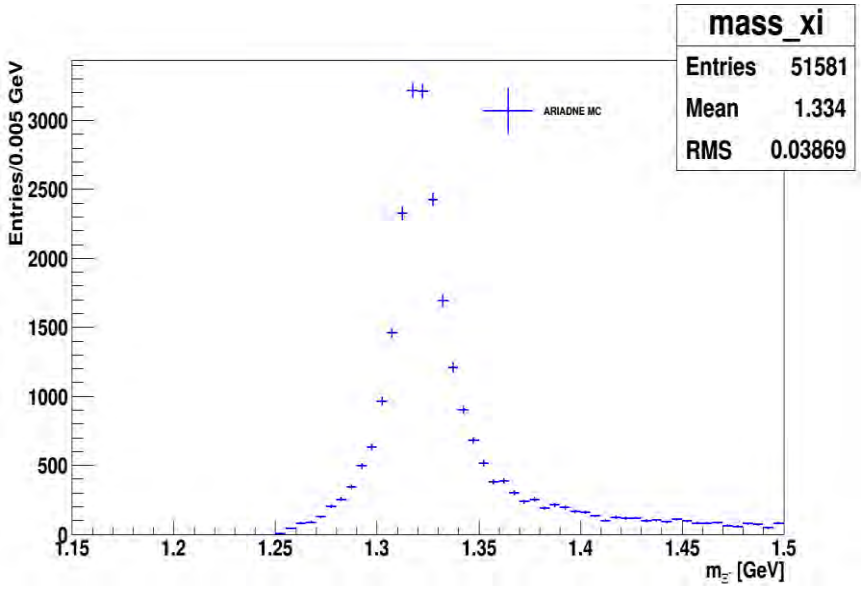

(b)

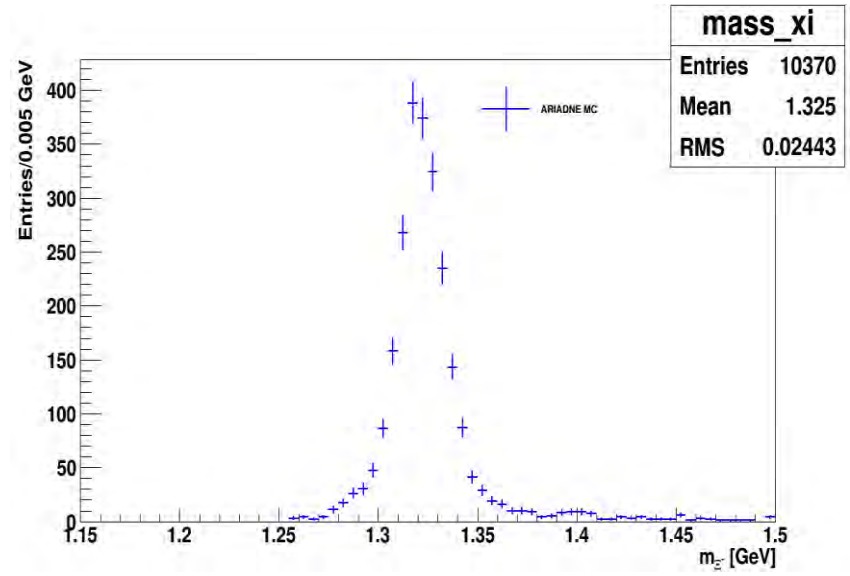

Figure 6.1: The matched reconstructed Ξ^- (a) before cuts and (b) after cuts using ARIADNE MC generator.

6.2 Functions and Fitting in Monte Carlo

The "goodness of fit" or better known as Chi-square, χ^2 test tells how well it is likely the observed distribution of data fits or matches with the model, or expected distribution. χ^2 is the sum of independent number degrees of freedom squared Gaussian variables with unit standard deviation. High correlation between MC and Data when the value of χ^2 is small, which means the observed data fits very well with the expected data. But having too low of χ^2 might also means the data uncertainties are overestimated, or the model contains excess parameters tuned to "over fit" the data. Vice versa, large χ^2 means either the data is not well described by the model or the uncertainties is underestimated.

Fitting is a process in minimizing a quantity in order to search for the best estimates for certain function parameters, and to test if the given data are properly explained by some hypothesized function. It involves in adjusting certain parameters to get the best fit of the spectrum distributions.

6.2.1 Λ candidate

The invariant mass distributions were fit using Gaussian function as in Equation 6.4.

$$f(x) = a_0 e^{\frac{-(x-a_1)^2}{2{a_2}^2}} \tag{6.4}$$

The total number of particles is given by Equation 6.5.

$$N_{particles} = \int f(x)dx = \frac{\sqrt{2\pi}}{w} a_0 a_2 \tag{6.5}$$

where $a_0$and $a_2$is the values of the 0th and 2nd parameters respectively, while w is the bin width.

Substituting $a_0 \equiv \frac{a_0}{\sqrt{2\pi}a_2}$,

$$f(x) = \left(\frac{a_0}{\sqrt{2\pi}a_2}\right) e^{\frac{-(x-a_1)^2}{(2{a_2}^2)}} \tag{6.6}$$

a_0, a_1 and a_2 are the fit parameters of the Gaussian distribution, where a_0 is the height of the peak, a_1 is the peak position of the Gaussian and a_2 is the bin width of the histograms. The number of particles observed is the total area under the Gaussian distribution that can be found by

$$N_{particles} = \int f(x)dx = \frac{a_0}{w} \tag{6.7}$$

where a_0 is the value of 0th Gaussian parameter after the fitting process and w is the bin width of the histogram. Figure 6.2 shows the simulated and reconstructed distributions of Λ candidates. The mass peak shown is around 1.116 GeV.

(a)

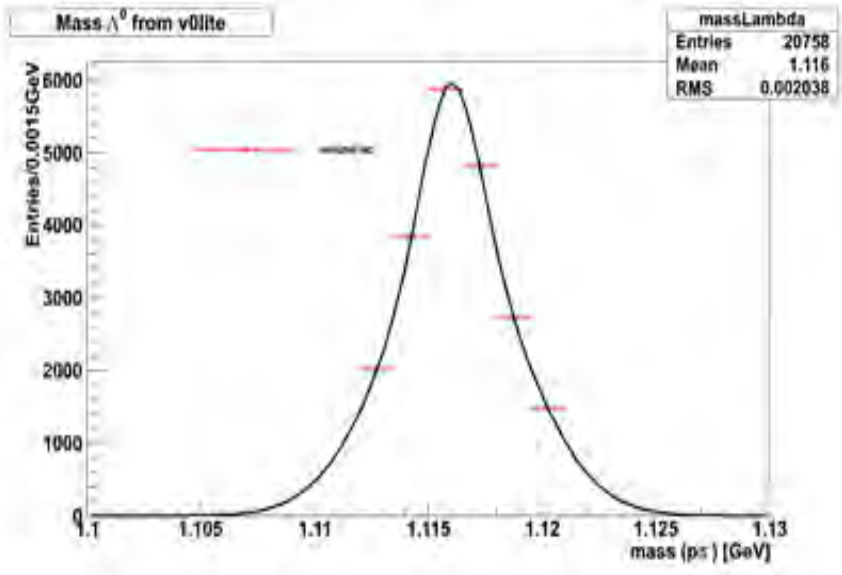

(b)

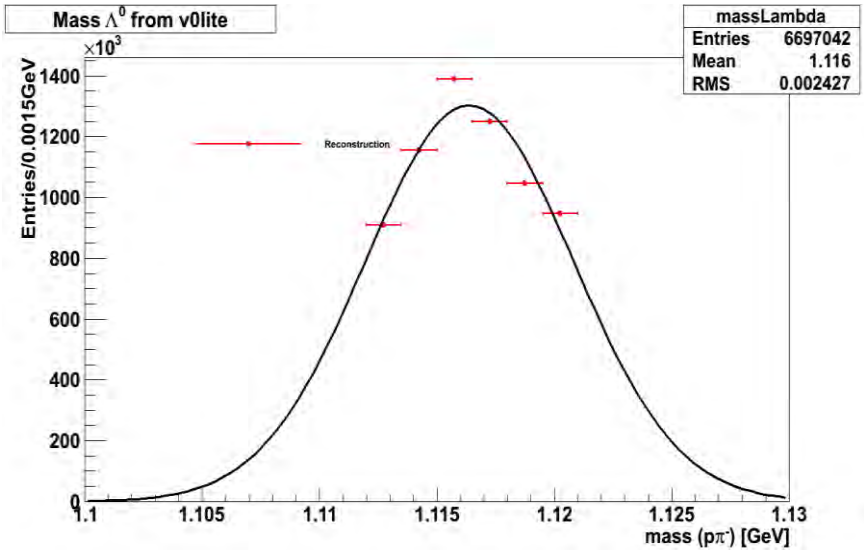

Figure 6.2: The mass distribution $m(p\pi)$ of all (a) simulated and (b) reconstructed Λ event candidates.

6.2.2 Ξ^- candidate

There were two attempts to fit the signal, using Breit-Wigner and Gaussian function and to fit the background, using 4th order of polynomial function and WA's function.

6.2.2.1 Breit-Wigner (BW)

BW (Weinstein, 1999) is an approximate line-shape model designed for an unstable particle or resonance propagator in quantum field theory, where it is well defined for fundamental particles such as the γ, Z^0 and $W^{\pm}$. In non-relativistic quantum mechanics, BW is popular through the hand-waving argument where the exponential decay law is encoded via wave function and also their Fourier transform, as in Equation 6.8.

$$|\psi(t)|^2 = |\psi(0)|^2 e^{-\Gamma t} \Rightarrow \psi(t) = \psi(0) e^{-\Gamma t} \tag{6.8}$$

where $\Gamma = 1/\tau$, with τ as the particle lifetime. The energy dependence is given by Equation 6.9 and Equation 6.10,

$$\bar{\psi}(E) = \int \psi(t)\, e^{iEt} dt \propto \frac{1}{E - M + (i\Gamma/2)} \tag{6.9}$$

$$\left|\bar{\psi}(E)\right|^2 \propto \frac{1}{E - M + (i\Gamma/2)} \tag{6.10}$$

Figure 6.3 shows the simulated distributions of Ξ^- candidates with full mass window and with the present of mass window using Breit-Wigner function. The signal is around 1.325 GeV. The mass distributions fitted gives $\chi^2/N_{dof} = 3.03$.

(a)

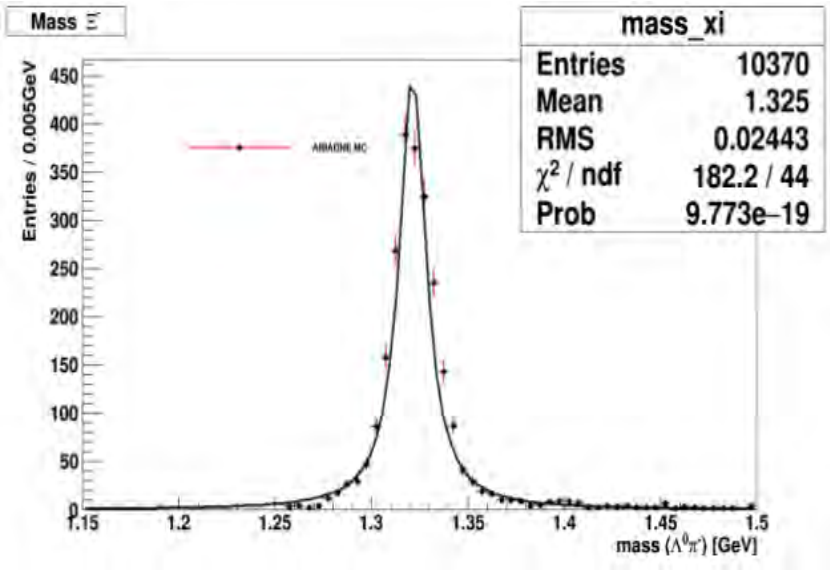

(b)

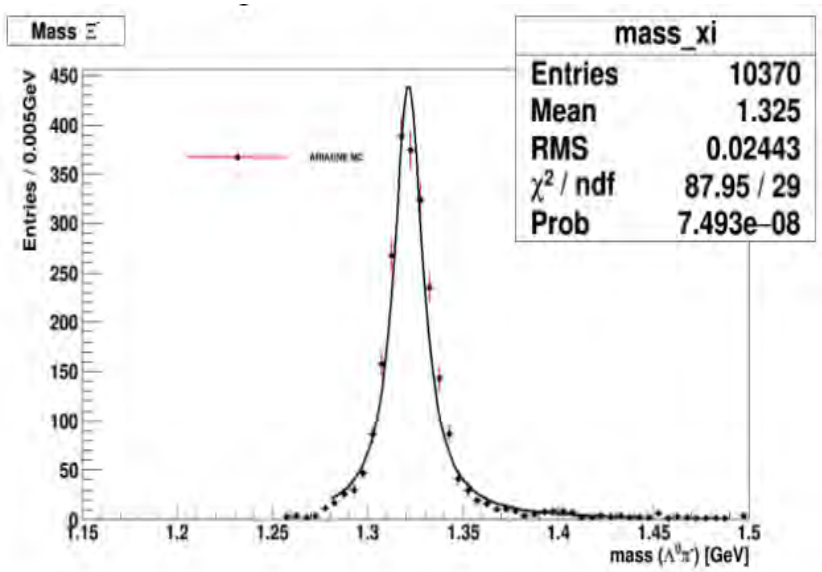

Figure 6.3: The mass distribution $m(\Lambda\pi^-)$ of all simulated $\Xi^-$with (a) full mass window and (b) present of mass window.

6.2.2.2 Gaussian functions

The invariant mass distributions were fit using two Gaussian functions as shown in Equation 6.11,

$$f(x) = a_0 e^{\frac{-(x-a_1)^2}{2{a_2}^2}} + a_3 e^{\frac{-(x-a_4)^2}{2{a_5}^2}} \tag{6.11}$$

The total number of particles is given by Equation 6.12,

$$N_{particles} = \int f(x)dx = \frac{\sqrt{2\pi}}{w} a_0 a_2 + \int f(x)dx = \frac{\sqrt{2\pi}}{w} a_3 a_5 \tag{6.12}$$

where a_0, a_2, a_3 and $a_5$is the values of the 0th, 2nd, 3rd, and 5th parameters respectively, while w is the bin width.

Substituting $a_0 \equiv \frac{a_0}{\sqrt{2\pi}a_2}$ and $a_3 \equiv \frac{a_3}{\sqrt{2\pi}a_5}$,

$$f(x) = \left(\frac{a_0}{\sqrt{2\pi}a_2}\right) e^{\frac{-(x-a_1)^2}{(2{a_2}^2)}} + \left(\frac{a_3}{\sqrt{2\pi}a_5}\right) e^{\frac{-(x-a_4)^2}{(2{a_5}^2)}} \tag{6.13}$$

$a_0, a_1, a_2,$ and $a_3, a_4, a_5,$ are the fit parameters of the Gaussian distribution, where $a_0$and a_3 is the height of the peak, a_1 and $a_4$is the peak position of the Gaussian and a_2 and $a_5$is the bin width of the histogram. The number of particle observed is the total area of Gaussian distribution which can be found by

$$N_{particles} = \int f(x)dx = \frac{a_0}{w} + \frac{a_3}{w} \tag{6.14}$$

where a_0 and a_3 is the value of 0th and 3rd Gaussian parameter after the fitting process and $w$is the bin width of the histogram. Figure 6.4 shows the simulated distributions of Ξ^- candidates with full mass window and with the present of mass window using two Gaussian functions. The signal obtained is around 1.325 GeV. The mass distributions fitted gives $\chi^2/N_{dof} = 0.96$.

(a)

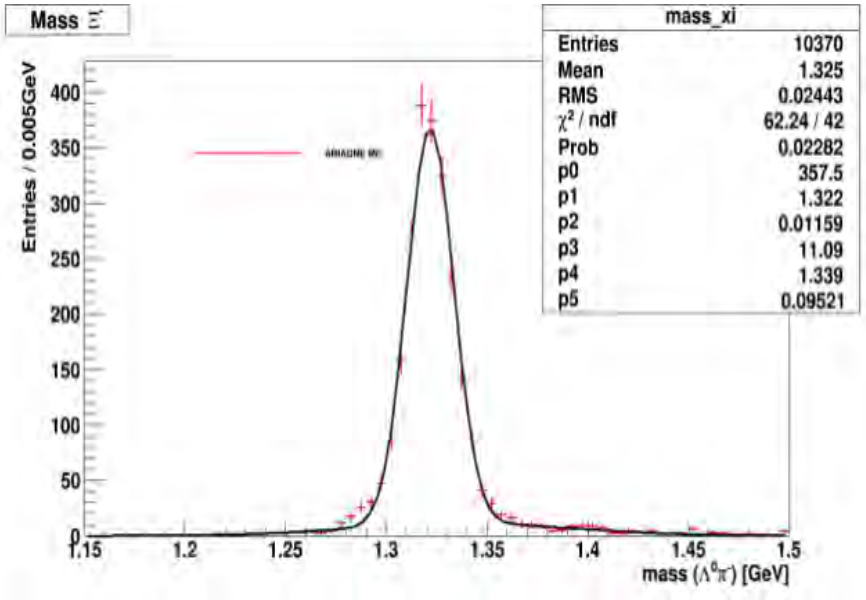

(b)

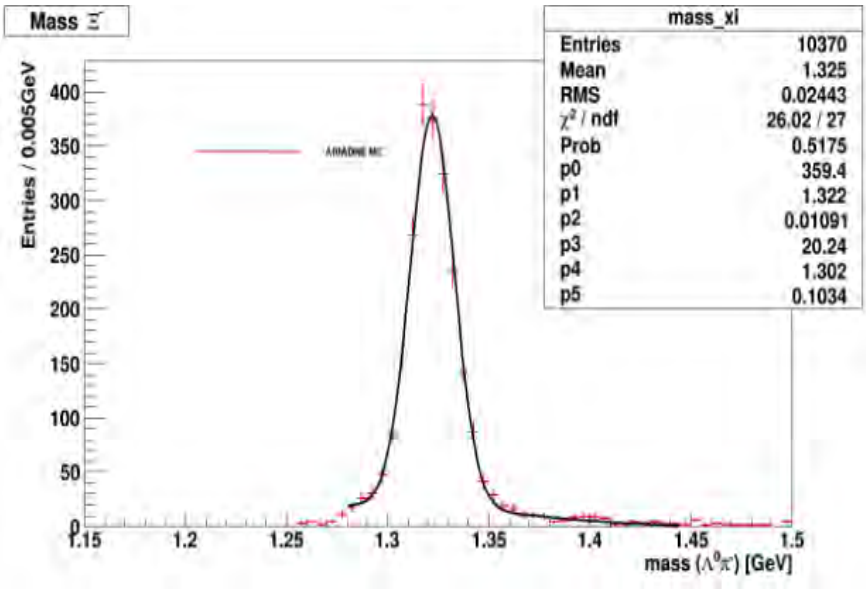

Figure 6.4: The mass distribution $m(\Lambda\pi^-)$ of all simulated signal $\Xi^-$with (a) full mass window and (b) present of mass window.

6.2.2.3 4th order polynomial function

The 4th order of polynomial, or also known as quartic polynomial was used to fit the background MC that can be expressed as Equation 6.15,

$$f(x) = ax^4 + bx^3 + cx^2 + dx + e = 0 \tag{6.15}$$

where $a \neq 0$. The mass distributions fitted gives $\chi^2/N_{dof} = 2.76$.

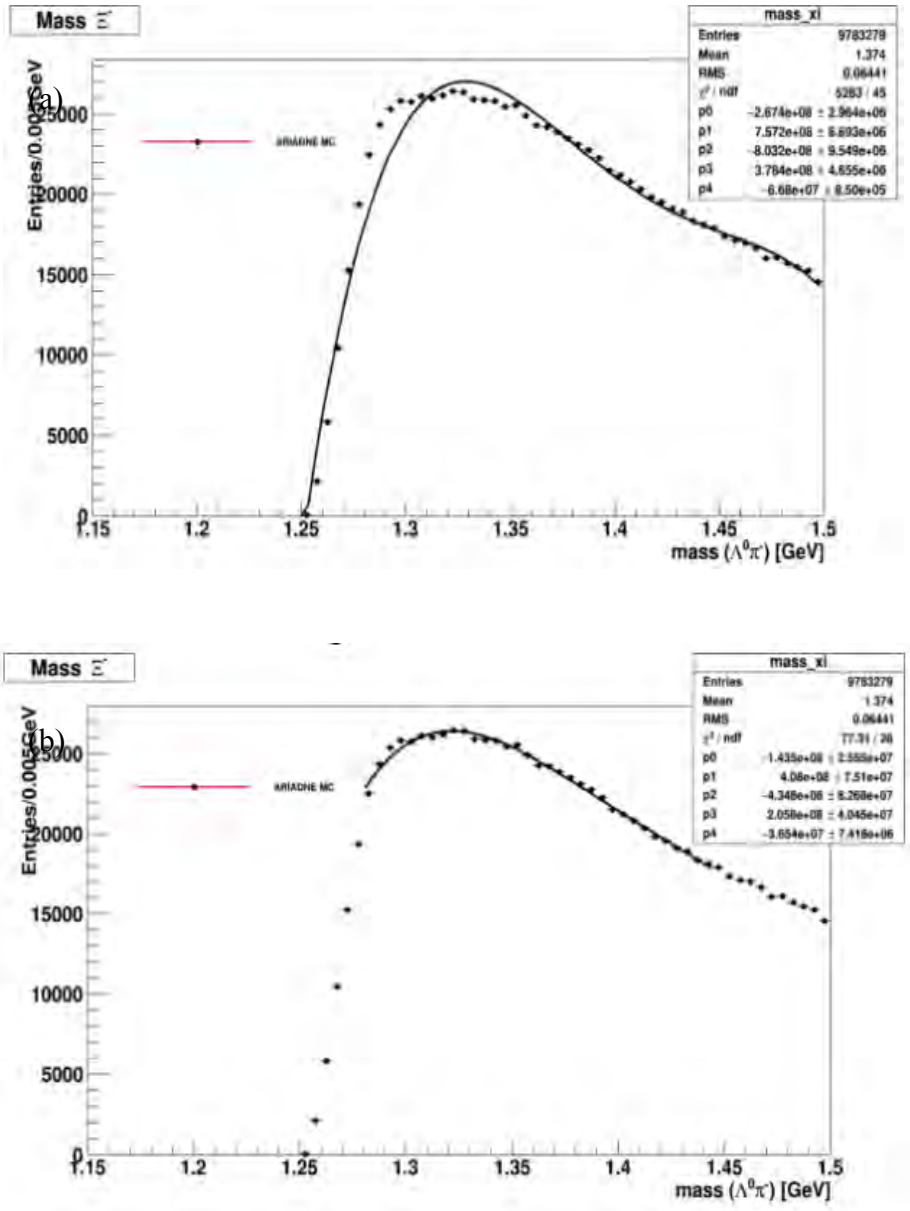

Figure 6.5: The mass distribution $m(\Lambda\pi^-)$ of all simulated background Ξ^- with (a) full mass window (b) present of mass window.

6.2.2.4 WA's function

Parametric estimations for background (Wan Abdullah, 1985) are carried out in such a way that the WA's function was used to fit the background MC. It is important to take note on the sharp rise at the threshold and the long tail at higher masses. WA's can be expressed as Equation 6.16,

$$f(x) = a_1 A(x) B(x) \tag{6.16}$$

Substituting $A(x) \equiv 1 - e^{-a_2(x-x_{thr})}$ and $B(x) \equiv e^{(-a_3(x-a_4))}$,

$$f(x) = a_1(1 - e^{-a_2(x-x_{thr})})(e^{(-a_3(x-a_4))}) \tag{6.17}$$

where $A(x)$ is the initial rapid rise and $B(x)$ is the tail of the background distribution. a_1, a_2, a_3, and a_4 are the constant coefficients to be fitted for, while x_{thr} is the threshold value. The fit was executed using the maximum likehood method, and it was found that the maximum somehow varies with the initial guesses for the coefficients. Thus, the starting values were varies to get an acceptable maximum likehood fit. In the region of greatest concern, the mass of Ξ^-'s and also the region which is near the threshold a_1 dominates the function shape. The mass distributions fitted gives $\chi^2/N_{dof} = 2.38$.

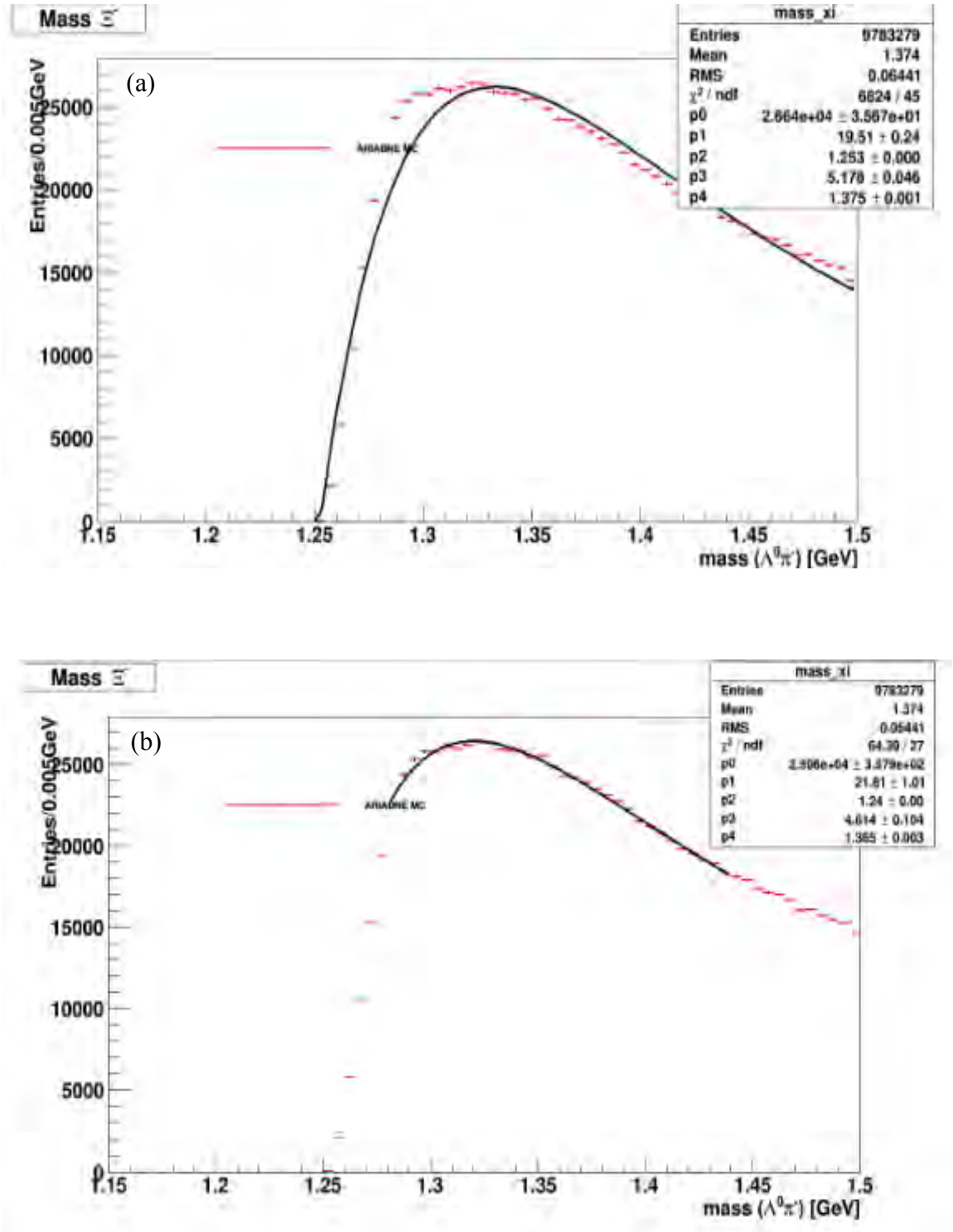

Figure 6.6: The mass distribution $m(\Lambda\pi^-)$ of all simulated background $\Xi^-$with (a) full mass window (b) present of mass window.

A fit of a mass spectrum was done not only because of the function needed, but it is because one would want to separate between signal and background. Therefore, certain assumptions about their shapes were made. For instance, signal is driven by Breit-Wigner, and background is driven by polynomial or exponent or whatever smooth function with not too many parameters. These gives an additional degree of freedom and one can separate between signal and background by looking into events in data which are the mixture of both signal and background. This becomes possible due to assumptions made about the shapes of signal and background; without any assumption about their shape, one cannot separate one from another.

A mass window functions to select events in a certain range dominated by signal. It is reasonable strategy to use the Gaussian function for signal samples or any other function which is suitable to describe the distributions. The two Gaussian functions give better fitting method in signal compared to BW function.

As for background, if it is "smooth" in the fitting area and does not have a threshold, typically it is needed to try several different polynomial orders and choose the minimum power that can describe the spectrum good enough. If the background clearly has a specific structure, for example a threshold, one typically needs to invent an appropriate function. As long as background is concerned, the fitting function really fully empirical and data-driven. From the figures shown above, WA's functions are much more relevant to choose due to smaller χ^2/N_{dof} obtained.

6.3 Functions and Fitting in HERA II Data

The signal and background functions, i.e. two Gaussian functions and WA's function were used to fit the whole spectrum in HERA II real data situation, as expressed,

$$Af_{sig}(x) + Bf_{bkg}(x) \tag{6.18}$$

$$f(x) = A(a_0 e^{\frac{-(x-a_1)^2}{2{a_2}^2}} + a_3 e^{\frac{-(x-a_4)^2}{2{a_5}^2}}) + B(a_1 A(x)B(x)) \tag{6.19}$$

$$f(x) = A(a_0 e^{\frac{-(x-a_1)^2}{2{a_2}^2}} + a_3 e^{\frac{-(x-a_4)^2}{2{a_5}^2}}) + B(a_1(1 - e^{-a_2(x-x_{thr})})(e^{(-a_3(x-a_4))})) \tag{6.20}$$

Substituting $A = 11.59$ and $B = 1.05$, the χ^2/N_{dof} obtained based on fitting for the certain sideband window was about 1.13. The A and B values improved to be 66.5 and 0.99 respectively, after being fitted.

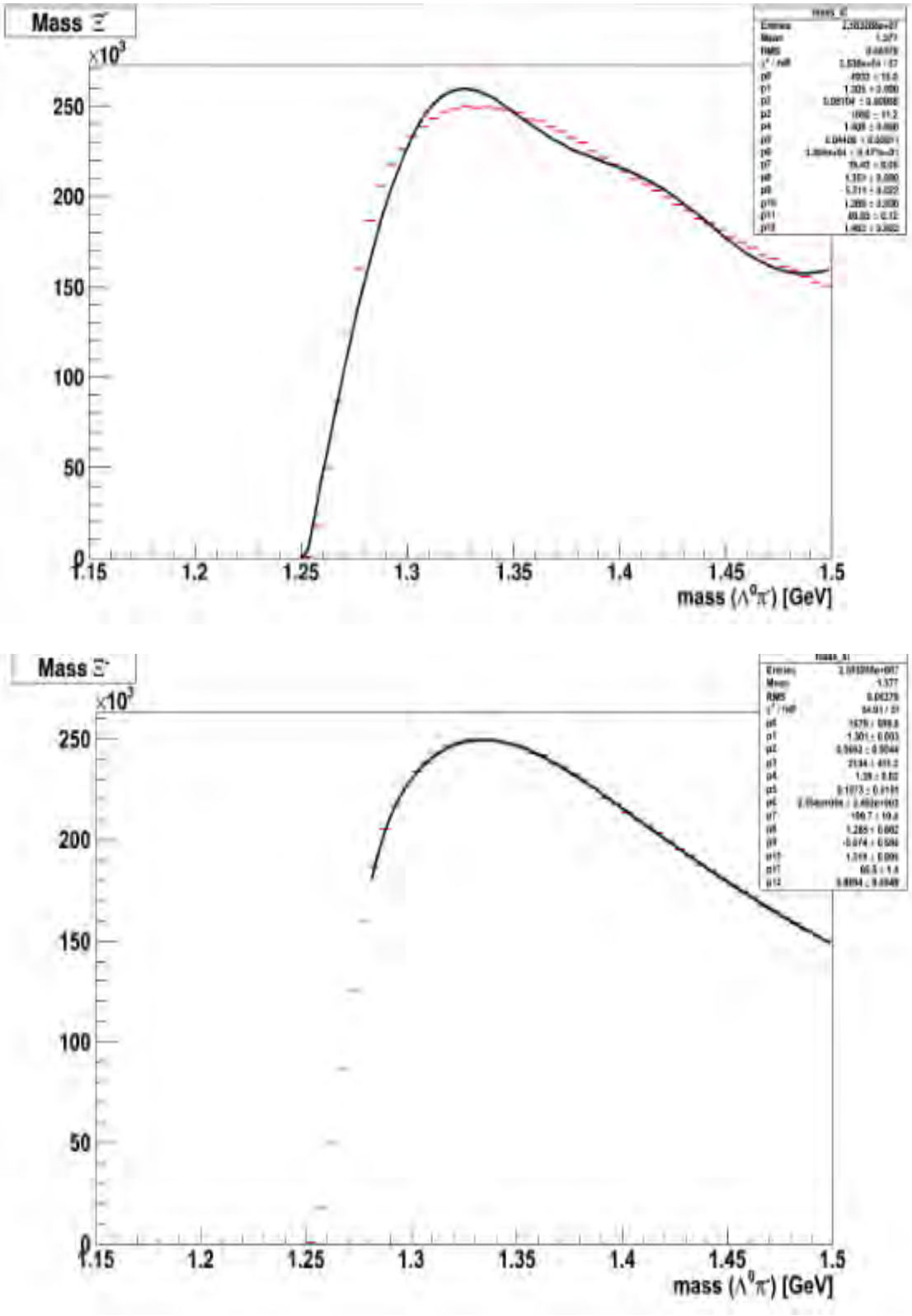

Figure 6.7: The mass distribution $m(\Lambda\pi^-)$ of all reconstructed $\Xi^-$with (a) full mass window (b) present of mass window.

6.4 Total Cross Section

In high energy physics world, total cross section means the probability of how many interactions occur during the collision between those tiny particles. In this case, it is the collision between electron, $\boldsymbol{e}$ and proton, $\boldsymbol{p}$. Usually, it is calculated by measuring the area under the graphs or histograms in the unit of area, namely barn. A barn is known as $\boldsymbol{10^{-28}m^2(100\ fm^2)}$. The total cross section, $\boldsymbol{\sigma}$ is defined as follows,

$$\sigma \approx \frac{N}{A.L.B_R} \tag{6.21}$$

where N is the total number of reconstructed Ξ^- at true level, A carries the acceptance, L is the integrated luminosity and B is the branching ratio of the selected decay channel. A is determined by Monte Carlo as definition in Section 5.8, while B_R gives the value of (99.89 ± 0.035) % following the decay channel $\Xi^- \rightarrow \Lambda + \pi^-$. The total cross section inclusive Ξ^- in HERA II data was found to be $13.98 \pm 0.002\ pb^{-1}$, while the cross section in HERA II MC $0.2 \pm 0.0039\ pb^{-1}$. HERA II data shows higher cross section compared to ARIADNE MC due to larger sample contains in data than Monte Carlo.

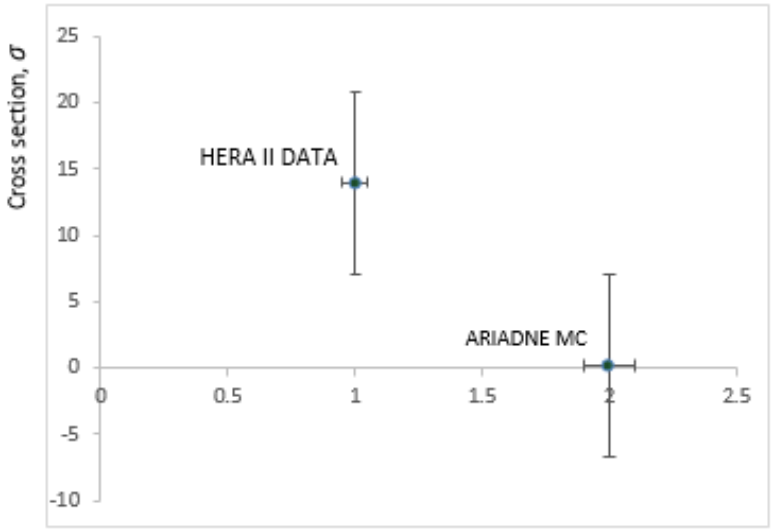

Figure 6.8: The comparison of cross section all generated and reconstructed Ξ^- using ARIADNE Monte Carlo and HERA II data.

CHAPTER 7: CONCLUSION

The analysis was carried out using HERA II data obtained from the ZEUS detector in the running time from 2002 up to 2007. The data consists of 355 million events with luminosity of 360 pb^{-1}, at center of mass of 318 GeV.

The matching procedure between generator level and reconstructed level has been done, and it was found that track efficiency to be 8 %. This is because of many Ξ^- candidate falls and was not detected due to large η track in the detector region.

Based on this research study to find Ξ^- in HERA II period, the particle was slightly possible to be found. From this analysis, the techniques of optimization cuts being used were crucial step because this could lessen the background. There are a few parameters being selected to under gone these cuts, as stated in Chapter 5. For the future works, more parameters can be used and tighter optimize cuts can be considered so that better signal peaks can be showed in HERA II data. In a nutshell, after going through optimization cuts, the total efficiency percentage were about 0.004% and 0.1961% Ξ^- candidates being found in MC and data respectively.

Apart from that, the shutdown of detector operation in purpose of increasing luminosity, has resulted in a large amount of background beam gas events and synchrotron radiation. Hence, to take useful physics data, some parts of the experiment needed to be modified because of the increasing multiple scattering process due to the additional material from the MVD. Thus, the peak of signal can hardly be seen in HERA II run. Apparently, in finding the configuration of any high energy physics experiment, one should aim to get the most physics results with least present of background. This applies on how well the CTD operates. A direct test should be done to test the effectiveness of MVD following the luminosity upgrade.

REFERENCES

Aaron, F. D., Abramowicz, H., Abt, I., Adamczyk, L., Adamus, M., Martin, M. A. D., ... & Antonov, A. (2010). Combined measurement and QCD analysis of the inclusive e±p scattering cross sections at HERA. *Journal of High Energy Physics*, *2010*(1), 109.

Abramowicz, H., Abt, I., Adamczyk, L., Adamus, M., Antonelli, S., Aushev, V., ... & Bloch, I. (2016). Search for a narrow baryonic state decaying to pKS0 and $\bar{p}$ KS0 in deep inelastic scattering at HERA. *Physics Letters B*, *759*, 446-453.

Abramowicz, H., Caldwell, A., & Sinkus, R. (1995). Neural network based electron identification in the ZEUS calorimeter. *Nuclear Instruments and Methods in Physics Research Section A: Accelerators, Spectrometers, Detectors and Associated Equipment*, *365*(2-3), 508-517.

Abt, I., Ahmed, T., Aid, S., Andreev, V., Andrieu, B., Appuhn, R. D., ... & Bán, J. (1997). The H1 detector at HERA. *Nuclear Instruments and Methods in Physics Research Section A: Accelerators, Spectrometers, Detectors and Associated Equipment*, *386*(2-3), 310-347.

Abt, I., Ahmed, T., Aid, S., Andreev, V., Andrieu, B., Appuhn, R. D., ... & Bán, J. (1997). The tracking, calorimeter and muon detectors of the H1 experiment at HERA. *Nuclear Instruments and Methods in Physics Research Section A: Accelerators, Spectrometers, Detectors and Associated Equipment*, *386*(2-3), 348-396.

Accomando, E., Andreazza, A., Anlauf, H., Ballestrero, A., Barklow, T., Bartels, J., ... & Bernreuther, W. (1998). Physics with e+ e− linear colliders. *Physics Reports*, *299*(1), 1-78.

Adamczyk, L., Andruszkow, J., Bold, T., Borzemski, P., Buettner, C., Caldwell, A., ... & Figiel, J. (2014). Measurement of the luminosity in the ZEUS experiment at HERA II. *Nuclear Instruments and Methods in Physics Research Section A: Accelerators, Spectrometers, Detectors and Associated Equipment*, *744*, 80-90.

Allison, J., Brun, R., Bruyant, F., Bullock, F. W., Chang, C. Y., Dumont, J. J., ... & Kawamoto, T. (1987). An Application of the GEANT3 Geometry Package to the Description of the OPAL Detector. *Computer Physics Communications*, *47*(1), 55-74.

Altarelli, G., & Wells, J. (2017). QCD: The Theory of Strong Interactions. In *Collider Physics within the Standard Model*. Springer, Cham.

Andrieu, B., Babayev, A., Ban, J., Banas, E., Barrelet, E., Bassler, U., ... & Besancon, M. (1993). The H 1 liquid argon calorimeter system. *Nuclear Instruments and Methods in Physics Research Section A: Accelerators, Spectrometers, Detectors and Associated Equipment*, *336*(3), 460-498.

Andruszkow, J., Borzemski, P., & Chwastowski, J. (2001). Luminosity Measurement in the ZEUS Experiment. *Acta Physica Polonica. Series B*, *32*(7-8), 2025-2057.

Antonelli, S. (2009). Study of production of high-PT leptons and limits on single top production at HERA. (Doctoral Dissertation).

Appuhn, R. D., Arndt, C., Barrelet, E., Barschke, R., Bassler, U., Boudry, V., ... & Claxton, B. (1997). The H1 lead/scintillating-fibre calorimeter. *Nuclear Instruments and Methods in Physics Research Section A: Accelerators, Spectrometers, Detectors and Associated Equipment*, *386*(2-3), 397-408.

Avery, P. (1992). Applied fitting theory V: track fitting using the Kalman filter. *CLEO Note CBX92-39*.

Bamberger, A., Boterenbrood, H., Bulmahn, J., Carlin, R., Cunitz, H., Dawson, J., ... & Klanner, R. (1997). The small angle rear tracking detector of ZEUS. *Nuclear Instruments and Methods in Physics Research Section A: Accelerators, Spectrometers, Detectors and Associated Equipment*, *401*(1), 63-80.

Baumgarten, C., Braun, B., Ciullo, G., Dalpiaz, P. F., Golendukhin, A., Graw, G., ... & Kolster, H. (2003). Measurements of atomic recombination in the HERMES polarized hydrogen and deuterium storage cell target. *Nuclear Instruments and Methods in Physics Research Section A: Accelerators, Spectrometers, Detectors and Associated Equipment*, *496*(2-3), 263-276.

Bentvelsen, S., Engelen, J., & Kooijman, P. (1992). *Reconstruction of (x, Q 2) and extraction of structure functions in neutral current scattering at HERA*.

Berkeley Lab. (2014). Scale of the Atom. Particle Data Group. Retrieved on June 22, 2015, from http://www.particleadventure.org/scale.html.

Bhadra, S., Crombie, M., Kirkby, D., & Orr, R. S. (1989). The ZEUS third-level trigger system. *Computer Physics Communications*, *57*(1-3), 321-324.

Bindi, M. (2008). Measurement of the charm production cross section in DIS events at HERA. (Doctoral Dissertation). Retrieved on July 15, 2015, from https://arxiv.org/pdf/1405.6915.pdf

Bjorken, J. D. (1969). Asymptotic sum rules at infinite momentum. *Physical Review*, *179*(5), 1547.

Boogert, S. T. (2003). Photoproduction of K , Å∞ s mesons and Œ› baryons in electron proton collisions at ZEUS. (Doctoral dissertation). Retrieved on January 10, 2014, from https://arxiv.org/abs/hep-ex/0701041.

Borisovich, O. L. (2012). ABC of Physics: A Very Brief Guide. *ABC of Physics: A Very Brief Guide.* New Jersey, United State of America: World Scientific Publishing Co. Pte. Ltd.

Brandelik, R., Braunschweig, W., Gather, K., Kadansky, V., Lübelsmeyer, K., Mättig, P., ... & Schmitz, D. (1979). Evidence for planar events in e+ e− annihilation at high energies. *Physics Letters B*, *86*(2), 243-249.

Brock, I. C. (2009). Heavy Quark Production at HERA. Retrieved on September 8, 2015, from https://arxiv.org/pdf/1612.02371.pdf.

CERN Collaboration et al., (2014). Retrieved on March 24, 2015, from http://www.stfc.ac.uk/research/particle-physics-and-particle-astrophysics/peter-higgs-a-truly-british-scientist/why-is-the-higgs-discovery-so-significant/

Chekanov, S., Derrick, M., Magill, S., Musgrave, B., Nicholass, D., Repond, J., ... & Molina, A. Y. (2007). Multijet production at low xBj in deep inelastic scattering at HERA. *Nuclear Physics B*, *786*(1), 152-180.

Close, F. (2004). *Particle Physics: A Very Short Introduction* (Vol. 109). Oxford University Press.

Cohen-Tannoudji, C., Dupont-Roc, J., & Grynberg, G. (1989). *Photons and Atoms: Introduction to Quantum Electrodynamics.* New York: Wiley.

Cooper-Sarkar, A. M., Devenish, R. C., & de Roeck, A. (1998). Structure functions of the nucleon and their interpretation. *International Journal of Modern Physics A*, *13*(20), 3385-3586.

Cowan, J. D. (1990). Discussion: Mcculloch-pitts and related neural nets from 1943 to 1989. *Bulletin of Mathematical Biology*, *52*(1-2), 73-97.

D'Agostini, G., & Nigro, A. (1997). *Deep Inelastic Scattering and Related Phenomena. In Deep Inelastic Scattering and Related Phenomena.* New Jersey, United State of America: World Scientific Publishing Co. Pte. Ltd.

Derrick, M., Krakauer, D., Magill, S., Musgrave, B., Repond, J., Sugano, K., ... & Ayed, R. (1992). A measurement of σtot (γp) at S= 210 GeV. *Physics Letters B*, *293*(3-4), 465-477.

Edin, A., Ingelman, G., & Rathsman, J. (1997). Quarkonium Production at the Fermilab Tevatron through Soft Color Interactions. *Physical Review D*, *56*(11), 7317.

Eichten, T. H., Faissner, H., Hasert, F. J., Kabe, S., Krenz, W., Von Krogh, J., ... & Van Doninck, W. (1973). Measurement of the Neutrino-Nucleon and Antineutrino-Nucleon Total Cross Sections. *Physics Letters B*, *46*(2), 274-280.

Elliot, C., & Teresa, E. (Eds.). (1998). *Calorimetry in High Energy Physics-Proceedings of The 7th International Conference*. New Jersey, United State of America: World Scientific Co. Pte. Ltd.

Feynman, R. P. (1969). Very high-energy collisions of hadrons. *Physical Review Letters*, *23*(24), 1415.

Fisher, R. A. (1936). The use of multiple measurements in taxonomic problems. *Annals of Human Genetics*, *7*(2), 179-188.

Gell-Mann, (2015). A schematic model of baryons and mesons. In *50 Years of Quarks*. Munich, Germany: World Scientific Co. Pte. Ltd.

Guzik, M. Reconstruction methods in Zeus note. (2011).

Haas, T. (1992). *Generating Monte Carlo events with MOZART*. Unpublished Note.

Hall-Wilton, R., McCubbin, N., Nylander, P., Sutton, M., & Wing, M. (1999). The CTD tracking resolution. *Internal ZEUS-Note*, 99-027.

Hartner, G. F. (1998). *VCTRAK Briefing: Program and Math.* Unpublished Note.

Heath, G. P., Foster, B., Short, T. L., Wilson, S. S., Lancaster, M., Shield, P. D., ... & Halsall, R. (1992). The ZEUS first level tracking trigger. *Nuclear Instruments and Methods in Physics Research Section A: Accelerators, Spectrometers, Detectors and Associated Equipment*, *315*(1-3), 431-435.

Herrero, M. (1999). The Standard Model. In *Techniques and Concepts of High Energy Physics X,* 1-59. Springer Netherlands.

Hilton, M., Li, Y. T., Loizides, J., Yue, M. M., Muhiddin, K., & Ramanlal, J. (1999). Electroweak Unification at HERA. Retrieved on February 25, 2015, from https://arxiv.org/abs/0705.4264.

Hoeger, K. C. (1991). Measurement of *x, y, Q** 2* in Neutral Current Events. Retrieved on May 29, 2016, from http://citeseerx.ist.psu.edu/viewdoc/

Honc, S. (2011). New applications of the multi variate analysis framework NeuroBayes for an inclusive b-jet cross section measurement at CMS. (Doctoral Dissertation). Retrieved on April 7, 2016, from https://ekp-invenio.physik.uni-karlsruhe.de/record/45231.

Jung, H. (1995). Hard diffractive scattering in high energy ep collisions and the Monte Carlo generator RAPGAP. *Computer Physics Communications*, *86*(1-2), 147-161.

Kalman, R. E. (1960). A new approach to linear filtering and prediction problems. *Journal of basic Engineering*, *82*(1), 35-45.

Kappes, A. (2001). Measurement of $e^- p \rightarrow e^- X$ differential cross-sections at high Q^2 and of the structure function xF_3 with ZEUS at HERA. (Doctoral Dissertation). Retrieved on May 7, 2016, from http://inspirehep.net/record/571844/files/diss.pdf

Klein, Uta. (2008). ZEUS Luminosity Calculation. Retrieved on September 21, 2016, from http://www-zeus.desy.de/physics/lumi/

Korcsak-Gorzo, K., Grzelak, G., Oliver, K., Dawson, M., Devenish, R., Ferrando, J., ... & Walczak, R. (2007). The optical alignment system of the ZEUS microvertex detector. *Nuclear Instruments and Methods in Physics Research Section A: Accelerators, Spectrometers, Detectors and Associated Equipment*, *580*(3), 1227-1242.

Kwiatkowski, A., Spiesberger, H., & Möhring, H. J. (1992). HERACLES: an event generator for ep interactions at HERA energies including radiative processes. *Computer Physics Communications*, *69*(1), 155-172.

Lajoie, L. (2009). Triggering and FEE Pipelining: ZEUS, H. Triggering in Particle Physics Experiments. Retrieved on August 24, 2017, from http://slideplayer.com/slide/5718584/

Libov, V. (2013). Measurement of charm and beauty-production in deep inelastic scattering at HERA and test beam studies of ATLAS pixel sensors.

Linde, A., Linde, D., & Mezhlumian, A. (1994). From the Big Bang theory to the theory of a stationary universe. *Physical Review D*, *49*(4), 1783.

Lisovyi, M. (2011). Measurement of charm production in deep inelastic scattering using lifetime tagging for D±meson decays with the ZEUS detector at HERA. (Doctoral Dissertation). Retrieved on July 23, 2015, from http://www-library.desy.de/preparch/desy/thesis/desy-thesis-11-033.pdf

Lönnblad, L. (1992). Ariadne version 4—A program for simulation of QDC cascades implementing the colour dipole model. *Computer Physics Communications*, *71*(1-2), 15-31.

Lönnblad, L. (2002). Correcting the colour-dipole cascade model with fixed order matrix elements. *Journal of High Energy Physics*, *2002*(05), 046.

Loveland, W. D., Morrissey, D. J., & Seaborg, G. T. (2017). *Modern Nuclear Chemistry*. New Jersey, United State of America: John Wiley & Sons.

Mankel, R., "ZEUS Tracking Tutorial", ZEUS Internal Report, Retrieved on January 15, 2017, from http://www-zeus.desy.de/lectures/tracking_lecture.ppt

Mansfield, M., O'Sullivan, C., (2011). *Understanding Physics (4th ed.)*. New Jersey, United State of America: John Wiley & Sons.

Metropolis, N., & Ulam, S. (1949). The Monte Carlo method. *Journal of the American Statistical Association*, *44*(247), 335-341.

Miller, G., Bloom, E. D., Buschhorn, G., Coward, D. H., DeStaebler, H., Drees, J., ... & Hartmann, G. C. (1972). Inelastic electron-proton scattering at large momentum transfers and the inelastic structure functions of the proton. *Physical Review D*, *5*(3), 528.

Mohammad Nasir, N., & Wan Abdullah, W.A.T. (2015). Production of Ξ^- in deep inelastic scattering with ZEUS detector at HERA. *American Institute of Physcis Conference Proceedings*, *1704, Negeri Sembilan, Malaysia.*

Narsky, I. (2006). Optimization of signal significance by bagging decision trees. *Statistical Problems in Particle Physics, Astrophysics and Cosmology* (pp. 143-146).

Okun, L. B. (2012). *ABC of Physics: A Very Brief Guide*. World Scientific.

Parker, C.B. (1994). *McGraw Hill Encyclopedia of Physics (2nd ed.), McGraw Hill.* Retrieved on June 18, 2015, from http://www.idc-online.com/technical_references/pdfs/electrical_engineering/Quantum_Mechanics_Polarization_Density.pdf

Patrignani, C., & Particle Data Group. (2016). Review of particle physics. *Chinese Physics C*, *40*(10), 100001.

Perez, E., & Rizvi, E. (2013). The quark and gluon structure of the proton. *Reports on Progress in Physics*, *76*(4), 046201.

Pitzl, D., Behnke, O., Biddulph, M., Bösiger, K., Eichler, R., Erdmann, W., ... & Kausch, M. (2000). The H1 silicon vertex detector. *Nuclear Instruments and Methods in Physics Research Section A: Accelerators, Spectrometers, Detectors and Associated Equipment*, *454*(2-3), 334-349.

Placakyte, R. (2011). Parton Distribution Functions. *Proceedings, 31st International Conference on Physics in Collisions (PIC 2011), Vancouver, Canada.*

Polini, A., Brock, I., Goers, S., Kappes, A., Katz, U. F., Hilger, E., ... & Adler, V. (2007). The design and performance of the ZEUS Micro Vertex detector. *Nuclear Instruments and Methods in Physics Research Section A: Accelerators, Spectrometers, Detectors and Associated Equipment*, *581*(3), 656-686.

Quadt, A., Devenish, R. C. E., Topp-Jørgensen, S., Sutton, M., Uijterwaal, H. A. J. R., Byrne, A. F., & Gingrich, D. M. (1999). The design and performance of the ZEUS central tracking detector second-level trigger. *Nuclear Instruments and Methods in Physics Research Section A: Accelerators, Spectrometers, Detectors and Associated Equipment*, *438*(2-3), 472-501.

Rutherford, E. (1911). LXXIX. The scattering of α and β particles by matter and the structure of the atom. *The London, Edinburgh, and Dublin Philosophical Magazine and Journal of Science*, *21*(125), 669-688.

Sjöstrand, T., Mrenna, S., & Skands, P. (2006). PYTHIA 6.4 physics and manual. *Journal of High Energy Physics*, *2006*(05), 026.

Smith, W. H., Ali, I., Behrens, B., Fordham, C., Foudas, C., Goussiou, A., ... & Silverstein, S. (1995). The ZEUS calorimeter first level trigger. *Nuclear Instruments and Methods in Physics Research Section A: Accelerators, Spectrometers, Detectors and Associated Equipment*, *355*(2-3), 278-294.

Spiridonov, A. (2008). Mathematical framework for fast and rigorous track fit for the ZEUS detector. Retrieved on March 4, 2017, from https://arxiv.org/abs/0812.1245.

Szuba, D., Wichmann, K., & Bokhonov, V. (2012). HERA Accelerator. Retrieved on October 23, 2014, from http://wwwzeus.desy.de/ZEUS_ONLY/analysis/primer/heraacc1.html

The Orange Homepage. (2014). Retrieved on August 10, 2016, from http://www-zeus.desy.de/ZEUS_ONLY/ analysis/orange/

Tuning, N. (2001). *ZUFOs: Hadronic Final State Reconstruction with Calorimeter, Tracking and Backsplash Correction.* Unpublished Note.

The Orange Ntuple. (2014). Retrieved on January 19, 2017, from http://www-zeus.desy.de/ZEUS_ONLY/analysis/orange/using_and_extending_the_orange_ntuple.html

Verena Schonberg Homepage. (2006). Retrieved on February 4, 2017, from http://www-zeus.desy. de/ ~vschoenb/

Wan Abdullah, W. A. T (1985). Strange and Multistrange Baryon Production in e^+ e^- Annihilation. (Doctoral Dissertation). Retrieved on June 8, 2016, from https://spiral.imperial.ac.uk / bitstream/10044/1/37888/2/Wan-Abdullah-WAT-1985-PhD-Thesis.pdf

Webber, B. R. (1999). Fragmentation and Hadronization. Retrieved on September 4, 2017, from https://arxiv.org/abs/hep-ph/9912292.

Weinstein, A. (1999). Breit Wigners and Form Factors.

Zenaiev, O. (2017). Charm Production and QCD Analysis at HERA and LHC. *The European Physical Journal C*, *77*(3), 151.

ZEUS collaboration, & Holm, U. (1993). *The ZEUS Detector.* Unpublished report,

ZEUS Collaboration. (2003). High-Q^2 neutral current cross sections in e+p deep inelastic scattering at $\sqrt{s}$= 318 GeV. Retrieved on May 18, 2015, from https://arxiv.org/abs/hep-ex/0401003.

ZEUS collaboration. (2008). Energy dependence of the charged multiplicity in deep inelastic scattering at HERA. *Journal of High Energy Physics*, *2008*(06), 061.

Ziegler, A. (2002). Measurement of Inclusive Xi-and Sigma (1385)+- Baryon Production in Neutral Current Deep Inelastic Scattering at HERA. (Doctoral Dissertation). Retrieved on October 2, 2015, from http://inspirehep.net/record/606108.

Zolkapli, Z. (2013). Strange Particle Production in High-Rnergy Electron Proton Collision. (Master Dissertation). Retrieved on July 17, 2016, from http://studentsrepo.um.edu.my/ 4876/2/ZukhaimiraThesisFinal.pdf

Zur Nedden, M. (2004). Measurement of the $b\bar{b}$ Cross Section at HERA-B. In *American Institute of Physics Conference Series*. 722, 57-62.

Zur Nedden. (2009). Charm Production: From HERA to LHC. Retrieved on March 23, 2015, from http://slideplayer.com/slide/4921536/

LIST OF PUBLICATIONS AND PAPER PRESENTED

Abramowicz, H., Abt, I., Adamczyk, L., Adamus, M., Antonelli, S., Aushev, V., … & **Mohammad Nasir, N.** (2016). Search for a narrow baryonic state decaying to pK 0 S and anti pK 0 S in deep inelastic scattering at HERA. *Physics Letters B*, *759*, 446-453.